Comenius University in Bratislava
Faculty of Mathematics, Physics and Informatics
Department of Nuclear Physics and Biophysics

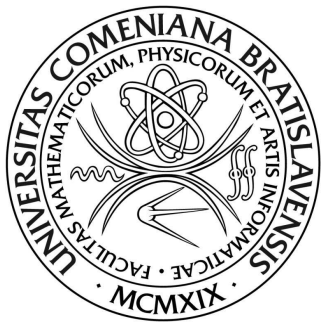

Alpha decay of neutron-deficient radium and francium isotopes

PhD Thesis

Branch of study: 4.1.5 Nuclear and Subnuclear Physics
Study program: Nuclear and Subnuclear Physics

Supervisor: doc. Mgr. Stanislav Antalic, PhD.

Mgr. Zdenka Kalaninová
Bratislava 2014

Comenius University in Bratislava
Faculty of Mathematics, Physics and Informatics

THESIS ASSIGNMENT

Name and Surname:	Mgr. Zdenka Kalaninová
Study programme:	Nuclear and Subnuclear Physics (Single degree study, Ph.D. III. deg., full time form)
Field of Study:	4.1.5. Nuclear And Subnuclear Physics
Type of Thesis:	Dissertation thesis
Language of Thesis:	English
Secondary language:	Slovak

Title: Alpha decay of neutron-deficient radium and francium isotopes

Literature: P.E. Hodgson, E. Gadioli and E. Gadioli Erba, Introductory Nuclear Physics, Oxford University Press, 1997.
K. Heyde, Basic Ideas and Concepts in Nuclear Physics, Institute of Physics Publishing, 3rd edition 2004.
R. Casten, Nuclear Structure from a Simple Perspective, Oxford University Press, 1990.
C. Wagemans, The Nuclear Fission Process, CRC Press, 1991.
K.S. Krane, Introductory Nuclear Physics, John Wiley & Sons, 1988.
Articles of current periodical journals.

Aim: Investigation of decay properties of neutron-deficient 197-202Fr and 201-203Ra isotopes produced in fusion-evaporation reactions at the velocity filter SHIP at GSI in Darmstadt.

Annotation: In the thesis decay properties of neutron-deficient radium and francium isotopes will be analyzed using alpha- and gamma-decay spectroscopy. Studied isotopes were produced in two experiments performed at the velocity filter SHIP using the reactions 56Fe+147,149Sm and 60Ni+141Pr. For some of the studied nuclides there is not much experimental information available up to now and in some cases published data are not consistent. Results of the thesis should bring more details on their structure a properties and improve known data. A search for a new isotope 197Fr will be performed.

Keywords: alpha decay, neutron-deficient isotopes, nuclear energy levels

Tutor:	doc. Mgr. Stanislav Antalic, PhD.
Department:	FMFI.KJFB - Department of Nuclear Physics and Biophysics
Head of department:	doc. RNDr. Stanislav Tokár, CSc.
Assigned:	18.10.2010
Approved:	18.10.2010

prof. RNDr. Jozef Masarik, DrSc.
Guarantor of Study Programme

.....
Student

.....
Tutor

I thank Dr. Stano Antalic for helping me with the analysis and interpretation of experimental data and for interesting discussions about results presented in this Thesis.
I also thank Prof. Andrei N. Andreyev and Dr. Fritz P. Heßberger for many discussions about subjects related to this work.

Thank you, Mou ☺

Abstrakt

V neutrónovo-deficitných jadrách nad uzavretou protónovou vrstvou $Z = 82$ môžeme študovať niekoľko zaujímavých javov súvisiacich s jadrovou štruktúrou. Príkladom je koexistencia stavov s rôznou deformáciou v rámci jedného jadra alebo výrazné zmeny tvaru medzi susednými nuklidmi. V dizertačnej práci boli skúmané jadrá z tejto oblasti — neutrónovo-deficitné nuklidy rádia ($Z = 88$) a francia ($Z = 87$). Izotopy boli produkované vo fúzno-výparných reakciách $^{56}\mathrm{Fe} + {}^{147,149}\mathrm{Sm}$ a $^{60}\mathrm{Ni} + {}^{141}\mathrm{Pr}$ na rýchlostnom filtri SHIP v GSI, Darmstadt (Nemecko). Dáta boli analyzované metódami rozpadovej α a γ spektroskopie.

K hlavným výsledkom práce patrí identifikácia nového izotopu ^{197}Fr a nových izomérnych stavov rozpadajúcich sa α rozpadmi v izotopoch ^{201}Ra a ^{198}Fr. V jadrách ^{200}Fr a ^{201}Fr boli identifikované nové izomérne hladiny rozpadajúce sa vnútornými prechodmi. Pre izotopy ^{202}Ra a ^{199}Fr sa podarilo výrazne upresniť známe rozpadové vlastnosti, keďže bolo registrovaných rádovo viac rozpadov než v predošlých meraniach. Dáta naznačujú zmenu deformácie základného stavu ^{199}Fr oproti ťažším izotopom francia s nepárnym počtom nukleónov. Pre α rozpad ^{202}Ra bola vyhodnotená vysoká redukovaná šírka, čo predstavuje nárast redukovaných šírok s klesajúcim počtom neutrónov pre párno-párne izotopy rádia. Nezvyčajne vysoká redukovaná šírka bola vyhodnotená aj pre α rozpad ^{197}Fr.

kľúčové slová: α rozpad, neutrónovo-deficitné izotopy, energetické hladiny v jadrách

Abstract

In neutron-deficient nuclei above the proton shell closure $Z = 82$, several interesting nuclear-structure phenomena can be observed, for example, states with different shapes coexisting within a single nucleus or large changes in deformation between neighboring nuclei. In this Thesis, neutron-deficient nuclei from this region were investigated, namely radium ($Z = 88$) and francium ($Z = 87$) isotopes. Nuclei were produced in fusion-evaporation reactions $^{56}\mathrm{Fe} + {}^{147,149}\mathrm{Sm}$ and $^{60}\mathrm{Ni} + {}^{141}\mathrm{Pr}$ at the velocity filter SHIP at GSI in Darmstadt (Germany). Data were analyzed using the methods of α- and γ-decay spectroscopy.

Main results of the Thesis comprise the identification of a new isotope ^{197}Fr and new isomeric α-decaying states in ^{201}Ra and ^{198}Fr. In ^{200}Fr and ^{201}Fr nuclei, new isomeric γ-decaying levels were identified. For ^{202}Ra and ^{199}Fr nuclei, known α-decay properties were significantly improved, since the collected statistics was higher than in previous measurements by one order of magnitude. Data indicate the change in the ground-state deformation of ^{199}Fr compared to heavier odd-A francium isotopes. For the α decay of ^{202}Ra, high value of reduced width was evaluated, that shows an increase of reduced α-decay widths with decreasing neutron number for even-even radium isotopes. A remarkably high reduced width was evaluated for the α decay of ^{197}Fr as well.

keywords: α decay, neutron-deficient isotopes, nuclear energy levels

Contents

List of Abbreviations

βDF	β-delayed fission
δ^2_α	reduced α-decay width
CERN	European Organization for Nuclear Research
CRIS	Collinear Resonance Ionization Spectroscopy
GARIS	GAs-filled Recoil Ion Separator
ISOLDE	on-line isotope mass separator
JYFL	Department of Physics of the University of Jyväskylä
LISOL	Leuven Isotope Separator On-Line
PSSD	Position-Sensitive Silicon Detector
RIKEN	Institute of Physical and Chemical Research
RITU	gas-filled recoil separator (Recoil Ion Transport Unit)
SHIP	Separator for Heavy Ion reaction Products
TOF	time of flight
CN	compound nucleus
ER	evaporation residue
FRDM	finite-range droplet model
FRLDM	finite-range liquid-drop model
HF	hindrance factor

Chapter 1

Introduction

At the beginning of the twentieth century, the concept of basic constituents of matter differed a lot from today's perspective. In 1904, J.J. Thomson described an atom as a sphere of uniformly distributed electric charge containing a number of moving 'corpuscles' of the opposite charge [Tho04]. In 1909, experiments performed by H. Geiger and E. Marsden [Gei09] showed that scattering of α particles passing through metal plates did not correspond to Thomson's idea of atomic structure. It was supposed that α particles traversing through matter would undergo a multitude of small scatterings. However, the final angular distribution of α particles did not correspond to this assumption. A small fraction of α particles showed a diffuse reflection as a result of their scattering. About 1 in 8000 α particles falling on a metal plate was deflected by an angle exceeding $90\,^{\circ}$. A simple calculation following the ordinary probability law resulted in an extremely small chance for such a reflection to occur [Gei10]. The behavior of α particles was explained in 1911 by E. Rutherford [Rut11]. He assumed that the positive charge is not distributed uniformly throughout the atom, but it is concentrated in a very small volume in the center of the atom. Interactions of α particles passing through matter with this central charge resulted in large deflection angles observed by Geiger and Marsden. The concept of the central charge existing within the atom was the beginning of the story of atomic nucleus.

Since the discovery of the atomic nucleus, a lot of effort has been made to understand its structure. It was found out that the nucleus consists of two types of nucleons: *protons* discovered by E. Rutherford in 1919 [Rut19] and *neutrons* discovered by J. Chadwick in 1932 [Cha32]. A new question arose: How are nucleons arranged within the nucleus? Trying to provide the answer, a lot of models describing the atomic nucleus have been developed.

The *liquid-drop model* compares the atomic nucleus to a drop of liquid and nucleons to molecules in that drop of liquid. This model explains, for example, nuclear masses, binding energies, energy distributions of nuclear reactions

and basic properties of radioactive decays (α, β, fission). This model supposes nuclear properties to vary smoothly as a function of the number of nucleons inside the nucleus. However, some nuclear properties, for example, proton and neutron separation energies, proved discontinuities at certain 'magic' numbers (2, 8, 20, 28, 50, 82, 126) of protons and neutrons.

The existence of magic numbers was explained by the *shell model*. This model assumes that nucleons within the nucleus are arranged in energy levels. Only a certain amount of them can occupy each level and in a ground state nucleons occupy the levels with the lowest energies. Levels are grouped into shells and when the outermost ('valence') shell is completely filled up with nucleons, the nucleus has a greater stability compared to the nucleus, whose valence shell is not fully filled up. The numbers of protons and neutrons inside the nucleus with closed (i.e. completely filled up) shells reproduce magic numbers.

First descriptions of nuclei with the shell structure assumed a spherical shape of the nucleus (see, e.g., [May49]). Later it was showed that in some cases greater stability is obtained not for a spherical nucleus, but for a deformed one with the same volume [Rai50, Boh51]. It is valid mainly for nuclei with numbers of protons and/or neutrons far from closed shells. Magic numbers present enhanced stability only for spherical nuclei. With increasing deformation, other numbers of protons and neutrons present a greater stability (see, e.g., Ref. [Jan05b]). The model calculating the order of single-particle levels as a function of nuclear deformation was originally presented by S.G. Nilsson in 1955 [Nil55]. Nowadays various models exist predicting the order of single-particle (also called 'Nilsson') levels for all nuclei across the nuclide chart (see, e.g., Ref. [Möl97]).

Although nuclear models describe some nuclear properties of known nuclei with excellent accuracy, the predictions can diverge for as-yet undiscovered nuclei. A nice example of such inconsistent theoretical predictions are calculated values for the nuclear mass — one of the most basic characteristics of the nucleus (see Fig. 1.1). Generally, the further the isotope is from the β-stability line, the less information is experimentally known about it. For optimization of theoretical models it is necessary to continue the investigation of nuclei far from the region of β stability.

In this work, we investigated neutron-deficient nuclei in the vicinity of a proton shell closure $Z = 82$. This region provides a unique possibility to investigate some interesting nuclear-structure phenomena, for example, shape coexistence (see, e.g., Refs. [Hey11, And00]), large changes in deformation between neighboring nuclei (see, e.g., Refs. [Bij95, Jul01]), or β-delayed fission (see, e.g., Refs. [Hal92, And13b]).

- In a number of nuclei, mainly near spherical shells or subshells, the phenomenon of *shape coexistence* was observed [Hey11]. In these nuclei, dif-

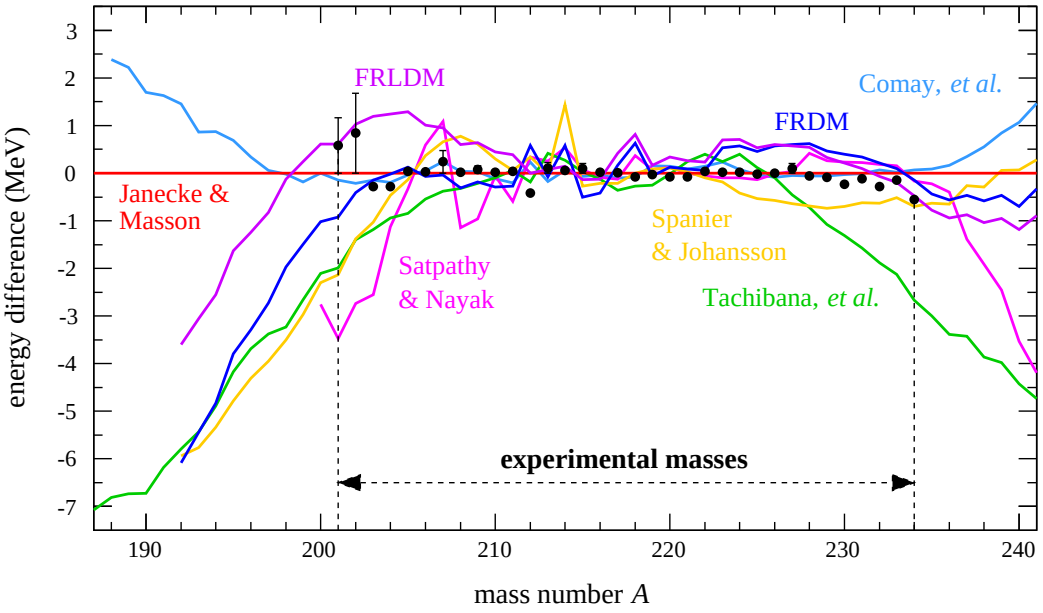

Fig. 1.1 Ground-state masses (energies) for radium isotopes ($Z = 88$) predicted by several theoretical models (colored lines). We selected the model of Janecke & Masson as the reference one and show the difference between masses predicted by other models and this model. We also show the difference between experimental masses (black full circles) and the ones according to the model of Janecke & Masson. Experimental values were taken from Ref. [Wan12] except for the values for ^{201,202}Ra, which are from our data and will be discussed later in this work. Theoretical values were taken from Ref. [lbnl].

ferent excitation energies are associated with different deformations. A rearrangement of only a few nucleons at the Fermi surface can result in a different nuclear shape [And00].

- A considerable *change in shape* of nuclei in this region is also present when moving from one isotope to another. Adding just one nucleon into the nucleus can completely change its deformation. For example, calculations for the ground-state quadrupole deformation based on the finite-range droplet macroscopic model and the folded-Yukawa single-particle microscopic model [Möl95] predict ^{194}Po and neighboring heavier polonium isotopes to be nearly spherical; ^{193}Po and ^{192}Po to have strongly deformed oblate shape; ^{191}Po and lighter polonium isotopes to have, on the contrary, strongly deformed prolate shape. This effect is illustrated in Fig. 1.2 showing ground-state quadrupole deformations of neutron-deficient isotopes in the vicinity of lead (proton shell closure $Z = 82$).

- *Beta-delayed fission* (βDF) is a two-step process. Firstly a nucleus undergoes β decay and then a daughter nucleus immediately fissions. This can occur when excited energy of a nucleus after the β decay is higher

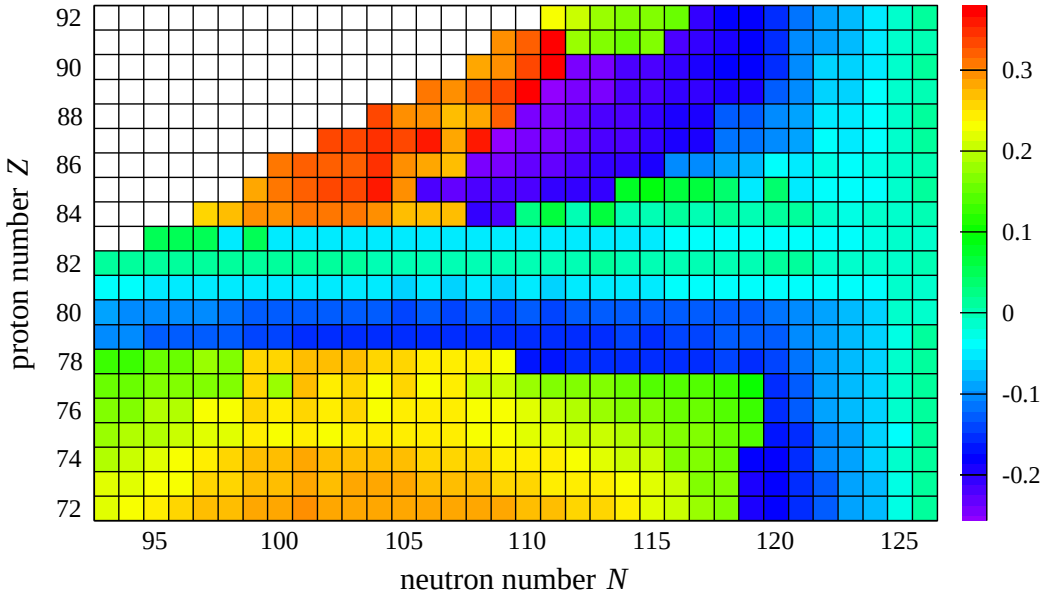

Fig. 1.2 Nuclear ground-state quadrupole deformation β_2 [Möl95] for nuclei in the vicinity of the proton shell closure $Z = 82$. The color scale corresponds to the various nuclear shapes: blue color represents an oblate shape and red color represents a prolate shape. Large changes in deformation from prolate ($\beta_2 > 0$) to oblate ($\beta_2 < 0$) shape can be seen between neighboring isotopes.

than or comparable with its fission barrier. The process of βDF extends the regions of the nuclide chart where low-energy fission can be studied.

In this Thesis, we focused on very neutron-deficient isotopes of radium, $^{201-203}$Ra ($Z = 88$), and francium, $^{197-202}$Fr ($Z = 87$). Both elements, radium and francium, were discovered in France; radium by M. Skłodowska-Curie and P. Curie in 1898 and francium by M.C. Perey in 1939. Since that time more than 30 isotopes have been identified for each of these elements and none of them is stable. The longest-living francium isotope is ^{223}Fr with the half-life of 22 minutes and the longest-living radium isotope is ^{226}Ra with the half-life of 1600 years.

As experimental techniques improve, the chains of known isotopes for each element are extending. The lightest radium isotope synthesized until now is ^{201}Ra; one nucleus of this isotope was observed nine years ago [Uus05]. In this work we report on the detection of another one ^{201}Ra nucleus. We also report on the detection of the lightest francium nucleus, ^{197}Fr, again with only one detected event. For some other isotopes discussed in this work, previously published data were based on low statistics as well. For example, the detection of only two ^{202}Ra nuclei was reported (each of them was measured in a different experiment [Lei96, Uus05]) and only five decay chains of ^{199}Fr were registered [Tag99]. One cannot avoid sizable uncertainties of measurements for such a small number of

detected events. However, detection techniques and data-acquisition systems continuously improve and available beam intensities increase. This progress enabled us to refine known decay properties of studied nuclides and to detect new isomeric states and transitions. We analyzed the experimental data by methods of α-, γ- and α-γ decay spectroscopy. These methods are very powerful tools, which reveal information helping to localize nuclear excited levels and determine their spins and parities, evaluate nuclear masses, Q values, fission-barrier heights, etc.

In the vicinity of studied nuclides, the energies of a number of excited single-particle levels within a given isotopic chain decrease when going towards the neutron mid-shell ($N = 104$). As a consequence, several single-particle levels, that may correspond to a different deformation, are located very close to the Fermi surface in the lightest nuclides. It has been proposed that the ground state for most of the neutron-deficient odd-A bismuth ($Z = 83$) and astatine ($Z = 85$) isotopes is related to a $\pi h_{9/2}$ spherical configuration (e.g., Refs. [Coe85, Smi99]). It has also been suggested that this ground state coexists with states related to a proton excitation to the $i_{13/2}$ orbital or a proton hole in the $s_{1/2}$ orbital, giving rise to an oblate deformation (e.g., Ref. [And04a]).

Recent experiments, aimed at a detailed investigation of the light odd-A francium isotopes ($Z = 87$), indicate the existence of coexisting shapes in these nuclides as well. An intruder $1/2^+$ state was identified in ^{201,203}Fr using α-decay spectroscopy [Uus05]. Isomeric $1/2^+$ and $13/2^+$ states were observed in ^{203}Fr [Jak13] and ^{205}Fr [Jak12] using prompt in-beam γ-ray, delayed γ-ray and electron spectroscopy, in addition to α-decay studies. Both the $1/2^+$ and $13/2^+$ states are assumed to possess oblate deformations and to coexist with the spherical $9/2^-$ ground state [Uus05, Jak13, Jak12].

For the even-even nuclides, coexisting structures were also seen in light polonium ($Z = 84$) (e.g., Ref. [Hel99]) and radon ($Z = 86$) (e.g., Ref. [Dob02]) isotopes. This effect can be also expected in radium ($Z = 88$) isotopes, but there is presently not much experimental information available.

In this Thesis, we present results from two experiments aimed at decay studies of $^{197-202}$Fr and $^{201-203}$Ra produced at the velocity filter SHIP. Goals of the Thesis are listed in *Chapter 2*. In *Chapter 3* we report on a physical background including nuclear decay modes, fusion-evaporation reactions and nuclear shapes. *Chapter 4* contains a description of an experimental setup used in measurements, a process of calibration, data analysis and methods of α- and α-γ decay spectroscopy. In *Chapter 5* we present experimental results and discussions for individual isotopes. The Chapter is divided into two parts: The first one includes the $^{201-203}$Ra and $^{200-202}$Fr isotopes produced in the reactions ^{56}Fe + ^{147,149}Sm. The second one includes the isotopes $^{197-199}$Fr produced in the

reaction $^{60}\mathrm{Ni} + ^{141}\mathrm{Pr}$. Results are summarized in *Chapter 6*. We note that all spins and parities attributed to nuclear energy levels in this Thesis are tentative. For simplicity we do not put tentative spins and parities in parentheses in the text, but we keep them in the figures. The Thesis has two Appendices. *Appendix A* contains tabular summary of all spectroscopic results obtained in this work. In *Appendix B* we report on GEANT 4 simulations of the α decay of $^{253}\mathrm{No}$.

Chapter 2

Goals of the Thesis

A subject of this Thesis is the investigation of decay properties of neutron-deficient radium and francium isotopes using the methods of α- and γ-decay spectroscopy. Data for these isotopes were collected in two experiments performed at the velocity filter SHIP at GSI in Darmstadt applying the fusion-evaporation reactions $^{56}\mathrm{Fe} + {}^{147,149}\mathrm{Sm}$ and $^{60}\mathrm{Ni} + {}^{141}\mathrm{Pr}$.

Specific goals of the Thesis are:

In the reactions $^{56}\mathrm{Fe} + {}^{147,149}\mathrm{Sm}$:

- Investigation of decay properties of the $^{201-203}$Ra and $^{200-202}$Fr isotopes. For some of these nuclides (especially radium isotopes) only very limited information has been known until now. Furthermore, there is a discrepancy for some published data (e.g., for ^{202}Ra). Results of our measurements should bring more details about decay patterns of mentioned isotopes.
- Search for the decay of a new isotope ^{200}Ra in the reaction $^{56}\mathrm{Fe} + {}^{147}\mathrm{Sm}$.

In the reaction $^{60}\mathrm{Ni} + {}^{141}\mathrm{Pr}$:

- Investigation of decay properties of the $^{198-199}$Fr isotopes. To our knowledge, there has been no published experimental information on decays of ^{198}Fr prior to our study, and the detection of only five decay chains of ^{199}Fr was reported [Tag99].
- Search for the decay of a new isotope ^{197}Fr.

Chapter 3

Physical background

3.1 Nuclear decay modes

3.1.1 α decay

In the α-decay process a decaying nucleus emits an α particle — a helium nucleus ${}^{4}_{2}He$. One of the main reasons why exactly the helium nucleus is emitted is its relatively high binding energy — 28.3 MeV. Thus, it is energetically more favorable for the nucleus to emit the α particle rather than other combination of nucleons. A process of the spontaneous α-particle emission can be written as

$$ {}^{A}_{Z}X_{N} \rightarrow {}^{A-4}_{Z-2}Y_{N-2} + {}^{4}_{2}He_{2}. \tag{3.1} $$

This process is possible only if the sum of binding energies (B) of the final system is greater than the binding energy of the initial nucleus. The difference between binding energies of the final and initial system, i.e. the Q value of the α decay (Q_α), can be written as:

$$ Q_\alpha = B(Z-2, A-2) + B(\alpha) - B(Z, A). \tag{3.2} $$

A typical energy range of emitted α particles is $(4-9)$ MeV. The kinetic energy available for the α particle (and the recoiling nucleus) comes from the mass decrease of the system after the radioactive disintegration. Using kinetic energies (T) and masses (M) of the parent (P) and daughter (D) nuclei we can express the Q_α value as:

$$ Q_\alpha = M_P c^2 - (M_D c^2 + M_\alpha c^2) = T_\alpha + T_D. \tag{3.3} $$

With high accuracy, the α decay can be considered as a non-relativistic process. From Eq. 3.3, considering the law of conservation of linear momentum, $|\vec{p}_\alpha| = |\vec{p}_D|$, we can find the relation between the α-particle kinetic energy and the Q

value of the decay:

$$Q_\alpha = \frac{1}{2}M_\alpha v_\alpha^2 + \frac{1}{2}M_D v_D^2 = \frac{1}{2}M_\alpha v_\alpha^2(1 + \frac{M_\alpha}{M_D}),$$
$$Q_\alpha \approx T_\alpha \frac{A}{A-4}. \tag{3.4}$$

Eq. 3.4 shows that most of the α-decay kinetic energy is carried by the α particle and only a small amount is taken by the recoiling nucleus. For example, for an α-decaying nucleus consisting of 200 nucleons with Q_α value of 7 MeV, the kinetic energy of the emitted α particle would be 6.86 MeV and the kinetic energy of the recoiling nucleus would only be remaining 140 keV.

The half-life of the α decay is correlated with its Q_α value. The existence of the relation between the α-decay half-life and the velocity of the emitted α particle was already considered in 1907 by E. Rutherford [Rut07]. Later in 1911 H. Geiger and J.M. Nuttall showed that there is a linear dependence between logarithms of the decay constant and the range of the α particle [Gei11]. Nowadays, this dependence is known as the Geiger-Nuttall law and can be written as

$$\log T_{1/2} = \frac{a(Z)}{\sqrt{Q_\alpha}} + b(Z), \tag{3.5}$$

where $a(Z)$ and $b(Z)$ are constants, which vary for each isotopic series. While Q value alters from nucleus to nucleus in the range of a few MeV, half-lives vary in the range of several orders of magnitude. The differences are significant even between isotopes within the same element. For example, for thorium, the limiting cases are ^{232}Th with $T_{1/2} = 1.4 \times 10^{10}$ years, $Q_\alpha = 4.08$ MeV and ^{218}Th with $T_{1/2} = 1.0 \times 10^{-7}$ s, $Q_\alpha = 9.85$ MeV [Kra88].

Another factor influencing the α-decay half-life is the difference between angular momenta of the parent (I_i) and daughter (I_f) nucleus. The α particle is composed of two protons and two neutrons. All four nucleons are arranged in the way that the total spin of the α particle is zero. That is the reason why in the α-decay process the angular momentum carried by the α particle has purely orbital character and can vary between $|I_i - I_f|$ and $|I_i + I_f|$. The parity change related to the α-particle emission can be written as: $\pi_i = \pi_f(-1)^{l_\alpha}$, where π_i and π_f is the parity of the initial and final state, respectively, and l_α is the angular momentum carried by the α particle. This results in the selection rule which respects the parity conservation: if the parities of the initial and final state are equal, l_α must be even and if the parities of the initial and final state are different, l_α must be odd [Kra88].

One of the possible explanations of the relation between the α-decay energy and half-life is quantum-mechanical theory of the α-particle emission suggested by G. Gamow [Gam28] in 1928 and independently by R.W. Gurney and E.U.

Condon [Gur28] in the same year. Following this theory, the α particle is formed within the parent nucleus before its disintegration. Considering only the classical mechanics, α particle has not enough energy to escape from the nucleus surrounded by the Coulomb barrier (B_C). From a quantum-mechanical point of view there is a certain probability of tunneling through this barrier even if $E_\alpha < B_C$.

The α transition favors connecting states with the same configuration. Such transitions are called unhindered. For example, α decays of even-even isotopes connecting 0^+ states in parent and daughter nuclei are usually unhindered. The increasing difference between configurations of the states connected by the α transition hampers the α-particle emission. The measure of suppression is expressed by a hindrance factor of the decay.

The hindrance factor can be calculated as the ratio of the experimental half-life ($T_{1/2,exp}$) for a given α transition and the expected partial α-decay half-life ($T_{1/2,theor}$) for an unhindered decay:

$$\mathrm{HF} = \frac{T_{1/2,exp}}{T_{1/2,theor}}. \tag{3.6}$$

There are equations for the calculation of the expected partial α-decay half-life of α emitters for unhindered decays, for example, a semi-empirical formula proposed by D.N. Poenaru, *et al.* [Poe80]:

$$\log T_{1/2} = (B_1 + B_2 y + B_3 z + B_4 y^2 + B_5 yz + B_6 z^2)\frac{K_S}{\ln 10} - 20.446, \tag{3.7}$$

where y and z are variables describing the relative placement of N and Z of the decaying nucleus between neutron and proton shell closures. Parameters $B_1 - B_6$ are obtained from the fit to experimental data. K_s is the coefficient depending on Q value, A and Z of nuclei included in the α-decay process. The relationship 3.7 is based on a fission theory of the α decay and takes into account the influence of shell effects. With increasing number of known α emitters the fit parameters are being improved in order to reproduce the experimental results better. The latest set of fit parameters $B_1 - B_6$ was presented particularly for even-even, even-odd, odd-even and odd-odd nuclei [Poe06].

A half-life for a cluster and α radioactivity can be calculated according to a relation derived by D.N. Poenaru, *et al.* [Poe06]:

$$\log T_{1/2} = -\log P_S - 22.169 + 0.598(A_e - 1), \tag{3.8}$$

where A_e is the mass number of an emitted cluster ($A_e = 4$ for an α particle) and P_S is the quantum penetrability of the external potential barrier. P_S is a function of Q value, Z and A of the emitted cluster and the daughter nucleus. This method is based on an assumption that a preformation probability of a cluster (including an α particle) at the nuclear surface in first approximation

only depends on the mass of the emitted cluster.

Another example of a simple formula for the calculation of half-lives of α decays as well as cluster decays was presented by C. Qi, *et al.* [Qi09]:

$$\log T_{1/2} = a\chi' + b\rho' + c, \tag{3.9}$$

where coefficients a, b and c are determined from experimental data fitting. χ' and ρ' depend on Q value, Z and A of particles included in the decay process. The Geiger-Nuttall law is a special case of Eq. 3.9. Unlike the Geiger-Nuttall law, the formula 3.9 is valid for all isotopic series.

Another method for the evaluation of an α-decay hindrance factor is a comparison of reduced α-decay width (δ_α^2) for a given α transition with δ_α^2 for unhindered α transitions in neighboring (often even-even) isotopes. Reduced α-decay width expresses the probability of α-particle emission and can be calculated using the procedure introduced by J.O. Rasmussen [Ras59]. Nuclides with 'magic' number of protons or neutrons have smaller δ_α^2 compared to their neighbors due to increased stability of shell closures. The reduced α-decay width is expressed by the equation [Ras59]:

$$\delta_\alpha^2 = \frac{\lambda h}{P}, \tag{3.10}$$

where λ denotes the decay constant, h is Planck's constant and P is the barrier penetration factor. Reduced α-decay width is in energy units (MeV).

In Sections 5.1 and 5.2 describing experimental results, we evaluated HFs for observed α transitions using the method of comparison of reduced α-decay widths (see the previous paragraph). As the reduced α-decay width according to Eq. 3.10 depends on the orbital angular momentum of the emitted α particle [Ras59] (which is included in the factor P), we have to consider the difference between spins of the initial and final state ΔL. We assumed $\Delta L = 0$ in the calculation of δ_α^2 in this work. In Section 5.3, we compare HFs calculated using several approaches (Eqs. 3.7, 3.8, and 3.9).

3.1.2 β decay

In the β-decay process a nucleus increases its stability by converting one neutron into proton (β^- decay) or vice versa (β^+ decay). The conversion is accompanied by the emission of an electron and antineutrino or a positron and neutrino:

$$\beta^- \text{ decay:} \qquad n \rightarrow p + e^- + \bar{\nu}, \tag{3.11}$$

$$\beta^+ \text{ decay:} \qquad p \rightarrow n + e^+ + \nu. \tag{3.12}$$

The competing process to the β^+ decay described by Eq. 3.12 is the electron capture (EC). In this process, one of the orbital electrons is captured by a proton from the atomic nucleus, thereby the proton is transformed into a neutron and

a neutrino is emitted:

$$EC: \qquad p + e^- \rightarrow n + \nu. \tag{3.13}$$

Q value of the β decay equals the sum of kinetic energies of the emitted electron (or positron) and the antineutrino (or neutrino). This is equivalent to the difference between the mass of the parent nucleus and the total mass of the daughter nucleus plus one electron:

$$Q_{\beta^-} = T_{e^-} + T_{\bar{\nu}} = M_P c^2 - (M_D c^2 + M_e c^2), \tag{3.14}$$

$$Q_{\beta^+} = T_{e^+} + T_{\nu} = M_P c^2 - (M_D c^2 + M_e c^2). \tag{3.15}$$

In the EC process only a neutrino is emitted, and thus the Q value equals the kinetic energy of the neutrino. This is equivalent to the mass difference between the parent nucleus plus one electron and the daughter nucleus. The electron mass has to be corrected for the binding energy of the n-shell (B_n), from which the electron was captured by the nucleus:

$$Q_{EC} = T_{\nu} = M_P c^2 + M_e c^2 - B_n - M_D c^2. \tag{3.16}$$

The above formulas for Q values (3.14, 3.15, 3.16) refer to β decays between ground states of parent and daughter nuclei. If the daughter nucleus is in an excited state after the β decay, the corresponding Q value of the decay is lower than the Q value between ground states by the excitation energy of the daughter nucleus.

After the β decay, if an excitation energy of a daughter nucleus is higher than the nucleon separation energy, the daughter nucleus can be unstable against one- or more-nucleon emission. Nucleons are emitted with the half-life of the β decay, as the emission occurs rapidly after the β decay. The process is called 'β-delayed particle emission'. When the excitation energy of the daughter nucleus is comparable with its fission barrier, a fission process can follow the β decay, which is called 'β-delayed fission'.

3.1.3 Internal transition

Most of radioactive decays populate excited levels in daughter nuclei. Although a small amount of these excited nuclei undergo further radioactive disintegration, most of them are promptly deexcited by an internal transition. Internal transition can proceed through a γ-ray emission (γ decay) or an internal-conversion emission. Firstly we briefly describe a process of the γ-ray emission and then a process of internal conversion.

γ decay

In the process of deexcitation by γ rays, one or more photons can be emitted. Their typical energy range is from several keV to several MeV. The deexcitation

may cause a re-arrangement of nucleons and lowers the total energy of the nucleus:

$$M_0^* c^2 = M_0 c^2 + E_\gamma + T_0, \tag{3.17}$$

where M_0 denotes a mass of the nucleus, T_0 is a recoil kinetic energy of the nucleus and E_γ is an energy of emitted γ ray(s). A linear-momentum conservation requires the sum of the momenta of the recoiling nucleus $\vec{p}_0$ and emitted photon(s) $\vec{p}_\gamma$ to be zero: $\vec{p}_0 + \vec{p}_\gamma = 0$. Considering this condition and the fact that the recoiling nucleus is with high accuracy non-relativistic, we can write the relation between T_0 and E_γ [Hey99]:

$$T_0 = \frac{p_0^2}{2M_0} = \frac{p_0^2 c^2}{2M_0 c^2} = \frac{E_\gamma^2}{2M_0 c^2}. \tag{3.18}$$

The equation 3.18 shows that the recoil kinetic energy of the nucleus is relatively small. If a 1-MeV photon is emitted from a nucleus consisting of 50 nucleons (which equals $\sim 50\,\mathrm{GeV}$ of mass), T_0 is only $\sim 10\,\mathrm{eV}$.

Each nuclear state is characterized by its spin and parity. Spins and parities of the initial and final state determine the possible angular momentum (multipolarity) of the γ transition (ΔL) between these states. A half-life of a single-particle electric or magnetic transition with multipolarity L (EL or ML, respectively) is described by the Weisskopf equations [Fir96]:

$$T_{1/2}(EL) \cong \ln 2 \frac{L((2L+1)!!)^2 \hbar}{2(L+1)e^2 R^{2L}} \left(\frac{3+L}{3}\right)^2 \left(\frac{\hbar c}{E_\gamma}\right)^{2L+1}, \tag{3.19}$$

$$T_{1/2}(ML) \cong \ln 2 \frac{L((2L+1)!!)^2 \hbar}{80(L+1)\mu_N^2 R^{2L-2}} \left(\frac{3+L}{3}\right)^2 \left(\frac{\hbar c}{E_\gamma}\right)^{2L+1}. \tag{3.20}$$

In order to obtain $T_{1/2}$ in seconds, the following constants and units are used: $\hbar = 6.58212 \times 10^{-19}\,\mathrm{keV\,s}$, $e^2 = 1.440 \times 10^{-10}\,\mathrm{keV\,cm}$, $R = R_0 A^{1/3}$ in cm ($R_0 = 1.2 \times 10^{-13}\,\mathrm{cm}$), $\hbar\, c = 197.327 \times 10^{-10}\,\mathrm{keV\,cm}$, E_γ is in keV, $\mu_N^2 = 1.5922 \times 10^{-38}\,\mathrm{keV\,cm^3}$.

The equations 3.19 and 3.20 represent some reference values for γ-decay rates. Generally, transitions with lower multipolarities are favored compared to higher multipolarities. Increasing L by one unit decreases the transition probability by several orders of magnitude. At a given multipolarity and energy the electric transition is preferred compared to the magnetic transition by a factor of about 2 orders of magnitude in medium and heavy nuclei [Kra88]. The ratio (B) of a single-particle half-life estimated using Weisskopf relations 3.19 and 3.20 ($T_{1/2\,SP}$) to an experimental half-life ($T_{1/2\,exp}$) gives the transition probability in Weisskopf units (W.u.) [Fir96]:

$$B(EL;ML) = \frac{T_{1/2}(EL;ML)_{SP}}{T_{1/2}(EL;ML)_{exp}}\ \text{W.u.}. \tag{3.21}$$

Internal conversion

Each internal transition has a certain probability to undergo internal conversion. In this process, a nucleus interacts directly with an electron from an atomic orbital. The electron gains the excitation energy of the nucleus and is emitted from the atom, if the excitation energy exceeds the binding energy of the electron. The kinetic energy of the electron T_e is given by the difference between the transition energy ΔE and the electron binding energy B:

$$T_e = \Delta E - B. \tag{3.22}$$

A vacancy left in the atomic orbital by the emitted electron is immediately filled by an electron from the higher atomic shell. The difference between binding energies of electrons causing initial and final vacancy is released as the emission of X-rays or Auger electrons. Both have characteristic energies for each element. A relative intensity of the γ-ray emission compared to the conversion-electron emission is described by the conversion coefficient α_{IC}:

$$\alpha_{IC} = \frac{n_{CE}}{n_\gamma}, \tag{3.23}$$

where n_{CE} denotes the number of emitted conversion electrons and n_γ the number of emitted γ rays. The total conversion coefficient is the sum of conversion coefficients for major shells and they are sums of conversion coefficients for subshells. Internal conversion can only occur on that shells, where the electron binding energy is smaller than the transition energy.

The internal-conversion probability depends on several factors. Conversion coefficient decreases as a function of increasing transition energy, decreasing nuclear mass and decreasing transition multipolarity. Magnetic transitions are more likely to be converted than electric ones. Theoretical conversion coefficients can be evaluated using a generic tool $BrIcc$ [Kib08].

The half-life of the single-particle transition $T_{1/2\,SP}$ calculated using Weisskopf equations 3.19 and 3.20 is not corrected for internal conversion. We can simply derive the relation between the total half-life of the internal transition $T_{1/2}$ (including both γ-ray and conversion-electron emission) and $T_{1/2\,SP}$. The ratio of n_{CE}/n_γ from Eq. 3.23 is equal to the ratio of probabilities of the CE emission and γ-ray emission $\lambda_{CE}/\lambda_\gamma$. Substituting this into Eq. 3.23 we have $\lambda_{CE} = \alpha_{IC}\lambda_\gamma$. This leads to the total probability for the given internal transition λ:

$$\lambda = \lambda_\gamma + \lambda_{CE} = \lambda_\gamma(1 + \alpha_{IC}). \tag{3.24}$$

Using Eq. 3.24 we can write the relation between $T_{1/2}$ of the internal transition and $T_{1/2\,SP}$:

$$T_{1/2} = \frac{\ln 2}{\lambda} = \frac{\ln 2}{\lambda_\gamma(1 + \alpha_{IC})} = \frac{T_{1/2\,SP}}{1 + \alpha_{IC}}. \tag{3.25}$$

The angular-momentum conservation law forbids the emission of a single

photon for transition between two spin-zero states of the same parity. The conversion coefficients for such $E0$ transition is not defined. These transitions proceed mostly through the conversion-electron emission. When transition energy exceeds $2m_ec^2$, nucleus can be deexcited by the creation of the electron–positron pair. The third possibility is the emission of two photons. However, this is a higher order process with a relative probability of $\sim(10^{-3}-10^{-4})$ and for practical purposes can be neglected [Kib08].

3.2 Fusion-evaporation reactions

Isotopes studied in this work were produced in fusion-evaporation reactions. In these reactions, an incident particle (projectile) is fully absorbed by a target nucleus resulting in a formation of a compound nucleus (CN). Then the CN evaporates particles and γ rays. The remaining nucleus is called the evaporation residue (ER). The fusion-evaporation reaction mechanism can be described as a two-step process:

$$a + A \rightarrow C^* \rightarrow b + B, \tag{3.26}$$

where a means projectile, A is target, C^* stands for the compound nucleus, b are evaporated particles and B is the evaporation residue. The process of the fusion-evaporation reaction is illustrated schematically in Fig. 3.1.

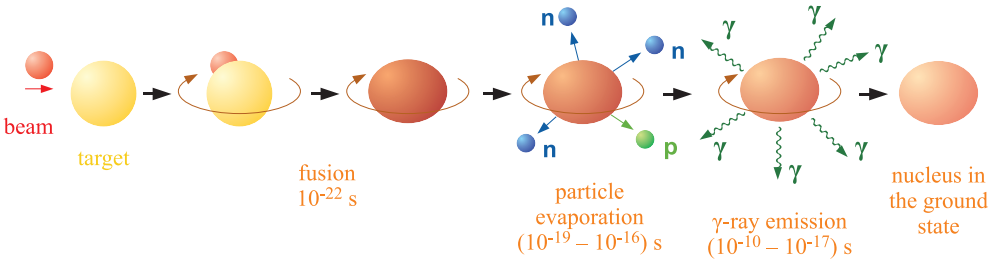

Fig. 3.1 Schematic drawing of the fusion-evaporation reaction.

The CN formed in heavy-ion reactions is usually in a highly-excited state with a typical excitation energy of several tens of MeV. That is enough excitation energy for the emission (called 'evaporation') of particles — mainly neutrons, protons and α particles (see Fig. 3.1). CN loses roughly 10 MeV of its excitation energy evaporating one nucleon. Generally, because the Coulomb barrier does not affect neutrons, they are more likely to be evaporated compared to protons. However, for a CN at the neutron-deficient side of the nuclide chart, the probability of proton evaporation increases. At a given excitation energy several evaporation channels can be active (with corresponding probabilities),

e.g., the emission of one proton plus one neutron (pn evaporation channel) can compete with the two-neutron emission ($2n$ evaporation channel). When the excitation energy of the CN is not sufficient for the evaporation for four independent nucleons, the α particle can still be evaporated due to its high binging energy.

After the evaporation of particles, the excitation energy of the evaporation residue is lower than an energy threshold for further particle evaporation, and the deexcitation proceeds through the emission of γ rays. Afterwards, the ER in its ground (or isomeric) state can live relatively long time until its radioactive disintegration.

We note that the *complete fusion* means that the projectile and target nucleus reach the fully-equilibrated compound-nucleus state. The process competing with the formation of the CN is the *quasi-fission*. In this process, the interacting system $a + A$ undergoes fission before the compound nucleus C is formed. We can detect fission-like fragments from this process.

The interaction probability between a projectile a and a target nucleus A is expressed by the reaction cross section. The cross section $\sigma(a, b)$ of the reaction $a + A \rightarrow b + B$ can be described as:

$$\sigma(a, b) = \sigma_C(a, A)\sigma(b), \tag{3.27}$$

where $\sigma_C(a, A)$ is the fusion probability of a and A, and $\sigma(b)$ is the probability for the evaporation of particle(s) b from the compound nucleus C.

Time that projectile needs to traverse the nucleus is $\sim(10^{-22} - 10^{-21})$ s. The CN formation takes several orders of magnitude longer, $\sim(10^{-19} - 10^{-16})$ s, because of time needed for re-sharing and re-distribution of the incident energy. As a result of relatively long life-time of the intermediate CN state, the process of its disintegration is independent on the reaction entrance channel $a + A$. This fact was experimentally confirmed, e.g., by the formation of the compound nucleus ^{64}Zn in the reactions $\alpha + {}^{60}$Ni and p $+ {}^{63}$Cu [Gho50]. The ratio of cross-sections $\sigma(\alpha, \mathrm{n}) : \sigma(\alpha, 2\mathrm{n}) : \sigma(\alpha, \mathrm{pn})$ in the reaction with the ^{60}Ni target was in agreement with the ratio of cross sections for the same exit channels $\sigma(\mathrm{p}, \mathrm{n}) : \sigma(\mathrm{p}, 2\mathrm{n}) : \sigma(\mathrm{p}, \mathrm{pn})$ in the reaction with the ^{63}Cu target.

At low excitation energies of the CN, the cross section for the production of a particular ER is limited by the fusion barrier between the projectile and target nucleus. At high excitation energies of the CN, the fission barrier is the limiting factor for the production of the certain ER. Thus, for the production of a given ER, we have to fulfill two contradictory demands: (a) a beam (projectile) energy must be high enough to overcome the Coulomb barrier between the projectile and target nucleus and (b) an excitation energy of the formed CN must not be too high to prevent its fission. Fulfilling these requirements we can find the

optimal reaction and beam energy for the production of a certain ER.

The dependence of a cross section for the production of a given ER on excitation energy of the CN is called an excitation function. An example of a systematic study of excitation functions for bismuth and polonium isotopes produced in fusion-evaporation reactions is given in Ref. [And05]. In reactions described in this work, the production cross sections were in the region of picobarns and nanobarns (see Sect. 5.4).

3.3 Shape of the nucleus

The shell model originally assumed a shperical shape of the nucleus. However, it was shown that some nuclei have a shape corresponding to a spheroid rather than a sphere [Rai50, Boh51]. Nuclear shape changes from spherical for nuclei with magic number of protons and/or neutrons to more deformed when moving further from closed shells. The effect of shell closures on the shape of nuclear ground state is illustrated in Fig. 3.2. Energies of single-particle levels and gaps between them change as a function of nuclear deformation.

Nuclear shapes can be different not only for different nuclides, but also for different states within one nuclide. It is supposed that this phenomenon, called *shape coexistence*, occurs in nuclei all over the nuclide chart (see, for example, reviews [Ham85, Hey83, Woo92, Hey11]). However, main regions occur near spherical shells or subshells with the most extensive demonstration in neutron-deficient isotopes around the shell closure $Z = 82$ [Hey11]. An interesting example of shape coexistence is the isotope ^{186}Pb, where spherical, oblate and prolate shapes were found to coexist [And00].

In a spherical potential, nuclear energy states are labeled as nl_j. The number n denotes the order of states with a certain l and can have integer values starting at $n = 1$. The numbers l and j represent an orbital and a total angular momentum of the level, respectively. The relation between l and j is: $j = l \pm 1/2$. For l the letters $(s(=0), p(=1), d(=2), f, g, h, i, ...$ and further alphabetically) are used similar to the description of orbital angular momenta of atomic electrons. A parity of the state is equal to $(-1)^l$. Each shell-model state l_j (e.g., $h_{9/2}$, $s_{1/2}$, ...) has a degeneracy of $(2j+1)$. It means that all $(2j+1)$ possible orientations of $\vec{j}$ are equivalent, as we can not define a symmetry axis in a spherical case. A particular level in a particular nucleus using shell-model notation can be denoted by πl_j or νl_j, where π and ν refer to proton and neutron, respectively. A number of particles (or holes) within the state can be denoted by a superscript. Positive number in the superscript refers to particles and negative number to holes. For example, $\nu f_{5/2}$ denotes one neutron in the orbital corresponding to $l = 3$ and $j = 5/2$, and $(\pi s_{1/2})^{-1}$ denotes one hole in the proton orbital corresponding to

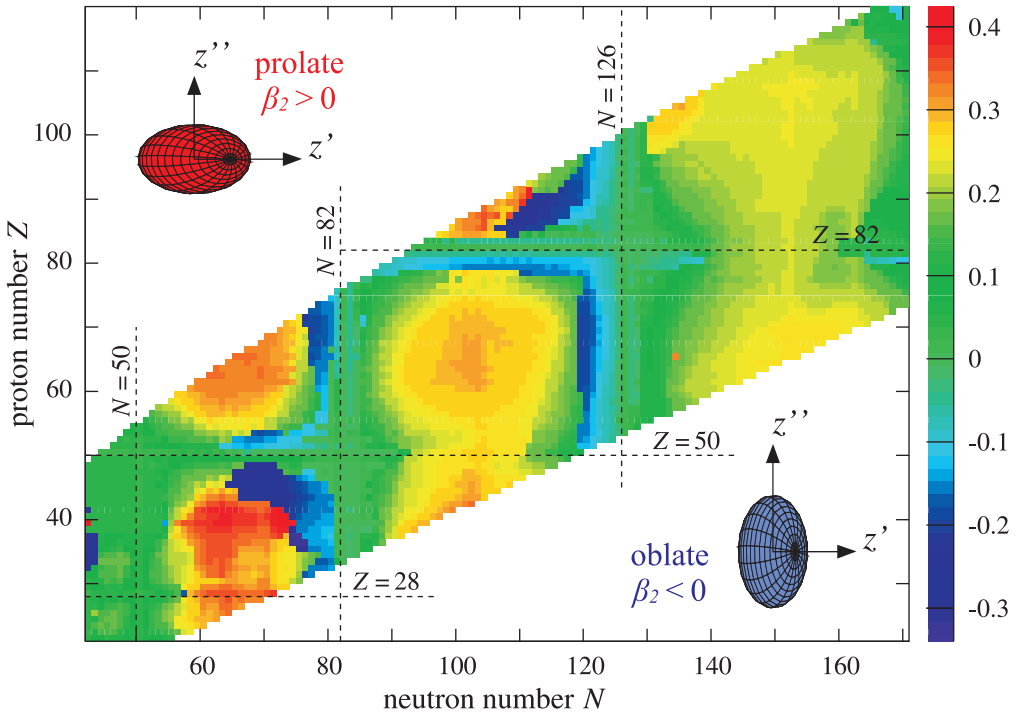

Fig. 3.2 Nuclear ground-state quadrupole deformations β_2 [Möl95] for most of the isotopes from the nuclide chart. Closed shells of protons and neutrons are denoted by dashed lines. Near the closed shells nuclei are spherical or almost spherical and moving further from closed shells nuclear shapes become deformed. The color scale represents the deformed nuclear shapes: blue color corresponds to an oblate shape and red color to a prolate shape. Corresponding deformed nuclear shapes are shown for $\beta_2 < 0$ (oblate) and $\beta_2 > 0$ (prolate). Nuclear symmetry axis and rotational axis are denoted by z' and z'', respectively.

$l = 0$ and $j = 1/2$.

In a case of axially symmetric deformed nuclei the situation is different from the spherical ones. For a single $\vec{j}$ in a deformed nucleus there are $(2j+1)$ different projections Ω on the nuclear symmetry axis. Usually a set of quantum numbers $\Omega^{\pi}[N_0, n_z, \Lambda]$ is used for a notation of single-particle levels in the deformed potential. N_0 is a quantum number denoting a major shell, i.e. the total number of oscillator quanta ($N_0 = 0, 1, 2, 3, ...$); π is a parity of the level and can be extracted from a relation $\pi = (-1)^{N_0}$; n_z is a number of oscillator quanta along the nuclear symmetry axis ($n_z = 0, 1, 2, ...$); Λ is a projection of an orbital angular momentum l on the nuclear symmetry axis. The sum of n_z and Λ is even if N_0 is even and odd if N_0 is odd. Sometimes a notation K is used instead of Ω. Usually Ω denotes the projection of the single-particle angular momentum along the nuclear symmetry axis and K denotes the projection of the total angular momentum along the nuclear symmetry axis. For low-lying states of

axially symmetric nuclei the rotational angular momentum is perpendicular to the symmetry axis, and therefore it does not contribute to K. Thus, we can substitute K for Ω [Cas90].

In a simplified way, we can imagine a motion of a nucleus to be composed of a collective and an individual-nucleon component. The situation is schematically illustrated in Fig. 3.3 for a rotating nucleus. A total angular momentum of the nucleus $\vec{I}$ is composed of an intrinsic motion of nucleons $\vec{J}$ and a collective motion of the nucleus $\vec{R}$: $\vec{I} = \vec{J} + \vec{R}$. Intrinsic motion of nucleons $\vec{J}$ is composed of total angular momenta of individual nucleons $\vec{j_1}, \vec{j_2}, \vec{j_3}$, ... However, nucleons within an even-even nucleus are paired resulting in a zero contribution to the angular momentum of the nucleus. In odd-A nuclei all but one nucleons are paired, and the intrinsic motion of the nucleus is given by one unpaired valence nucleon. In odd-odd nuclei or excited nuclei, the intrinsic motion of the nucleus is given by total angular momenta of all unpaired nucleons. For example, if a nucleus has two unpaired nucleons with total angular momenta j_1 and j_2, the final intrinsic motion of the nucleus can have values from $|j_1 - j_2|$ to $|j_1 + j_2|$ in integer steps. For the simplicity in Fig. 3.3 there is only one valence nucleon, and thus $\vec{j} = \vec{J}$. Total angular momentum of the nucleon $\vec{j}$ is the sum of an orbital angular momentum of a nucleon $\vec{l}$ and an intrinsic spin of a nucleon $\vec{s}$: $\vec{j} = \vec{l} + \vec{s}$. If Ω, Λ and Σ represent the projections of $\vec{j}$, $\vec{l}$ and $\vec{s}$, respectively, along the nuclear symmetry axis, we can write: $\Omega = \Lambda + \Sigma$. Possible values for Σ are $\pm 1/2$. Possible values for Ω are $1/2$, $3/2$, ..., j. If more valence nucleons contribute to the intrinsic motion of the nucleus $\vec{J}$, the projection of $\vec{J}$ along the symmetry axis is usually denoted by K: $K = \Omega_1 + \Omega_2 + \Omega_3 + ...$.

Each intrinsic spin of a nucleus $\vec{J}$ (with its projection K along the nuclear symmetry axis) has associated quantized rotational motion called a *rotational band*. A state with a total angular momentum of the nucleus $I = K$ is called a bandhead of the rotational band. Excited states of the rotational band have total angular momenta of $K + 1$, $K + 2$, $K + 3$, ... There is one exception: if $K = 0$, states of the rotational band only have even total angular momenta: $I = 0, 2, 4, 6, ...$ [Cas90]. As a rotational axis of the nucleus is perpendicular to the nuclear symmetry axis, each state of the rotational band has the same projection along the symmetry axis (K). Energies of rotational levels can be calculated from the relation [Kra88]:

$$E = \frac{\hbar^2}{2\mathcal{J}} I(I+1), \tag{3.28}$$

where $\mathcal{J}$ is a moment of inertia. Rotational motion can be only observed in a non-spherical nucleus. A representative of a shape of a non-spherical nucleus is a spheroid (ellipsoid of revolution). A spheroid is created by rotating an ellipse about one of its principal axes; a *prolate* shape is obtained by rotating about

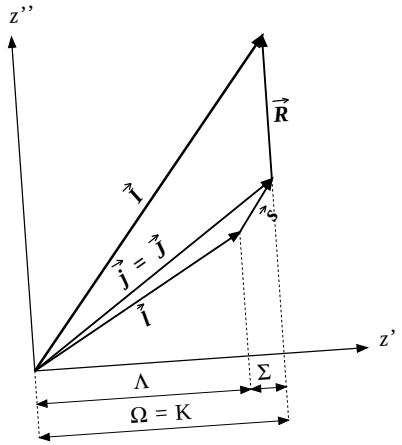

Fig. 3.3 Nuclear angular-momentum diagram for a rotating nucleus. A total angular momentum of the nucleus $\vec{I}$ is composed of an intrinsic motion of nucleons $\vec{J}$ and a collective rotational motion of the nucleus $\vec{R}$. The intrinsic motion of nucleons is in the illustrated case created by one unpaired nucleon with a total angular momentum $\vec{j}$ composed of an orbital angular momentum of the nucleon $\vec{l}$ and an intrinsic spin of the nucleon $\vec{s}$. Nuclear symmetry axis and rotational axis are denoted by z' and z'', respectively. See the text for more details

its major axis and an *oblate* shape is obtained by rotating about its minor axis (see Fig. 3.4). We can define a deformation parameter β_2, which is related to the eccentricity of an ellipse as [Kra88]:

$$\beta_2 = \frac{4}{3}\sqrt{\frac{\pi}{5}}\frac{\Delta R}{R_{av}}, \tag{3.29}$$

where ΔR is the difference between the semi-major and semi-minor axes of the ellipse and R_{av} is equal to $R_0 A^{1/3}$. A shape of the nucleus is prolate when $\beta_2 > 0$ and oblate when $\beta_2 < 0$.

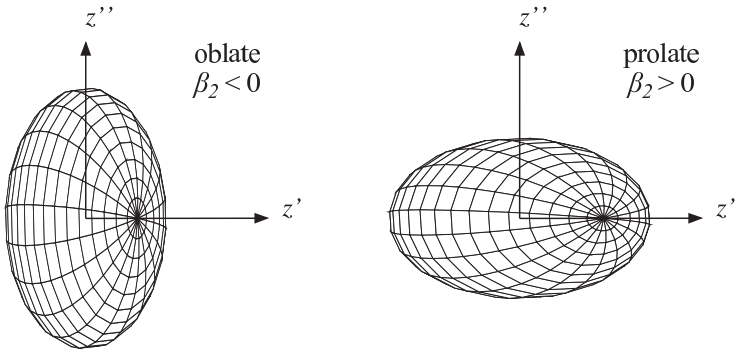

Fig. 3.4 Deformed axially symmetric nuclear shapes: *oblate* on the the left side and *prolate* on the right side. Nuclear symmetry axis and rotational axis are denoted by z' and z'', respectively.

Chapter 4

Experiment

4.1 Experimental Setup

4.1.1 SHIP

SHIP (**S**eparator for **H**eavy **I**on reaction **P**roducts) is one of the most successful facilities aimed at production and studies of heavy and superheavy elements [Mün79]. New elements with proton numbers from 107 to 112 were identified at SHIP in years $1981-1996$. Nowadays spectroscopic experiments aimed at investigation of neutron-deficient nuclei, mass measurements and nuclear-reaction studies are in progress at SHIP. Beam is provided by the UNILAC (**UNI**versal **L**inear **AC**celerator) accelerator. UNILAC can deliver beam of all stable elements up to uranium ($Z = 92$) with energies up to 20 MeV/u [Ant05]. Accuracy of the beam energy is ± 0.01 MeV/u and beam intensities can reach $3.0\,p\mu$A for $^{40}Ar^{8+}$, $1.2\,p\mu$A for $^{58}Fe^{8+}$ and $0.4\,p\mu$A for $^{82}Se^{12+}$ ($1\,p\mu\text{A} = 6.24 \times 10^{12}$ particles/s) [Hof00].

The beam is focused on a target area to a spot with a diameter of ~ 5 mm. Eight foils with a thickness of $(0.1-1.0)$ mg/cm^2 are used as targets. The target material is evaporated on a carbon backing with a thickness of $(35-60)$ μg/cm^2 and covered with another ~ 10-μg/cm^2 carbon foil to reduce radiation damage of the target material and to increase its emissivity. To increase a melting temperature of the targets, they are often made as compounds with some admixture material with high melting point [Lom02]. In our experiments, the admixture of F_3 was added to the main target materials (^{141}Pr, ^{147}Sm, ^{149}Sm). Target foils are mounted on a wheel rotating synchronously to the beam macro-structure (usually 5 ms beam on and 15 ms beam off). Another carbon foil with a thickness of $(30-60)$ μg/cm^2 is placed ~ 20 cm behind the target. The foil is used to equilibrate a charge state of reaction products, as the filter is optimized for the transmission of particles with a particular charge state, and particles with other charge states are suppressed. Reaction products are leaving the target

at different angles due to scattering in the target material and evaporation of particles. In order to focus and gather nuclei from the maximum solid angle, two electromagnetic lenses arranged as quadrupole triplets are placed at the beginning and at the end of the ion-optical system (see Fig. 4.1).

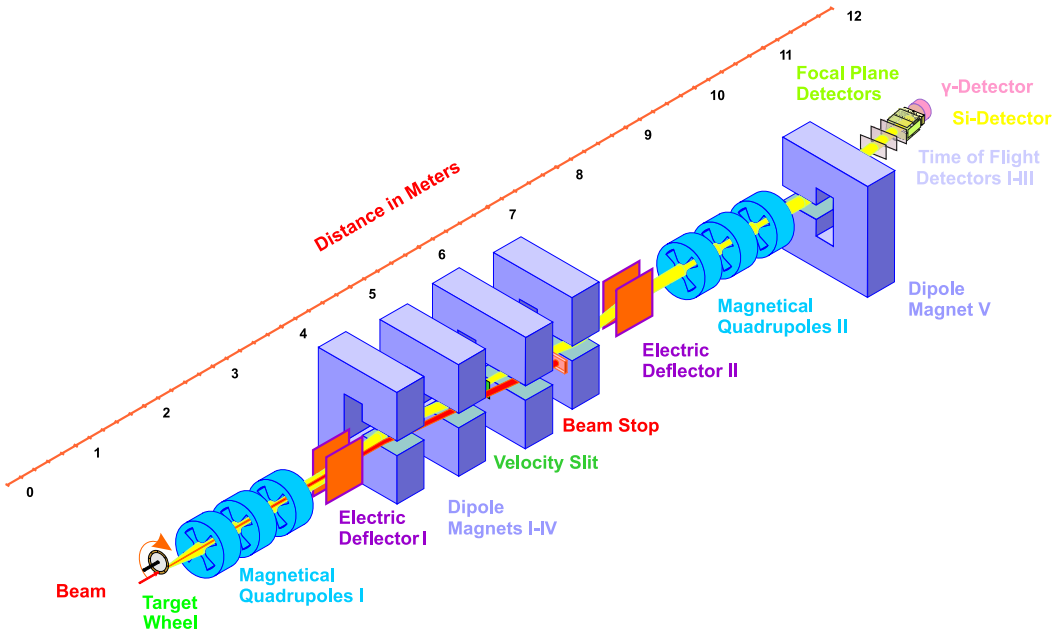

Fig. 4.1 Velocity filter SHIP.

SHIP is an electromagnetic separator designed for in-flight separation of complete-fusion reaction products. In contrast to classical Wien-filter, SHIP has separated electric and magnetic field improving its efficiency and primary-beam suppression, which can reach a factor of $10^7 - 10^{11}$. Suppression of beam particles with full energy is even some orders of magnitude higher ($10^{12} - 10^{14}$). This allows the collection of reaction products in the beam direction and measurements of isotopes with small production cross sections. Especially for heavier compound nuclei produced by light projectiles with proton number less than 36 (= krypton), background suppression is so high that there is no problem with background even for beam intensities higher than 10^{12} particles/s. High background suppression along with the short separation time (∼ microseconds) enables the investigation of unstable isotopes in neutron-deficient regions up to the heaviest nuclei ($Z > 100$). Reaction products are accepted within the angle of 3 degrees in axial direction and are effectively transmitted within ±5 % from the expected mean velocity of complete-fusion reaction products and ±10 % from the mean charge state. Transmission of SHIP is from 10 % for asymmetric reactions to 60 % for more symmetric reactions [Mün79].

The overall configuration of the filter is $QQQEMMMMEQQQ$ (see Fig. 4.1). Q means magnetic quadrupole, E is electric deflector, M is magnetic dipole. An additional magnetic dipole with deflecting angle between 0 and 15 degrees (typically 7.5 degrees) was added behind the last quadrupole triplet in 1994. It helps to reduce background in some cases [Hof00]. A main part of the separator consists of electric deflectors and magnetic dipoles. A maximum field strength of dipole magnets is 0.7 T [Mün79]. The velocity filter utilizes the different velocity between complete-fusion-reaction products and other particles (i.e. elastically scattered projectiles, scattered products of inelastic reactions like transfer reactions or incomplete fusion) for separation. The specific E/B ratio permits only particles with particular velocity to pass the filter.

4.1.2 Detectors

After separation, reaction products enter a system of detectors (see Fig. 4.2).

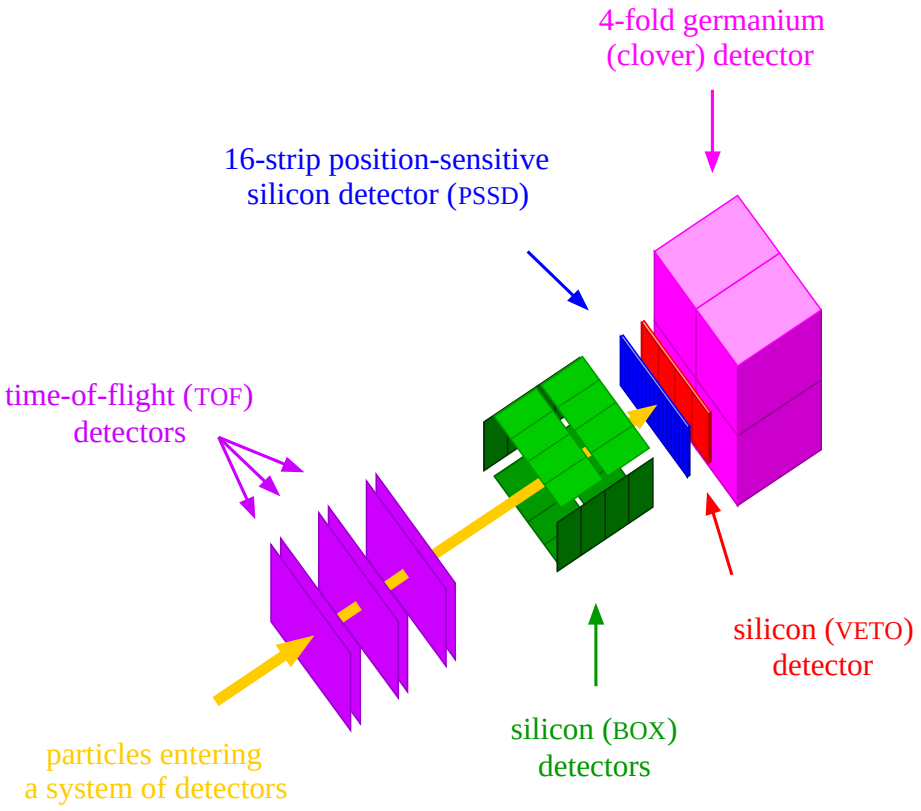

Fig. 4.2 Detection system used at SHIP.

PSSD

Studied nuclei are implanted into a 16-strip position-sensitive silicon detector (PSSD) with an active area of $(80 \times 35)\,\mathrm{mm}^2$ and a thickness of $300\,\mu$m placed at the focal plane of the separator. A resistive layer provides a position sensitivity in a vertical direction through charge distribution. A position resolution for α particles in experiments described in this work was $(0.8 - 1.0)\,$mm (FWHM), which was equivalent to a system of more than 560 single detectors with an area of $(1 \times 5)\,\mathrm{mm}^2$. A thickness of a dead layer is $11.6\,\mu\mathrm{g/cm}^2$ [Hof07].

Efficiency for the detection of full energy of α particles depends on an implantation depth of an evaporation residue (ER) and a range of α particles in silicon. Typical implantation depth of the ER is a few micrometers and the range of 7-MeV α particles in silicon is $\sim 40\,\mu$m. Assuming these values we have the geometric efficiency of $\sim 54\,\%$ for the detection of α particles with full-energy release in the PSSD. In a fission process, the efficiency for the detection of both fission fragments with full energy reaches $\sim 60\,\%$, considering the implantation depth of $(4 - 5)\,\mu$m for the ER and the range of $20\,\mu$m for fission fragments in silicon. These are typical values for heavy nuclei with total kinetic energy of fission fragments $\sim 240\,$MeV [Hof07]. Energy resolution for α particles is $\sim 30\,$keV (FWHM).

BOX detectors

Particles escaped from the PSSD to the backward direction can be detected by a system of six silicon detectors (denoted as 'BOX' in the following text) placed upstream the beam. BOX detectors are divided into 28 segments (altogether). A geometrical efficiency of the BOX system amounts 80 % of 2π [And04b]. Energy resolution for α particles measured by the PSSD + BOX system is $\sim 70\,$keV (FWHM). Compared to the PSSD the resolution of the BOX system is worse because particles registered in the BOX detectors must pass through both dead layers of the PSSD and BOX detectors.

VETO detector

Another silicon 'VETO' detector is placed behind the PSSD. It helps to recognize particles, mostly high-energy protons, which came from the separator, passed through the PSSD and were not registered by a time-of-flight system (see next paragraph). These particles are recognized by requiring coincidence signals from both PSSD and VETO detector. All the silicon detectors are cooled down to $-10\,$℃.

TOF detectors

In front of the PSSD three time-of-flight (TOF) detectors (for more details see Ref. [Šár96]) are installed giving both START and STOP signals for passing particles. The STOP signal can be taken from the PSSD as well. Each TOF detector consists of two 30-$\mu\mathrm{m/cm}^2$ thick carbon foils placed 40 mm far from

each other. When ions cross the first foil, secondary electrons are emitted. They are accelerated by a voltage of 3.8 kV applied on the second foil and deflected by a magnetic field to a microchannel plate working as an amplifier. Time resolution of TOF detectors is ~ 700 ps. In experiments described in this work the detection efficiency was 98.4 % when two TOF detectors were used and 99.4 % when three TOF detectors were used. The number of TOF detectors used in particular experiments is a compromise between a maximization of the detection efficiency and a minimization of energy losses in carbon foils.

An (anti)coincidence condition between signals from the PSSD and the TOF system allows nuclei coming from the separator to be distinguished from nuclei decaying behind the TOF system. By measuring time of flight and kinetic energy of implanted events, complete-fusion reaction products are distinguished from other implanted particles, for example, scattered projectiles or transfer-reaction products.

Clover detector
For the detection of γ rays several large-volume germanium 'clover' detectors can be placed closely behind the PSSD. They are composed of four identical crystals (Clover $1-4$). One of two Clover detectors with different volumes is usually used at SHIP: either the larger one with a diameter of 70 mm and a length of 140 mm shaped to form a block of $(124 \times 124 \times 140)\,\mathrm{mm}^3$ or the smaller one with a diameter of $(50-55)$ mm and a length of 70 mm shaped to form a block of $(102 \times 102 \times 70)\,\mathrm{mm}^3$. In experiments described in this work the smaller Clover was used. Gamma rays are measured as individual events or in a coincidence with signals from the PSSD within a time window of $5\,\mu$s. Energy resolution of germanium detectors is $\sim$(1.4-2.1) keV (FWHM). A detection efficiency amounts ~ 10 % and ~ 12 % for γ rays with $E_\gamma \approx 120$ keV for the larger and smaller detector, respectively (see Fig. 4.3).

4.2 Electronics and data analysis

During an experimental run different kinds of particles enter a system of detectors consisting of different types of detectors (see Sect. 4.1.2). They register events in a wide energy range from several keV (for example, low-energy photons) to hundreds of MeV (for example, projectiles which passed through the separator). Therefore, the electronic system used at SHIP is divided into two branches optimized for low- and high-energy events:

- In silicon detectors, a *low-energy branch* registers events up to ~ 16 MeV. This branch is optimized for α-decay measurements.

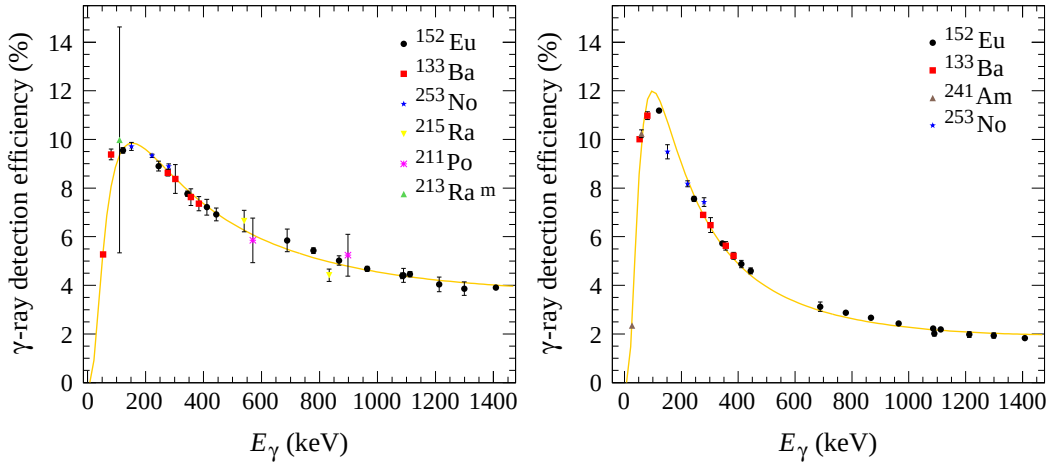

Fig. 4.3 Gamma-ray detection-efficiency curves for germanium clover detectors used at SHIP [Kal10]. One of two Clovers with different volumes of crystals is used: the larger one with a size of $(124\times124\times140)\,\mathrm{mm}^3$ (left side) or the smaller one with a size of $(102\times102\times70)\,\mathrm{mm}^3$ (right side) (see the text for more details). In experiments described in this work the smaller detector was used. For the estimation of a relative efficiency, we used external γ-ray sources: ^{152}Eu (black circles) and ^{133}Ba (red squares). For the estimation of an absolute efficiency, we used decays of nuclei implanted into the PSSD (remaining colored symbols).

In germanium crystals, events up to $\sim 1.4\,\mathrm{MeV}$ are registered in the low-energy branch.

- A *high-energy branch* registers events up to $\sim 300\,\mathrm{MeV}$ in silicon detectors. This branch is suitable for the detection of fission fragments and implanted compound nuclei from fusion-evaporation reactions.

  In germanium crystals, the high-energy branch detects events up to $\sim 8\,\mathrm{MeV}$, for example, high-energy γ rays from a fission process.

Signals in the low-energy branch are about 10 times more amplified than the ones in the high-energy branch.

Data are registered as one event within a coincidence time window of $5\,\mu$s. After this period follows a ~ 17-μs long dead time of the acquisition system. After the dead time, signals within a 5-μs long period are taken as another event. Within one event, time differences between signals from the PSSD and germanium crystals are measured with a TAC. A trigger for data acquisition in experiments described in this work was set to the signal from the PSSD. Signals from germanium crystals are delayed for about $0.8\,\mu$s, that allows to measure events in crystals preceding events in the PSSD. Times of events in germanium crystals occurring after events in the PSSD are measured up to $\sim 2.6\,\mu$s [Ant11]. Time resolution of the TAC is $\sim 300\,\mathrm{ns}$.

For each event registered in the PSSD a signal from both top and bottom of the strip is taken separately. The total energy signal is obtained as a sum of both

signals (top+bottom). By comparing the single signals from top and bottom with the total signal (top+bottom) we estimate a position within the strip where the event appeared. The information on the exact position is utilized in the search for *correlated events*. For example, we can search for a signal from the implantation of a nucleus followed by a signal of its α decay (ER-α1 correlation) or signals from several subsequent α decays of one particular nucleus (parent, daughter, granddaughter, ... decay, i.e. α1-α2-α3-... correlation). We require all the signals from correlated events to come from the same position within the same strip of the PSSD. Usually a position window of $\pm(0.4 - 0.5)$ mm is sufficient for the search of ER-α and α-α correlations. The α particles escaped from the PSSD releasing there only part of their energy have larger uncertainty of position estimation. In such cases usually a position window of ± 1.5 mm is used. However, the width of the position window can vary a bit and must be checked for each experiment particularly. In data analysis described in this work we used position windows of ± 0.5 mm for the search of ER-α and α-α correlations detected in the PSSD and ± 1.5 mm for the search of α particles detected with the PSSD + BOX system.

We used time and position correlations of implanted ERs and their subsequent α decays when identifying the studied isotopes. The time windows Δt(ER-α1), Δt(α1-α2), ... were selected as a compromise between minimizing random correlations and covering most of the true correlations. The correlation method is highly selective and enables tracking of decays of particular nuclei at rather low production cross sections (down to picobarns). For more details on the correlation method see Ref. [Hof79].

Data can be analyzed either on-line during an experimental run or off-line after the end of the experiment. In this work, we present results of the off-line analysis using the analysis code based on ROOT [Bru97] optimized for the SHIP setup implemented in the GO4 (**G**SI **O**bject **O**riented **O**n-line **O**ff-line system) framework. We modified the analysis part of the program to match particular settings used in each experiment.

4.3 Calibrations

Before the actual data analysis silicon and germanium detectors must be properly calibrated. Calibrations must be performed separately for low- and high-energy electronic branch. Several calibrations are applied:

- Detector response to the particle with a specific energy depends on a position within the strip of the PSSD, where an event occurs. In order to reduce this dependence a *ballistic calibration* of the PSSD is done for each strip. Elimination of the position dependence of energy of registered events

improves the energy resolution for each strip. For this type of calibration we use a 2nd-order polynomial as a calibration function.

- For an *energy calibration* of the PSSD we can use external α sources or α decays of nuclei implanted into the detector. However, external sources have two main disadvantages: (a) α particles from the external source lose part of their energy in the dead layer of the detector. This effect does not occur in case of studied nuclei, which are implanted into the detector. (b) In the α-decay process a part of the kinetic energy is carried by the recoiling nucleus. This contribution is not included in calibration using external sources.

  In this work we used α decays of nuclei implanted into the PSSD for the energy calibration. The α emitter selected for calibration should have similar mass as the studied isotope to guarantee similar energy distribution between the emitted α particle and the recoil of the ER. It is convenient to use even-even isotopes, because most of their α decays usually connects 0^+ ground states in parent and daughter nuclides. When the α decay populates excited levels in the daughter nucleus, the 'energy-summing effect' may occur. It means that energy of conversion electrons (and also X-rays) from the deexcitation process can be summed with the energy of the α particle. Energy summing hampers the identification of α lines in the α-decay spectrum and makes the calibration less precise. For more details on the energy-summing effect see Sect. 4.4.

  Energy calibration must be done for each strip of the PSSD. For high-energy calibration, besides α lines, we can also use projectiles with full energy, which passed through the separator. In our analysis we use a linear function for energy calibration.

- A *position calibration* of the PSSD reconciles positions measured by the low- and high-energy branch of electronics. We need the positions measured by both branches to be in line with each other, when we are analyzing, for example, ER-α correlations. A signal from the ER implantation is usually recorded by the high-energy branch, while α decays are recorded by the low-energy branch. (Actually, they are recorded by both branches, but the low-energy branch has better resolution, as it covers about 20 times smaller energy range with the same number of channels.) Differences in positions between both branches can be caused by the different amplification applied in each case. Amplification used in the low-energy branch is about 10 times lower than in the high-energy branch. The position calibration can be performed in two ways:

  - We can use events with measured position signals in both low- and high-energy branch of electronics.
  - We can use two correlated events with expected signals from the same position in the PSSD, one in the low-energy branch and the other in the high-energy branch. This method is applicable if some short-lived α emitter is produced in the measurement and is implanted into the PSSD. The ER implantation provides a position signal for the high-energy branch and its subsequent α-decay provides a position signal for the low-energy branch.

  Calibration function applied in our analysis is the 4th-order polynomial. The calibration coefficients are extracted for signals from both top and bottom of the PSSD strips.

- *An energy calibration* of germanium detectors is mostly done using the sources ^{133}Ba and ^{152}Eu emitting γ rays in a wide energy range from $\sim 50\,\mathrm{keV}$ up to $\sim 1.4\,\mathrm{MeV}$. Due to a non-linearity of germanium crystals, the calibration function is fitted by the 3rd-order polynomial.

4.4 α- and γ-decay spectroscopy

Although each α emitter emits α particles of specific energies, it may not be easy to identify them in an α-decay energy spectrum. In experiments at SHIP, various evaporation residues are produced in different evaporation channels of complete-fusion reactions. Besides the studied nuclides with proton number Z and neutron number N, isotopes with similar Z and N are also transmitted through the separator and implanted into a detector system. Alpha-decay energy spectra measured in the PSSD are then rather complex and contain peaks from different isotopes.

The alpa-decay pattern of a single isotope could also be complex, since it might populate various excited level in a daughter isotope. An example of the isotope with such a complex decay scheme is ^{255}No: 58 % of its α decays populate a 200-keV level in ^{251}Fm ($E_\alpha = 8095\,\mathrm{keV}$), 19 % of decays populate a 558-keV level ($E_\alpha = 7742\,\mathrm{keV}$), and 11 % of decays populate a 392-keV level ($E_\alpha = 7903\,\mathrm{keV}$). A few other excited levels in ^{251}Fr are populated with relative intensities of a few % each [Heß06]. The α-decay energy spectrum of such isotopes contains several α lines. From α-decay energies and partial half-lives we can extract information about hindrance factors for each transition. A measure of hindrance helps us to determine the difference in structure between the states connected by a given α transition. (Some of the methods for the evaluation of hindrance factors are described in Sect. 3.1.1.)

To test if α lines stem from the same level and populate different levels in a daughter nucleus (i.e. α-decay fine structure), we can look for γ rays coming in coincidence with α signals. The detection of a prompt α-γ coincidence means that an α decay populates a state promptly deexciting by a γ-ray emission. If the difference between Q values of two α decays equals the γ-ray energy coming in coincidence with the lower-energy α line, it is a strong indication for the α-decay fine structure. Considering a γ-ray detection efficiency and probability of the internal conversion, this test is possible only if we have at least several hundreds of counts within studied α lines.

Detailed information on nuclear energy levels can be acquired by a combination of two complementary techniques: γ-ray spectroscopy and conversion-electron spectroscopy. A comparison of numbers of detected γ rays and conversion electrons enables the estimation of the internal-conversion coefficient for a given transition. By comparing the experimental internal-conversion coefficient with expected values for various multipolarities (e.g., from Ref. [Kib08]), we can assign a multipolarity to the studied transition. Information about the transition multipolarity can help us to determine a change of spin and parity between the states connected by the internal transition.

(Isomeric) states decaying by a cascade of internal transitions can be identified and investigated by the detection of γ-γ and/or electron-γ coincidences. Such studies require even higher number of produced nuclei (at least thousands) than are needed in α- or α-γ spectroscopic studies.

Analyzing α-decay spectra, one must be aware of the 'energy-summing' effect. This effect occurs when α emitters implanted into a detector decay to excited levels in daughter nuclei. Conversion electrons emitted in the deexcitation process leave full or part of their energy in the detector. This energy is summed with the α-particle energy and in the output signal from the detector we usually cannot distinguish these components. To a lesser extent also the energy of γ and X-rays can be summed with the α-particle energy, which is valid mostly for low-energy photons. High-energy γ rays tend to escape from the detector undetected. Energy-summing effect causes a shift of α peaks to higher energies or change in their shapes and relative intensities or even the occurrence of additional lines in the α-decay spectra [Heß89]. An example of an isotope with a decay scheme resulting in the complex α-decay spectrum is ^{253}No. This nucleus decays mainly by the emission of an 8004- ($\sim$96 %) or 8075-keV α particle ($\sim$4 %). These decays populate excited levels in a daughter isotope ^{249}Fm (at 279.5 and 209.3 keV, respectively). Thus, the α-decay spectrum of ^{253}No is more complex than just two peaks at corresponding energies due to the energy-summing effect. A valuable tool for the analysis of such complex decay patterns are computer Monte-Carlo simulations. We performed simulations of the α decay of ^{253}No using GEANT 4 and discuss the results in Appendix B.

Chapter 5

Results and discussions

In this chapter we present and discuss results from two experiments aimed at the investigation of decay properties of very neutron-deficient radium and francium isotopes. Studied nuclides, $^{197-202}$Fr and $^{201-203}$Ra, were produced in fusion-evaporation reactions $^{56}\mathrm{Fe} + ^{147,149}\mathrm{Sm}$ and $^{60}\mathrm{Ni} + ^{141}\mathrm{Pr}$ at SHIP (GSI, Darmstadt). Prior to this work, only very limited statistics were recorded for some of the studied nuclides, namely $^{201-203}$Ra and ^{199}Fr, and no experimental decay data were published for ^{197,198}Fr. Our goal was to extract detailed information on nuclear structure of these nuclides. Results are described in next sections for each isotope separately.

5.1 Reaction $^{56}\mathrm{Fe} + ^{147,149}\mathrm{Sm}$

In this section we describe decay properties of very neutron-deficient radium, $^{201-203}$Ra, and francium, $^{200-202}$Fr, isotopes. These isotopes are in the region of the nuclide chart known for interesting nuclear-structure phenomena, e.g., shape coexistence and β-delayed fission. Recent experiments indicated the coexistence of states with different shapes in light francium isotopes [Uus05, Jak13, Jak12]. We expect shape coexistence to be present in neutron-deficient radium isotopes as well. However, the experimental information on these isotopes is very limited up to now. This motivated us to investigate decay properties of mentioned nuclides.

Our experiment was performed at SHIP (for the description of SHIP see Sect. 4.1.1) using the fusion-evaporation reaction $^{56}\mathrm{Fe} + ^{147,149}\mathrm{Sm} \rightarrow {}^{203,205}\mathrm{Ra}^{*}$. Irradiations were performed at several beam energies in the range of (244 − 275) MeV in front of the target. An average beam intensity was $\sim 600\,p$nA (particle nA), i.e. $\sim 30\,\mu$A (electric μA) in the pulse ($1\,p\mathrm{nA} = 6.242 \times 10^9$ particles/s). A charge state of the projectiles was 13+. Targets were prepared as SmF_3 compounds. An average thickness of enriched $^{147}SmF_3$ material was $\sim 500\,\mu\mathrm{g/cm}^2$,

which is equivalent to a contribution of $\sim 360\,\mu g/cm^2$ of pure ^{147}Sm. An average thickness of enriched $^{149}SmF_3$ material was $\sim 450\,\mu g/cm^2$, which is equivalent to a contribution of $\sim 330\,\mu g/cm^2$ of pure ^{149}Sm.

In this experiment all three TOF detectors were used. Energy resolution of single strips of the PSSD for α particles was ~ 25 keV (FWHM). For energy calibration of the PSSD we used α lines at 6311(5), 6609(5), 6699(5), and 6843(3) keV from decays of ^{191}Bi, $^{195}Po^g$, $^{195}Po^m$, and ^{194}Po isotopes [Fir04], respectively, produced in the reaction $^{56}Fe + ^{141}Pr$ [And09, And13a] applied before the irradiation of samarium targets. For the energy calibration of the germanium detector we used γ lines from ^{133}Ba and ^{152}Eu sources.

Results presented in this section were published in *Physical Review C* [Kal14].

5.1.1 Isotope ^{202}Ra

Experimental data known prior to this work

Before our study, the observation of ^{202}Ra was reported in two experiments; each one of them detecting only one α-decay event attributed to ^{202}Ra. Both events were registered in experiments at the gas-filled recoil separator RITU (**R**ecoil **I**on **T**ransport **U**nit) at the Department of Physics of the University of Jyväskylä (JYFL) in Finland. The measurements reported significantly different values for the α-decay energies and life-times of ^{202}Ra. One decay chain was produced in the reaction $^{36}Ar + ^{170}Yb$ at a beam energy of 201 MeV yielding a parent (^{202}Ra) α-decay energy of 7860(60) keV and a half-life of $0.7^{+3.3}_{-0.3}$ ms [Lei96]. The α particle tentatively assigned to the decay of ^{202}Ra was followed by two escaped α particles. The production cross section for ^{202}Ra in that measurement was 2 nb. Another triple-α correlation chain was observed in the reaction $^{63}Cu + ^{141}Pr$ at a beam energy of $(278 - 288)$ MeV yielding a parent (^{202}Ra) α-decay energy of 7740(20) keV and a half-life of 16^{+30}_{-7} ms [Uus05]. In this case the daughter α particle escaped while the granddaughter decay was registered with full energy. The cross section for the ^{202}Ra production in that experiment was 25 pb. Reduced widths for α decays evaluated from both measurements were (in spite of large uncertainties) very different (430^{+2020}_{-260} [Lei96] and 44^{+83}_{-20} keV [Uus05]) and will be discussed later in this section.

Our experimental results

We collected decay data for ^{202}Ra at several beam energies in the range of $(244 - 275)$ MeV in front of the ^{149}Sm target. The corresponding excitation energy of the compound nuclei was in the range of $(30 - 53)$ MeV for production at 2/3 of the target thickness, which we consider to be the most probable location for the formation of evaporation residues. At these beam energies, mainly fran-

cium and radon isotopes were produced in pxn and $2pxn$ evaporation channels, respectively (see Fig. 5.1).

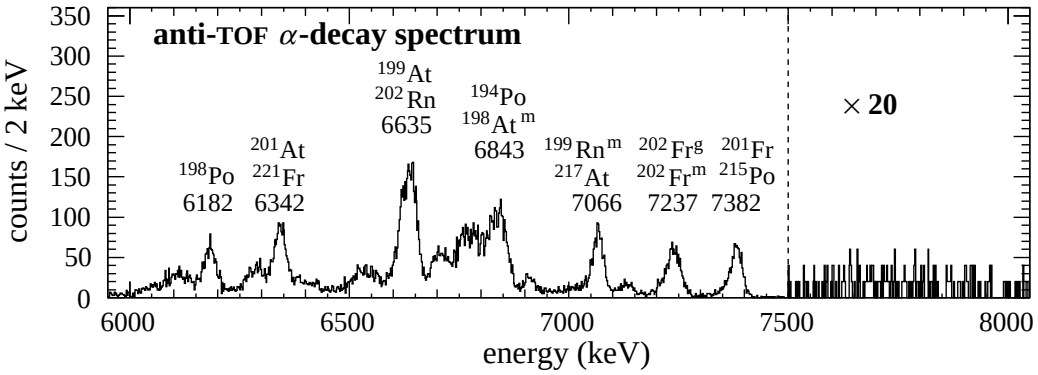

Fig. 5.1 Alpha-decay energy spectrum measured in the PSSD in anticoincidence with the TOF detectors in the reaction $^{56}\mathrm{Fe} + {}^{149}\mathrm{Sm}$ at $\mathrm{E}_{beam} = 244$ and 256 MeV.

ER-α1-α2-α3 correlations We were searching for the decays of ^{202}Ra by searching for the time- and position-correlated events consisting of signals from an implantation of an evaporation residue and its subsequent α decays (ER-α1-α2 chains). The α-decay properties of ^{198}Rn, the α-decay daughter of ^{202}Ra, are known. Thus, in the detected ER-α1-α2 correlation chain with the daughter α2 decay corresponding to the decay of ^{198}Rn, the parent α1 activity originates from ^{202}Ra.

In our data we used correlation time windows of $\Delta t(\text{ER-}\alpha 1) < 50$ ms and $\Delta t(\alpha 1\text{-}\alpha 2) < 300$ ms to search for ^{202}Ra. Correlation parent(α1)-daughter(α2) energy spectrum using these time windows is shown in Fig. 5.2. Sixteen ER-α1-α2 decay chains were registered with daughter decay characteristics (α-decay energy of 7198(6) keV and a half-life of 38^{+13}_{-8} ms) corresponding to ^{198}Rn (reference values: $E_\alpha = 7205(5)$ keV, $T_{1/2} = 64(2)$ ms [Bij95]). Therefore, we assigned the parent α1 activity with an α-decay energy of 7722(7) keV and a half-life of $3.8^{+1.3}_{-0.8}$ ms to ^{202}Ra (see Tab. 5.1).

For all the ER-α1-α2 chains we found the correlated granddaughter α3 decay with an α-decay energy of 6846(7) keV and a half-life of 340^{+110}_{-70} ms. These properties correspond to ^{194}Po (reference values: $E_\alpha = 6842(6)$ keV, $T_{1/2} = 392(4)$ ms [Wau93]), which confirms that 16 detected chains originate from ^{202}Ra. The α-decay scheme of ^{202}Ra is shown in Fig. 5.3.

The Q_α value of the 7722(7)-keV decay is 7878(7) keV. The maximum cross section for the production of ^{202}Ra, 0.2(1) nb, was measured at $E_{beam} = 244$ MeV ($E^*_{CN} = 30$ MeV). One of the 16 detected events of ^{202}Ra was registered in the irradiation of the ^{147}Sm target. However, in this case we suppose that ^{202}Ra was produced in the reaction with ^{149}Sm, which was a 0.53-% admixture in the ^{147}Sm

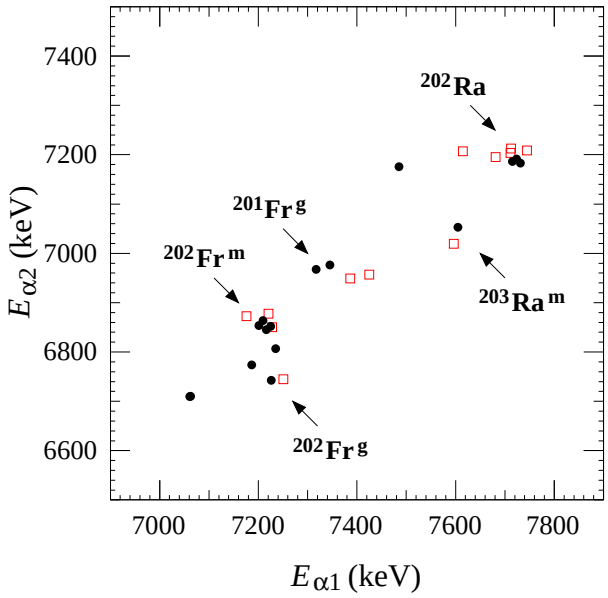

Fig. 5.2 Correlation parent-daughter $\alpha 1$-$\alpha 2$ energy spectrum measured in the PSSD + BOX system in the reaction ^{56}Fe + ^{149}Sm at E_{beam} = 244 and 256 MeV. Correlation search times were Δt(ER-$\alpha 1$) < 50 ms and Δt($\alpha 1$-$\alpha 2$) < 300 ms. Full circles represent events with both $\alpha 1$ and $\alpha 2$ particles fully stopped in the PSSD, while open squares represent cases where the $\alpha 1$ or $\alpha 2$ particle (or both) were registered with the PSSD + BOX system.

Tab. 5.1 The α-decay properties of ^{202}Ra.

isotope	E_α (keV)	$T_{1/2}$ (ms)	δ^2_α (keV)	ref.
^{202}Ra	7722(7)	$3.8^{+1.3}_{-0.8}$	210^{+70}_{-50}	this work
	7740(20)	16^{+30}_{-7}	44^{+83}_{-20} [a]	[Uus05]
	7860(60)	$0.7^{+3.3}_{-0.3}$	430^{+2020}_{-260} [a]	[Lei96]

[a] Values of δ^2_α were calculated according to Rasmussen prescription [Ras59] using input values (E_α and $T_{1/2}$) from cited references.

target, as the production cross section for the reaction ^{149}Sm(^{56}Fe,3n)^{202}Ra is considerably higher than for ^{147}Sm(^{56}Fe,1n)^{202}Ra.

We observed the correlated $\alpha 3$ decay of ^{194}Po for all 16 detected ER-$\alpha 1$(^{202}Ra)-$\alpha 2$(^{198}Rn) chains. Thus, considering 16 α decays and zero β decays[1] of ^{194}Po, we obtain the lower limit of 88 % for the α-decay branch in ^{194}Po. This value agrees with the value of 93(7) % reported previously [Wau93]. The same consideration can also be applied on the second member of the correlation chain, ^{198}Rn. As

[1] zero observed events with assumed Poisson's distribution have an upper 1σ limit of 1.84 [Sch84]

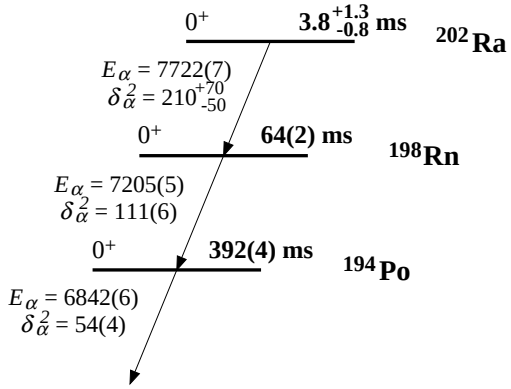

Fig. 5.3 Partial α-decay scheme of ^{202}Ra. The values for ^{202}Ra are from our work and for ^{198}Rn, ^{194}Po from Refs. [Bij95, Wau93]. Alpha-decay energies and reduced widths are in keV.

we observed correlated $\alpha 2$ (^{198}Rn) decays for all detected ER-$\alpha 1$(^{202}Ra) pairs, we evaluate the lower limit for the α branch in ^{198}Rn to be more than 88 %.

Discussion

The α-decay properties for the two ^{202}Ra events registered in previous experiments resulted in reduced α-decay widths of 430^{+2020}_{-260} [Lei96] and 44^{+83}_{-20} keV [Uus05]. One of them indicated a tendency of lowering δ^2_α at decreasing neutron number in radium isotopes, while the other indicated an increasing trend. Both trends have been observed for even-even isotopes of neighboring elements (see Fig. 5.4(a)) and their interpretation is discussed in Ref. [And13c].

We deduced the reduced α-decay width using the Rasmussen prescription [Ras59] assuming $\Delta L = 0$ and obtained $\delta^2_\alpha = 210^{+70}_{-50}$ keV for the 7722-keV α decay of ^{202}Ra, confirming unambiguously the trend of increasing δ^2_α. Recent results also show the tendency of increasing δ^2_α in neighboring thorium [Her10] and radon [And06, Ket01] isotopes.

The improved values of Q_α (7.878(7) MeV) and atomic mass excess (10.6(1) MeV) for ^{202}Ra obtained from our measurement follow the trends of Q_α values and atomic mass excesses for radium isotopes (see Fig. 5.4(b) and Fig. 5.10 in next Sect. 5.1.2 on ^{201}Ra).

We note that the event with the α-decay energy of 7860(60) keV and a half-life of $0.7^{+3.3}_{-0.3}$ ms attributed to ^{202}Ra in previous measurement at RITU [Lei96], may have actually originated from ^{201}Ra.

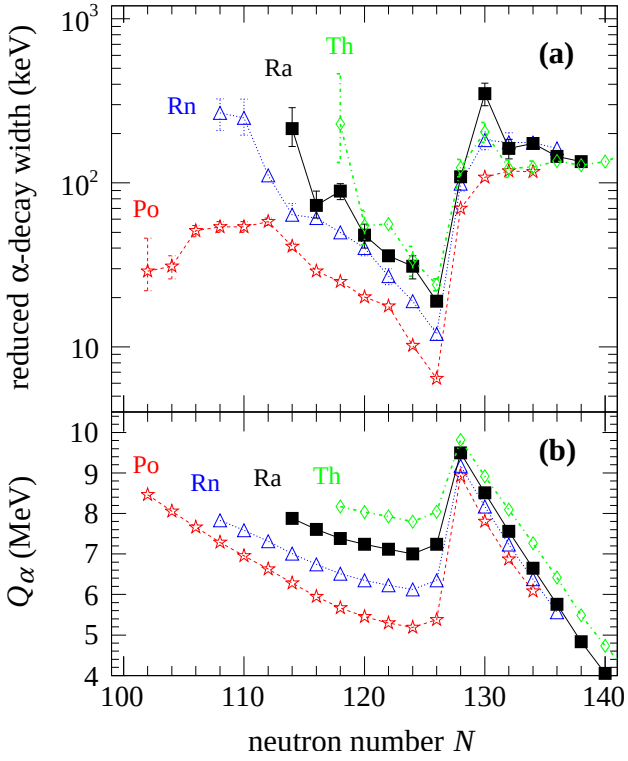

Fig. 5.4 (a) Systematics of reduced α-decay widths for even-even isotopes of elements from polonium ($Z = 84$) to thorium ($Z = 90$) in the vicinity of the shell closure $N = 126$. (b) Systematics of Q_α values for the nuclides from (a). The values of reduced α-decay widths are taken from Refs. [And13c, Her10, nndc] except for the value for ^{202}Ra, which is from our data.

5.1.2 Isotope ^{201}Ra

Experimental data known prior to this work

Only one ER-α1-α2-α3(escaped) decay chain originating from ^{201}Ra was observed before our measurement. The chain was recorded in an experiment performed at RITU at JYFL [Uus05]. The event was produced in the reaction $^{63}\mathrm{Cu} + {}^{141}\mathrm{Pr}$ at a beam energy of $(278-288)$ MeV. Measured α-decay energy for ^{201}Ra was 7905(20) keV and a half-life $1.6^{+7.7}_{-0.7}$ ms. The α2 and α3 decays were attributed to originate from the $13/2^+$ states in ^{197}Rn and ^{193}Po, respectively. A spin and parity of $13/2^+$ was also assigned to the corresponding state in ^{201}Ra, because the α1 decay was considered to be unhindered based on the comparison of measured and calculated α-decay half-lives. The production cross section for ^{201}Ra in that reaction was 25 pb.

Our experimental results

In the reaction $^{56}\mathrm{Fe} + {}^{147}\mathrm{Sm}$ at a beam energy of 249 MeV corresponding to an excitation energy of 27 MeV of a compound nucleus $^{203}\mathrm{Ra}^{*}$, mainly radon and astatine isotopes were produced (see Fig. 5.5). The corresponding evaporation channels for their production are αxn and αpxn, respectively.

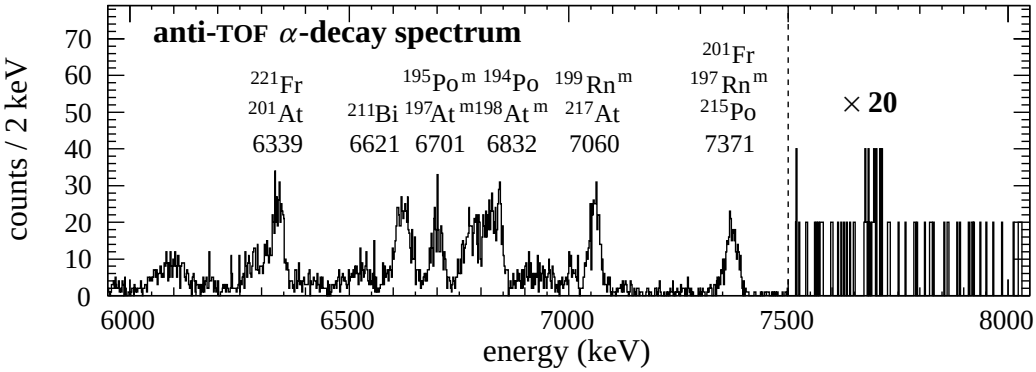

Fig. 5.5 Alpha-decay energy spectrum measured in the PSSD in anticoincidence with the TOF detectors in the reaction $^{56}\mathrm{Fe} + {}^{147}\mathrm{Sm}$ at $\mathrm{E}_{beam} = 249\,\mathrm{MeV}$.

ER-α1-α2-α3 correlation chain We registered one ER-α1-α2(escaped)-α3 correlation chain with parent α-decay energy of 7842(12) keV and a life-time of 12.0 ms in the reaction with the ^{147}Sm target at a beam energy of 249 MeV (see Fig. 5.6). The parent α1 decay was followed by the daughter α2 decay after 51 ms. The α2 particle escaped from the PSSD, depositing only part of its energy (4191 keV). The α3 decay with an energy of 6947(12) keV was detected with full energy in the PSSD 644 ms after the α2 decay. The α1 and α3 decays were registered in the pause between beam pulses, while the α2 decay was recorded in the pulse. The decays were registered in the last strip (No. 16) of the PSSD and in the 1/4 of the strip length. The positions from the bottom and top of the strip for correlated signals of the decay chain are shown in Fig. 5.6.

The energy of the ER before the implantation into the PSSD calculated by LISE++ [Tar08] is 53 MeV. The registered energy of implanted ER was only 21.6 MeV. The detected energy is lower than the expected one due to the pulse-height defect, which may be up to several tens of % [Ant01]. The location of the ER in a two-dimensional plot showing the time of flight and energy of implanted particles is shown in Fig. 5.7. Three groups of events are visible in the plot: the scattered projectiles (on the right side), the complete-fusion reaction products (in the middle) and the scattered target or target-like nuclei from elastic scattering or transfer reactions, respectively (below the complete-fusion reaction products).

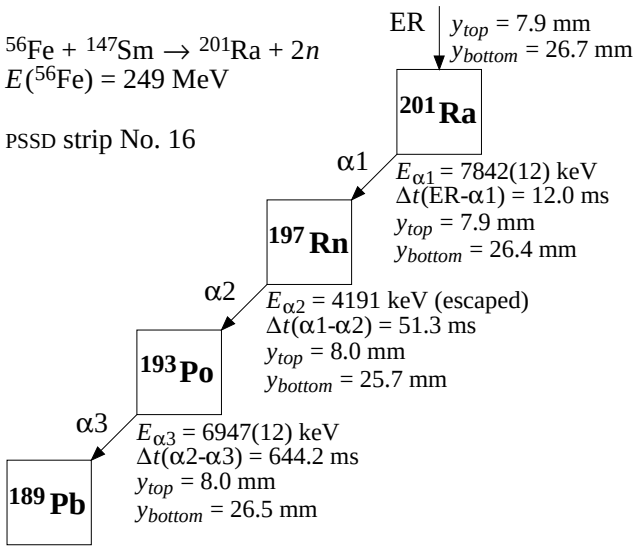

Fig. 5.6 Correlation α-decay chain attributed to ^{201}Ra observed in the reaction ^{56}Fe + ^{147}Sm at $E_{beam} = 249\,\mathrm{MeV}$. Measured energies in the PSSD, time differences between subsequent signals and positions obtained from the top (y_{top}) and bottom (y_{bottom}) of the strip are shown. The $\alpha 1$ and $\alpha 3$ particles were fully stopped in the PSSD, while the $\alpha 2$ particle escaped.

We assign the $\alpha 3$ decay to the known decay of the $3/2^-$ state in ^{193}Po (with reference values $E_\alpha = 6949(5)\,\mathrm{keV}$, $T_{1/2} = 450(40)\,\mathrm{ms}$ [Wau93]). The measured time difference between $\alpha 1$ and $\alpha 2$ decays, $\Delta t(\alpha 1\text{-}\alpha 2) = 51\,\mathrm{ms}$, agrees with the known half-life of the $3/2^-$ state in ^{197}Rn (reference value is $65^{+25}_{-14}\,\mathrm{ms}$ [Enq96a]). Based on the properties of the $\alpha 2$ and $\alpha 3$ decay, we attribute the parent 7842(12)-keV $\alpha 1$ decay with a half-life of $8^{+40}_{-4}\,\mathrm{ms}$ to ^{201}Ra (see Tab. 5.2).

Tab. 5.2 The α-decay properties of ^{201}Ra.

isotope	I^π	E_α (keV)	$T_{1/2}$ (ms)	δ^2_α (keV)	ref.
^{201}Ra	$3/2^-$	7842(12)	8^{+40}_{-4}	43^{+204}_{-20}	this work
	$13/2^+$	7905(20)	$1.6^{+7.7}_{-0.7}$	140^{+680}_{-70} [a]	[Uus05]

[a] Value of δ^2_α was calculated according to Rasmussen prescription [Ras59] using input values (E_α and $T_{1/2}$) from cited reference.

The $\alpha 3$ decay of the ^{201}Ra decay chain registered in our measurement populates the $3/2^-$ state in ^{189}Pb. Its half-life is $39(8)\,\mathrm{s}$ [Sau09]. This state in ^{189}Pb decays predominantly by the EC/β^+ decay. Only less than 1 % of decays proceeds through an α-particle emission (with an energy of 5764(6) or 5619(5) keV)

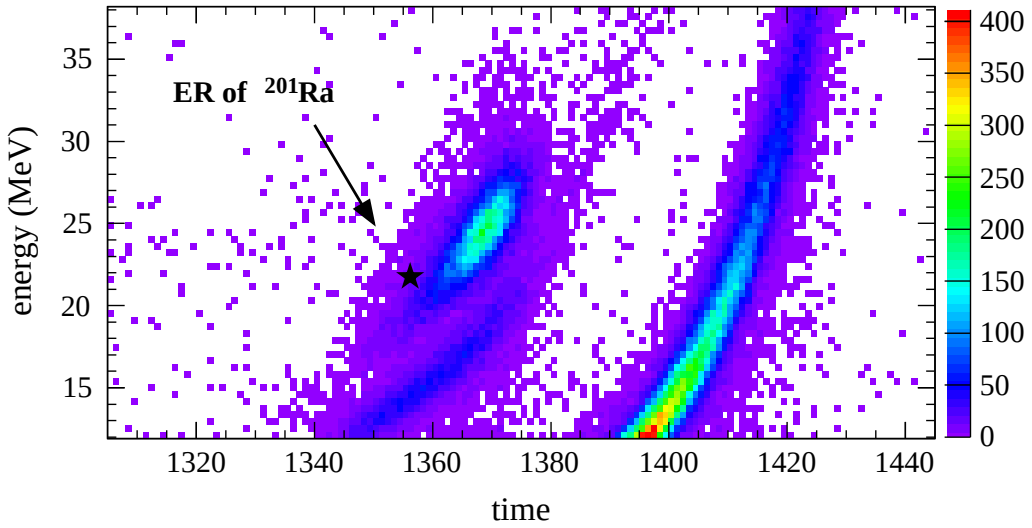

Fig. 5.7 A two-dimensional plot showing time of flight (horizontal axis) and energy (vertical axis) of implanted particles. A position of the evaporation residue (ER) attributed to ^{201}Ra is marked by the black full star. The color scale corresponds to the number of events in one pixel. Events on the right side are scattered projectiles, events in the middle are complete-fusion reaction products and below them are the scattered target or target-like nuclei from elastic scattering or transfer reactions, respectively. Time on the horizontal axis is not calibrated and is in reverse order: higher values correspond to shorter times of flight and vice versa.

[Sau13]. The detector setup at SHIP is not optimized for the detection of the EC/β^+ decay mode due to a high rate of single γ rays and electron threshold of around 100 keV in this measurement. However, we were looking for the $\alpha 4$ decay correlated to the observed ER-$\alpha 1$-$\alpha 2$-$\alpha 3$ decay chain originating from ^{201}Ra within a time window of 200 s after the $\alpha 3$ decay, but no appropriate $\alpha 4$ decay was found.

The probability for the detection of the ER-$\alpha 1$-$\alpha 2$-$\alpha 3$ correlation chain randomly is 10^{-8} (see Ref. [Sch84] for the detailed description of the error analysis in case of low statistics). In the calculation we used time windows of Δt(ER-$\alpha 1$) < 90 ms, $\Delta t(\alpha 1$-$\alpha 2) < 530$ ms and $\Delta t(\alpha 2$-$\alpha 3) < 4.2$ s. The energy range for the $\alpha 1$ particle was taken from 7500 to 9000 keV. The energy windows for the $\alpha 2$ and $\alpha 3$ particles covered the whole range of $(500 - 7500)$ keV, as we also included the α particles escaped from the PSSD.

We obtained $Q_\alpha = 8001(12)$ keV for the observed 7842(12)-keV decay of ^{201}Ra. The production cross section for ^{201}Ra was evaluated to 40^{+80}_{-30} pb at $E_{beam} = 249$ MeV ($E^*_{CN} = 27$ MeV).

Discussion

The reduced width of the observed 7842(12)-keV α decay from ^{201}Ra is 43^{+204}_{-20} keV. The reduced α-decay widths for heavier even-A radium isotopes are 210^{+70}_{-50} (^{202}Ra [this work]) and 73^{+16}_{-12} keV (^{204}Ra [Lei96]). For the heavier odd-A radium isotopes ^{203}Ra and ^{205}Ra, reduced α-decay widths of around 60 keV are known for both, the $3/2^-$ and $13/2^+$, α-decaying states [Uus05, Lei96]. Based on these values we assume no change in spin and parity between the states connected by the 7842(12)-keV $\alpha 1$ transition from ^{201}Ra.

As we assigned the observed $\alpha 2$ and $\alpha 3$ decays to the $3/2^-$ state in daughter nuclei ^{197}Rn and ^{193}Po, respectively, we conclude that the triple-α correlation chain originates from the $3/2^-$ state in ^{201}Ra (see the proposed α-decay scheme in Fig. 5.8).

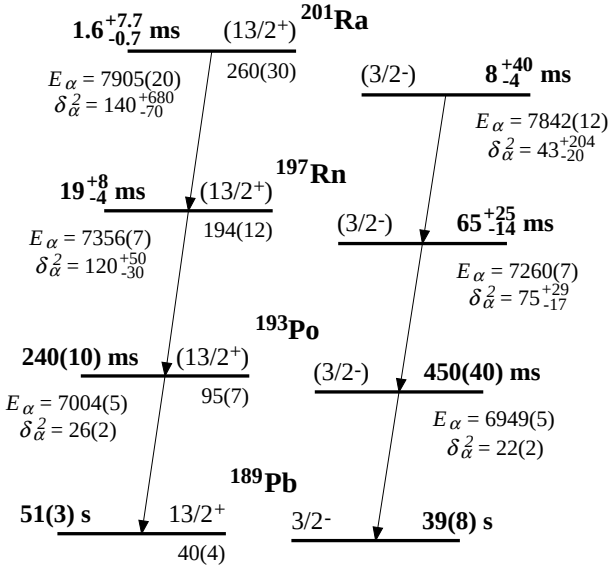

Fig. 5.8 Proposed α-decay scheme for ^{201}Ra. Values for the $3/2^-$ ground state and the excitation energy of the $13/2^+$ isomeric state in ^{201}Ra are from this work; other values are from Refs. [Uus05, Enq96a, Wau93, Sau13]. Alpha-decay energies, reduced widths and energies of excited levels are in keV.

Alpha-decay energies of all isotopes in correlation chains detected in our work and in previous study at RITU [Uus05] are different, which indicates that a different state was populated in each study. However, we recall that the $\alpha 2$ particle escaped from the PSSD in our measurement, and thus we could not evaluate the reduced α-decay width for this transition. Its assignment to the decay of the $3/2^-$ state in ^{197}Rn is therefore only tentative. The production cross section of the $3/2^-$ state obtained from our data (40^{+80}_{-30} pb) is similar to the production cross section of the $13/2^+$ state (25 pb [Uus05]).

In most of the light radium and radon isotopes, the ground-state spin and parity is $3/2^-$ (see Fig. 5.9). Nevertheless, the energy of the $13/2^+$ level decreases with lowering neutron number and we can expect both levels to lie close in energy in the most neutron-deficient region. The spin of the ground and isomeric state in ^{189}Pb were determined unambiguously as 3/2 and 13/2, respectively, by in-source laser spectroscopy at the on-line isotope mass separator ISOLDE at the European Organization for Nuclear Research CERN in Switzerland [Sau13]. In that study the $13/2^+$ isomeric level was located at 40(4) keV above the $3/2^-$ ground state of ^{189}Pb, which enabled to establish the excitation energies of the $13/2^+$ levels in ^{193}Po and ^{197}Rn at 95(7) and 194(12) keV, respectively. On this basis we determine the excitation energy of the $13/2^+$ level in ^{201}Ra to be 260(30) keV.

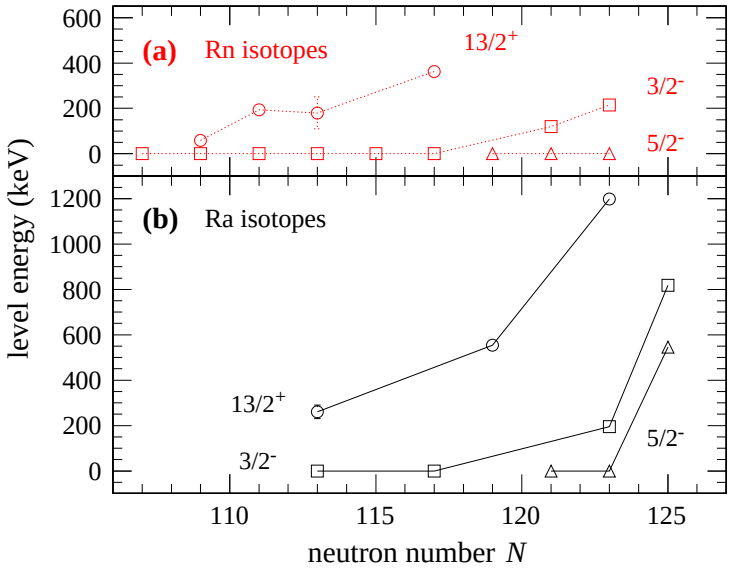

Fig. 5.9 Single-particle level systematics for odd-A (a) radon ($Z = 86$) and (b) radium ($Z = 88$) isotopes. The values of excitation energies are taken from Refs. [Sau13, nndc] except for the value for ^{201}Ra, which is from our data.

Assuming that we registered the α decay from the $3/2^-$ ground state of ^{201}Ra, the evaluated experimental atomic mass excess for ^{201}Ra is 13.4(1) MeV, which fits into the systematics of experimental atomic mass excesses for radium isotopes (see Fig. 5.10(a)). For the comparison of experimental values of atomic mass excesses with theoretical predictions of several models [lbnl] for radium isotopes see Fig. 5.10(b). Both values for ^{201}Ra and ^{202}Ra obtained from our data are in excellent agreement with the values predicted by the finite-range liquid-drop model (FRLDM) [Möl95]. Commonly used finite-range droplet model (FRDM) [Möl95] predicts values by more than 1 MeV different from experimental data for ^{201,202}Ra, but for the heavier isotopes (from $A = 203$) the FRDM model reproduces the experimental data better than the FRLDM model.

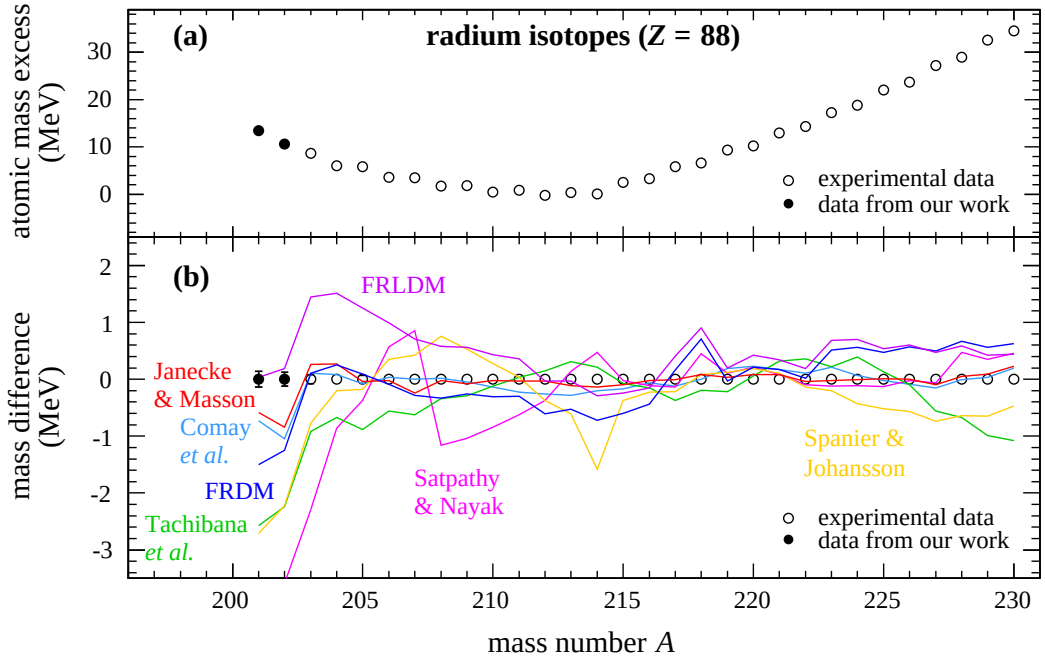

Fig. 5.10 (a) Experimental atomic mass excesses for radium isotopes. (b) The relative differences between experimental (black circles) and theoretical values (colored lines) for atomic mass excesses of radium isotopes. Experimental values were set to zero and values predicted by several models are compared with them. Experimental values were taken from Ref. [Wan12] (open circles) except for ^{201,202}Ra (full circles), which are from our data. Theoretical values were taken from Ref. [lbnl].

5.1.3 Isotope ^{203}Ra

Experimental data known prior to this work

Seven decay chains assigned to ^{203}Ra were observed in the fusion-evaporation reaction $^{35}\mathrm{Cl} + {}^{175}\mathrm{Lu}$ at a beam energy of $(191 - 208)$ MeV at RITU at JYFL [Lei96]. Six decay chains were assigned to the $13/2^+$ state and one decay chain was assigned to the $3/2^-$ state. The maximum production cross section for ^{203}Ra in that reaction was 4 nb. A subsequent measurement with improved precision was performed at RITU using the reactions $^{65}\mathrm{Cu} + {}^{141}\mathrm{Pr}$ at a beam energy of $(283-293)$ MeV and $^{36}\mathrm{Ar} + {}^{170}\mathrm{Yb}$ at a beam energy of $(180-185)$ MeV [Uus05]. In this later study, two α-decaying states were also observed. For both states altogether several tens of events were registered. The production cross section for ^{203}Ra in that measurement was 4 nb. Decay properties from both studies are in agreement except for the half-life of the $3/2^-$ state, for which values of $1.0^{+5.0}_{-0.5}$ ms [Lei96] and 31^{+17}_{-9} ms [Uus05] were measured (see Tab. 5.3). Resulting reduced α-decay widths for this transition are very different (2200^{+11200}_{-1200} [Lei96] and 66^{+36}_{-20} [Uus05]), although uncertainties are large.

Tab. 5.3 The α-decay properties of ^{203}Ra and its daughter ^{199}Rn.

isotope	I^π	E_α (keV)	$T_{1/2}$ (ms)	δ^2_α (keV)	ref.
^{203}Ra	$3/2^-$	7575(10)	50^{+40}_{-15}	45^{+37}_{-14}	this work
	$3/2^-$	7589(8)	31^{+17}_{-9}	66^{+36}_{-20} [a]	[Uus05]
	$3/2^-$	7577(20)	$1.0^{+5.0}_{-0.5}$	2200^{+11200}_{-1200} [a]	[Lei96]
	$13/2^+$	7607(8)	37^{+37}_{-12}	48^{+48}_{-16}	this work
	$13/2^+$	7612(8)	24^{+6}_{-4}	72^{+18}_{-13} [a]	[Uus05]
	$13/2^+$	7615(20)	33^{+22}_{-10}	51^{+35}_{-17} [a]	[Lei96]
^{199}Rn	$3/2^-$	6978(10)	340^{+280}_{-110}	120^{+100}_{-40}	this work
	$3/2^-$	6989(6)	1100^{+900}_{-400}	34^{+28}_{-12} [a]	[Uus05]
	$3/2^-$	6995(10)	620(25)	57(5) [a]	[Cal84]
	$13/2^+$	7050(10)	120^{+120}_{-40}	190^{+190}_{-70}	this work
	$13/2^+$	7060(6)	260^{+80}_{-50}	82^{+26}_{-16} [a]	[Uus05]
	$13/2^+$	7059(10)	325(25)	66(7) [a]	[Cal84]

[a] Values of δ^2_α were calculated according to Rasmussen prescription [Ras59] using input values (E_α and $T_{1/2}$) from cited references.

Our experimental results and discussion

We were searching for decays of ^{203}Ra in the same reaction and beam energies as in case of ^{202}Ra (^{56}Fe + ^{149}Sm, $E_{beam} = (244-275)$ MeV, $E^*_{CN} \approx (30-53)$ MeV). The α-decay energy spectrum measured in the PSSD in this reaction is shown in Fig. 5.1.

ER-α1-α2 correlations To identify decays of ^{203}Ra we searched for correlated ER-α1(^{203}Ra)-α3(^{199}Rn) decay chains. We used time windows Δt(ER-α1) $<$ 300 ms and Δt(α1-α2) $<$ 3 s. We observed nine decay events, which can be divided into two groups:

- The first one comprising five α-decay chains had a parent α1-decay energy of 7575(10) keV and a half-life of 50^{+40}_{-15} ms. A daughter α2-decay energy was 6978(10) keV and a half-life was 340^{+280}_{-110} ms.
- The second group of four α-decay chains yielded a parent α1-decay energy of 7607(8) keV and a half-life of 37^{+37}_{-12} ms. A daughter α2-decay energy was 7050(10) keV and a half-life was 120^{+120}_{-40} ms.

These two groups of ER-α1-α2 chains were attributed to the decays of the $3/2^-$ and $13/2^+$ states in ^{203}Ra, respectively, based on previously measured reference values for ^{203}Ra and its α-decay daughter ^{199}Rn (see Tab. 5.3). Our results are in agreement with the later measurement at RITU [Uus05]. We measured a maximum cross section of 0.2(1) nb for the sum of both α-decaying states in

^{203}Ra at $E_{beam} = 244\,\mathrm{MeV}$ ($E^*_{CN} = 30\,\mathrm{MeV}$).

The ratio of decays from the $13/2^+$ and $3/2^-$ state from our data is 0.8(5). In contrast to this, more decays were seen from the $13/2^+$ state than from the $3/2^-$ state in both previous studies with reported ratio of ~ 6 [Lei96] and ~ 3 [Uus05]. However, the statistics in all experiments were low (9 events in our work, 7 events in Ref. [Lei96] and ~ 30 events in Ref. [Uus05]).

Spins and parities of $3/2^-$ and $13/2^+$ were previously assigned to the two α-decaying states in ^{203}Ra [Lei96]. We confirm these assignments based on reduced α-decay widths obtained from our data (see Tab. 5.3) and the assumed unhindered character of the α decays. We note that energy difference between the ground $3/2^-$ and isomeric $13/2^+$ states is not known, either for ^{203}Ra or for its α-decay daughters.

5.1.4 Search for the decay of ^{200}Ra

We expected the production of a new isotope ^{200}Ra in the $3n$ evaporation channel in the fusion-evaporation reaction $^{56}\mathrm{Fe} + {}^{147}\mathrm{Sm}$. We were searching for the decay of this isotope applying ER-α1(^{200}Ra)-α2(^{196}Rn) and ER-proton(^{200}Ra)-α(^{199}Fr) correlation search. Thus, as a daughter decays we were searching for the α decays of ^{196}Rn and ^{199}Fr, which have α-decay energies and half-lives of $7461(9)\,\mathrm{keV}$ and $4.4^{+1.3}_{-0.9}\,\mathrm{ms}$ (^{196}Rn) [Ket01] and $\sim 7657\,\mathrm{keV}$ and $\sim 6\,\mathrm{ms}$ (^{199}Fr) [this work], respectively. We set the correlation search time between the decay of ^{200}Ra and the daughter decay to 60 ms and the energy window for a daughter decay to $(7300 - 7800)\,\mathrm{keV}$. The time window between the implantation of an evaporation residue and the decay of ^{200}Ra was set to 100 ms. As we also considered the case of escaped α particle or proton from the decay of ^{200}Ra, we set the energy window for this decay to $(100 - 9000)\,\mathrm{keV}$. However, no appropriate chain fulfilling given conditions was found.

Although no decay event of ^{200}Ra was found, we can still estimate the upper limit for the production of this isotope. Each number of counts measured in an experiment has its standard error. Zero events have an upper error of 1.84 [Sch84]. Using this value we evaluated the upper limit of 30 pb for the production cross section of ^{200}Ra at a beam energy of 263 MeV ($E^*_{CN} = 37\,\mathrm{MeV}$) corresponding to the expected maximum of the ^{200}Ra excitation function according to HIVAP calculations [Rei81] (see Fig. 5.38 in Sect. 5.4 on cross sections).

5.1.5 Isotope ^{200}Fr

Experimental data known prior to this work

The detection of the isotope ^{200}Fr was reported for the first time at the **GA**s-filled **R**ecoil **I**on **S**eparator (GARIS) at the Institute of Physical and Chemical

Research (RIKEN) in Japan [Mor95]. Six ER-α1-α2 decay chains were observed. The same number of six events was also obtained at RITU at JYFL [Enq96b]. Half-life values from these two studies were 570^{+270}_{-140} ms [Mor95] and 19^{+13}_{-6} ms [Enq96b] leading to different values of reduced α-decay widths (see Tab. 5.4). Later, in an experiment carried out at the ISOLDE facility at CERN, significantly higher statistics for ^{200}Fr were collected and a half-life of 49(4) ms was measured [DeW05] (see Tab. 5.4).

Tab. 5.4 The α-decay properties of ^{200}Fr and its daughter ^{196}At.

isotope	E_α (keV)	I_α (%)	$T_{1/2}$ (ms)	δ^2_α (keV)	ref.
^{200}Fr	7470(5)		46(4)	48(5)	this work
	7473(12)		49(4)	44(5) [a]	[DeW05]
	7468(9)		19^{+13}_{-6}	120^{+80}_{-40} [a]	[Enq96b]
	7500(30)		570^{+270}_{-140}	$3.1^{+1.6}_{-1.0}$ [a]	[Mor95]
^{196}At	7045(5)	96(2)	350(90)	29(7)	this work
	6732(8)	4(2)		16(9)	this work
	7048(12)		350^{+290}_{-110}	27(2)	[Uus13]
	7055(12)		389(54)	25(4) [a]	[DeW05]
	7048(5)		388(7)	27(1) [a]	[Smi00]
	7065(30)		253(9)	36(9) [a]	[Pu97]
	7044(7)		390^{+270}_{-120}	28^{+19}_{-9} [a]	[Enq96b]
	7053(30)		320^{+220}_{-90}	31^{+23}_{-12} [a]	[Mor95]

[a] Values of δ^2_α were calculated according to Rasmussen prescription [Ras59] using input values (E_α and $T_{1/2}$) from cited references.

Our experimental results

In our experiment, the ^{200}Fr isotope was produced in the complete-fusion reaction $^{56}\mathrm{Fe} + {}^{147}\mathrm{Sm}$. Data were collected at beam energies of 260 and 263 MeV resulting in $E^* \approx 35$ and 37 MeV of the compound nuclei, respectively. At these beam energies, mainly francium and radon isotopes were produced in pxn and $2pxn$ (or αxn) evaporation channels, respectively (see Fig. 5.11).

ER-α1-α2 correlations Searching for correlated α decays of ^{200}Fr and its daughter ^{196}At we used time windows $\Delta t(\text{ER-}\alpha 1) < 0.3\,\text{s}$ and $\Delta t(\alpha 1\text{-}\alpha 2) < 2\,\text{s}$. A two-dimensional plot of correlated parent-daughter (α1-α2) events is shown in Fig. 5.12. In this spectrum we marked as 'A' and 'B' two groups, which have the same decay properties of the parent α1 decay ($E_{\alpha 1} = 7470(5)\,\text{keV}$, $T_{1/2} = 46(4)\,\text{ms}$ for group A and $E_{\alpha 1} = 7463(12)\,\text{keV}$, $T_{1/2} = 89^{+61}_{-26}\,\text{ms}$ for group B). We attributed this α1 decay to the transition connecting ground states of

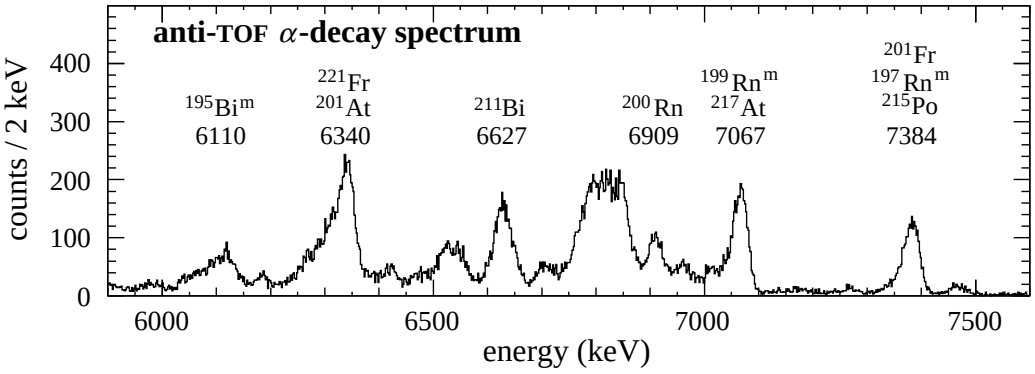

Fig. 5.11 Alpha-decay energy spectrum measured in the PSSD in anticoincidence with the TOF detectors in the reaction $^{56}\mathrm{Fe} + {}^{147}\mathrm{Sm}$ at $\mathrm{E}_{beam} = 260$ and 263 MeV.

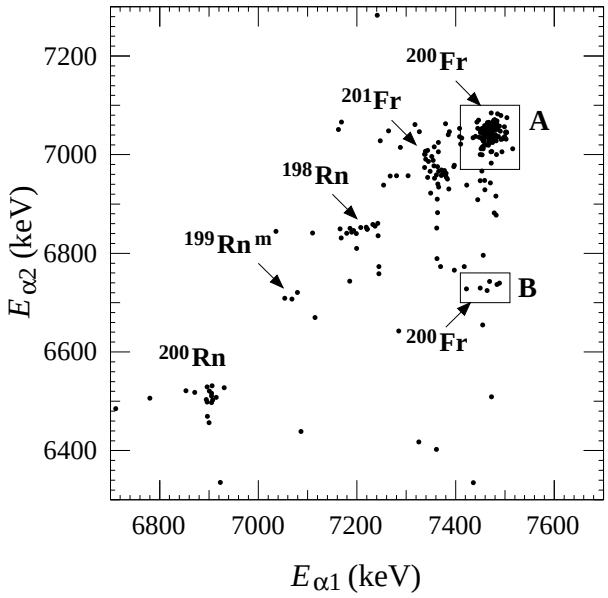

Fig. 5.12 Parent-daughter α1-α2 correlation energy spectrum measured in the PSSD in anticoincidence with the TOF detectors in the reaction $^{56}\mathrm{Fe} + {}^{147}\mathrm{Sm}$ at $E_{beam} = 260$ and 263 MeV. The correlation search times were $\Delta t(\mathrm{ER}\text{-}\alpha 1) < 0.3\,\mathrm{s}$ and $\Delta t(\alpha 1\text{-}\alpha 2) < 2\,\mathrm{s}$.

^{200}Fr and ^{196}At (see Tab. 5.4). The maximum cross section of 1.8(2) nb was measured for the production of ^{200}Fr at $E_{beam} = 263$ MeV ($E^*_{CN} = 37$ MeV).

The daughter α2-decay properties of group A ($E_{\alpha 2} = 7045(5)$ keV, $T_{1/2} = 340(90)$ ms) correspond to the transition connecting ground states of ^{196}At and ^{192}Bi. For the α2 decay of group B the measured energy and half-life are 6732(8) keV and 670^{+460}_{-200} ms. One α2 particle from group B came in coincidence with a γ ray at 76.5(6) keV. This energy agrees with the energy of $K_{\alpha 1}$ X-rays of bismuth ($E_{K_{\alpha 1}} = 77.107$ keV [Fir04]). We assume that the α2 decay of group B represents a transition into an excited level of ^{192}Bi not observed

previously (see Fig. 5.14). Our assumption was confirmed by the observation of a weak α transition from ^{196}At with $E_\alpha = 6742\,\text{keV}$ in a recent experiment at ISOLDE [Tru14]. The half-life for ^{196}At obtained from events of both groups, A and B, is 350(90) ms. Relative intensities of 96(2) % for the stronger line (group A) and 4(2) % for the weaker line (group B) were extracted from our data. From the difference of Q_α values for both transitions we estimate the energy of the level populated in ^{192}Bi by the 6732-keV transition to be 320(10) keV.

In addition, we observed one ER-α1-α2 correlation attributed to ^{200}Fr-^{196}At in the reaction with the ^{149}Sm target. Both α particles were fully stopped in the PSSD and the event is seen in Fig. 5.16. The decay chain was registered at $E_{beam} = 275\,\text{MeV}$, $E^*_{CN} = 53\,\text{MeV}$, with a production cross section of $23^{+53}_{-19}\,\text{pb}$.

β-delayed fission In the reaction ^{56}Fe + ^{147}Sm at $E_{beam} = 263\,\text{MeV}$ one high-energy event was detected 67 ms after the ER implantation in the same position of the PSSD as the ER. The event was registered in the pause between beam pulses with signals from both PSSD and BOX detectors. The measured energy (not corrected for the pulse-height defect) of the event was 136(30) MeV (129 MeV in the PSSD and 7 MeV in the BOX system). We note that the energy calibration was performed using α lines and was extrapolated to higher energies from α-decay energy region. Since no spontaneous-fission branch is known in any of the produced isotopes, we consider the observed event to be a candidate for β-delayed fission (βDF). The probability for the detection of the ER-fission correlation randomly is 10^{-3}. Considering only fission events in the beam pauses, the 136(30)-MeV event was the only one between 50 and 250 MeV observed during the ^{147}Sm irradiation of roughly 70 hours. In the comparably long measurement with the ^{149}Sm target, no event was registered between 50 and 250 MeV in the beam pauses. The process of βDF was measured at SHIP recently in several other neutron-deficient isotopes above $Z = 82$, namely ^{192,194}At [And13a] and ^{186,188}Bi [Lan13].

The ER-fission correlation was detected at a beam energy close to the expected maximum of the ^{200}Fr excitation function. The half-life of the fission event ($T_{1/2} = 47^{+220}_{-20}$ ms) is in excellent agreement with the 46(4)-ms half-life of ^{200}Fr. Besides ^{200}Fr, from the half-life point of view, the only other candidate for the observed fission is ^{201}Fr ($T_{1/2} = 64(3)$ ms) considering all nuclides produced in the reaction. However, we exclude ^{201}Fr for two reasons: firstly, βDF of odd-even nuclei is suppressed compared to odd-odd nuclei [And13b]; and secondly, we did not register any fission event in the measurement with the ^{149}Sm target, in which about six times more ^{201}Fr decay chains were collected compared to the measurement with the ^{147}Sm target (see Sect. 5.1.6). Therefore we consider βDF of ^{200}Fr to be the most probable source for the observed fission event. Recently, βDF events attributed to ^{200}Fr were observed in the measurement at

ISOLDE as well [Ghy14].

(ER-γ)-α1 correlations Fig. 5.13(a) shows a part of the γ-ray spectrum detected in the clover detector. The γ rays from panel (a) detected within a 5-μs coincidence time with ERs implanted into the PSSD are shown in Fig. 5.13(b). Panel (c) shows γ rays from (b) followed by the α decay of ^{200}Fr within 300 ms. Insets in each panel show broader energy range for corresponding spectra. Pb X-rays in panel (b) along with the intensive γ lines in the inset of panel (b) arise from the 11-μs isomer in ^{190}Pb [Dra98] produced in reactions with target contaminations. Because the most intensive lines in panels (a) and (b) (e.g., the 511-keV peak and γ-ray lines from the 11-μs isomer in ^{190}Pb) are not present in panel (c), we assume that the lines in panel (c) are not random, but may arise from the decay of a short-lived isomeric state in ^{200}Fr. The energies of γ lines at 83.8 (2 counts) and 86.6 keV (1 count) agree with $K_{\alpha 2}$ and $K_{\alpha 1}$ X-rays of francium, respectively. Reference values are: $E_{K_{\alpha 2}} = 83.231$ keV, $E_{K_{\alpha 1}} = 86.105$ keV

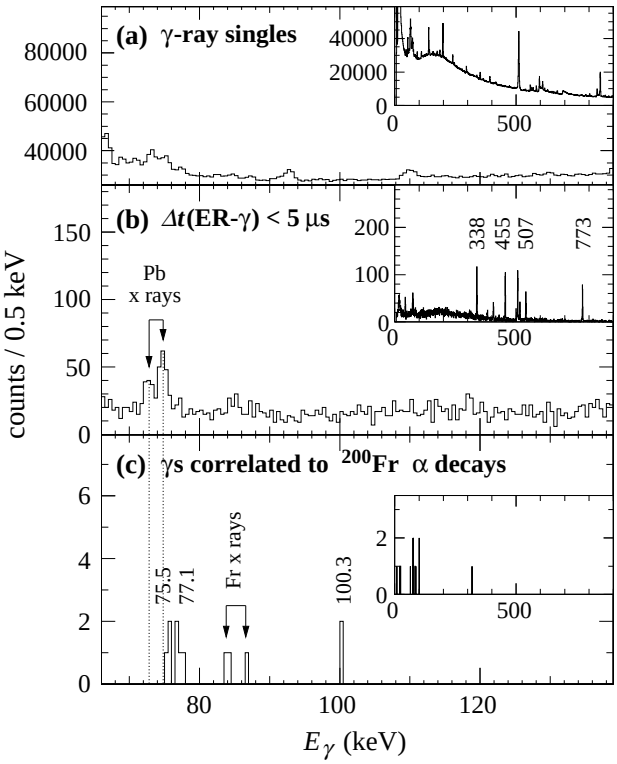

Fig. 5.13 (a) A part of the γ-ray spectrum detected in the germanium clover detector in the reaction ^{56}Fe + ^{147}Sm at $E_{beam} = 260$ and 263 MeV. (b) Gamma rays from (a) within a 5-μs coincidence time with ERs implanted into the PSSD. (c) Gamma rays from (b) correlated with α decays of ^{200}Fr. Insets in each panel show unzoomed spectra from 0 to 900 keV. Pb X-rays in panel (b) and intensive γ lines in the inset of panel (b) arise from the 11-μs isomer in ^{190}Pb [Dra98] produced in reactions with target contaminations.

[Fir04]. Three other γ lines were registered at energies 75.5 (3 counts), 77.1 (4 counts) and 100.3 keV (2 counts) (see Fig. 5.13(c)). All these energies are below the K-shell atomic-electron binding energy of francium (101.13 keV [Fir04]). However, if we assumed the three detected events at 83 and 86 keV to be the K X-rays of francium, the excitation energy of the isomer would be higher than 101.13 keV (see Fig. 5.14). The half-life of this isomer is $0.6^{+0.5}_{-0.2}\,\mu$s.

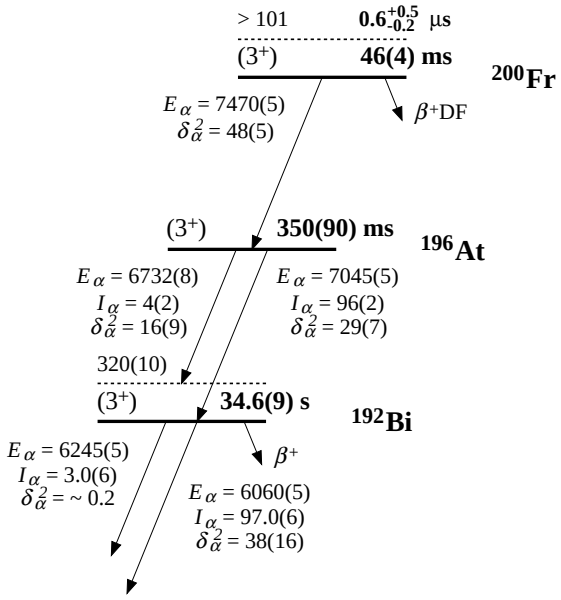

Fig. 5.14 Alpha-decay scheme for ^{200}Fr. The values for ^{200}Fr and ^{196}At are from our data and for ^{192}Bi are from Ref. [Van91]. Alpha-decay energies, reduced widths and energies of excited levels are in keV and relative intensities are in %.

Discussion

Our measurement confirms known α-decay properties of ^{200}Fr from previous studies (see Tab. 5.4) by the detection of the 7470(5)-keV α-decay connecting the 3^+ states in ^{200}Fr and ^{196}At. We observed a new α line for the daughter nucleus ^{196}At at 6732(8) keV populating a 320(10)-keV level in ^{192}Bi (see the decay scheme in Fig. 5.14). The reduced α-decay width for this transition is 16(9) keV calculated using the measured relative intensity of 4 % for this α line and an α branch of 97.5(1) % for ^{196}At [Tru14]. This decay is unhindered compared to the transitions connecting ground states with the same spins and parities between ^{200}At and ^{196}Bi with $\delta^2_\alpha = 18(2)$ keV [Huy92] and between ^{202}At and ^{198}Bi with $\delta^2_\alpha = 12(2)$ keV [Huy92]. Compared to the α transitions connecting ground states with the same spins and parities of ^{196,198}At and ^{192,194}Bi with reduced widths of 29(7) and 39(5) keV [this work], respectively, the 6732(8)-keV decay is hindered up to about a factor of two.

Besides the α-decay mode of ^{200}Fr, we also registered one β-delayed fission event attributed to this isotope. The β-decay daughter of ^{200}Fr is ^{200}Rn. The information on β-decay branching ratio of ^{200}Fr is needed for the evaluation of the probability of βDF of ^{200}Fr. However, in the reaction $^{56}\mathrm{Fe} + ^{147}\mathrm{Sm}$, where we produced ^{200}Fr in the $p2n$ evaporation channel, we also produced ^{200}Rn in the $2pn$ evaporation channel. Thus, we could not estimate the β branch of ^{200}Fr directly from our data. Based on the calculated partial β^+/EC-decay half-lives, the β branch can be estimated as about 1 % (according to the gross theory of β decay [Tak73]), less than 2 % or about 4 % (according to the proton-neutron quasiparticle random-phase approximation models, [Hir93] and [Möl97], respectively). From the experimental data measured at ISOLDE at CERN the β branch of less than 2.5 % was estimated for ^{200}Fr [Ghy14], which is close to theoretical predictions. Based on the ratio of detected α decays of ^{200}Fr and one event attributed to β-delayed fission of ^{200}Fr, which is 460^{+1060}_{-140}, and the estimated β branch of ^{200}Fr of less than 2.5 %, we determine the probability of β-delayed fission to be more than 1.4 %. This is one of the highest observed values for the probability of βDF. In the neutron-deficient region around lead, the βDF probabilities in the range of $(10^{-2} - 10^{-5})$ were measured in thallium, bismuth and astatine isotopes [And13b].

5.1.6 Isotope ^{201}Fr

Experimental data known prior to this work

Two α-decaying states in ^{201}Fr were measured at RITU at JYFL [Uus05]. The isotope was produced in the reactions $^{63}\mathrm{Cu} + ^{141}\mathrm{Pr}$ at $E_{beam} = (278 - 288)$ MeV and $^{36}\mathrm{Ar} + ^{170}\mathrm{Yb}$ at $E_{beam} = (180 - 185)$ MeV. The stronger activity was assigned to the known decay of the $9/2^-$ ground state. The weaker one comprising three correlation chains was assigned to the decay of the intruder $1/2^+$ state. This assignment was based on the correlations with the known α decay of the $1/2^+$ state in the daughter nucleus ^{197}At.

Our experimental results

We collected the main part of the data for ^{201}Fr at $E_{beam} = 275$ MeV in front of the ^{149}Sm target, corresponding to a compound nucleus excitation energy of 53 MeV. The α-decay energy spectrum from this reaction is shown in Fig. 5.15. Dominant α lines in this spectrum are decays of radon and astatine isotopes produced in the $2pxn$ and $3pxn$ evaporation channels, respectively.

ER-α1-α2 correlations A two-dimensional plot of correlated α-decay parent-daughter (α1-α2) events is shown in Fig. 5.16. The dominant transition observed in our data connecting $9/2^-$ ground states of ^{201}Fr and ^{197}At has decay

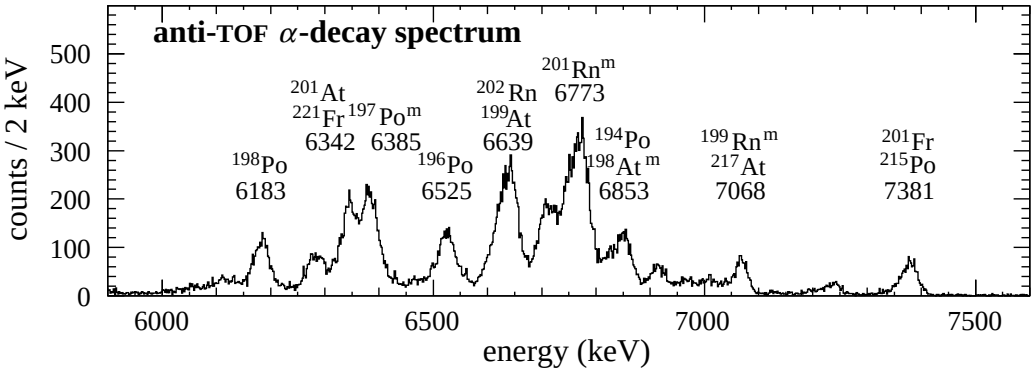

Fig. 5.15 Alpha-decay energy spectrum measured in the PSSD in anticoincidence with the TOF detectors in the reaction $^{56}\mathrm{Fe} + {}^{149}\mathrm{Sm}$ at $\mathrm{E}_{beam} = 275\,\mathrm{MeV}$.

properties consistent with reference values (see Tab. 5.5). The weak group of three events with $E_{\alpha 1} = 7445(8)\,\mathrm{keV}$, $T_{1/2} = 8^{+12}_{-3}\,\mathrm{ms}$ for the parent $\alpha 1$ decay and $E_{\alpha 2} = 6698(16)\,\mathrm{keV}$, $T_{1/2} = 2.8^{+3.8}_{-1.0}\,\mathrm{s}$ for the daughter $\alpha 2$ decay was attributed to the decay of the intruder $1/2^+$ state in ^{201}Fr, which confirms the observation of this isomer at RITU [Uus05]. From the Q_α values of ground- and isomeric-state decays and from the known excitation energy of the $1/2^+$ level in ^{197}At, we estimate the excitation energy of the $1/2^+$ state in ^{201}Fr to be $130(14)\,\mathrm{keV}$.

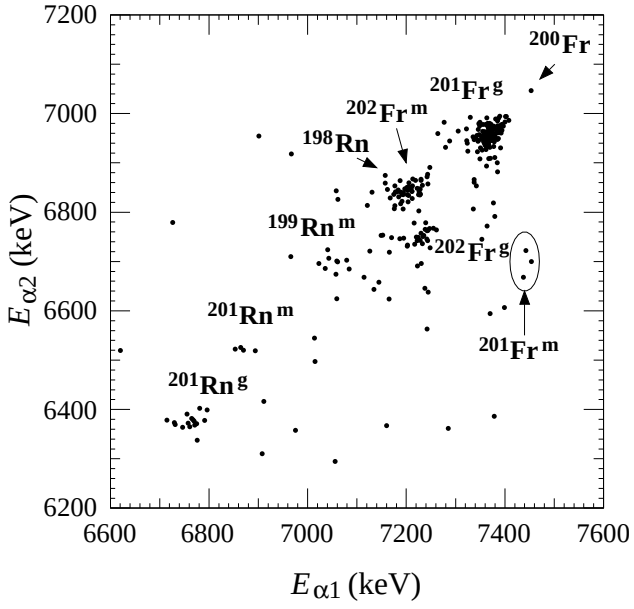

Fig. 5.16 Parent-daughter $\alpha 1$-$\alpha 2$ correlation energy spectrum measured in the PSSD in anticoincidence with the TOF detectors in the reaction $^{56}\mathrm{Fe} + {}^{149}\mathrm{Sm}$ at $E_{beam} = 275\,\mathrm{MeV}$. The correlation search times were optimized for $^{201}\mathrm{Fr}^m$: $\Delta t(\mathrm{ER}\text{-}\alpha 1) < 0.1\,\mathrm{s}$ and $\Delta t(\alpha 1\text{-}\alpha 2) < 12\,\mathrm{s}$.

This is in agreement with the value of 146 keV quoted previously [Uus05]. The isomeric ratio calculated from our data is 0.02(1). The cross section for the production of ^{201}Fr (both $9/2^-$ and $1/2^+$ states) of 4.0(4) nb was measured at $E_{beam} = 275$ MeV ($E^*_{CN} = 53$ MeV) corresponding to the expected maximum of the ^{201}Fr excitation function. We did not observe any ^{201}Fr^m-^{197}At^g correlations.

Tab. 5.5 The α-decay properties of ^{201}Fr^{g,m} and its daughter ^{197}At^{g,m}.

isotope	I^π	E_α (keV)	$T_{1/2}$ (ms)	δ^2_α (keV)	ref.
^{201}Fr	$9/2^-$	7369(5)	64(3)	72(4)	this work
	$9/2^-$	7379(7)	67(3)	64(4)	[DeW05]
	$9/2^-$	7369(8)	53(4)	87(8) [a]	[Uus05]
	$9/2^-$	7361(7)	69^{+16}_{-11}	71^{+17}_{-12} [a]	[Enq96b]
	$9/2^-$	7388(15)	48(15)	83(28) [a]	[Ewa80]
	$1/2^+$	7445(8)	8^{+12}_{-3}	300^{+500}_{-100}	this work
	$1/2^+$	7454(8)	19^{+19}_{-6}	130^{+130}_{-40} [a]	[Uus05]
^{197}At	$9/2^-$	6963(5)	354^{+17}_{-15}	57^{+4}_{-3}	this work
	$9/2^-$	6963(4)	390(16)	51(3)	[DeW05]
	$9/2^-$	6959(6)	340(20)	61(5) [a]	[Uus05]
	$9/2^-$	6960(5)	388(6)	53(2) [a]	[Smi99]
	$9/2^-$	6956(5)	370^{+90}_{-60}	57^{+14}_{-10} [a]	[Enq96b]
	$1/2^+$	6698(16)	2800^{+3800}_{-1000}	70^{+90}_{-30}	this work
	$1/2^+$	6706(9)	1100^{+1100}_{-400}	160^{+160}_{-60} [a]	[Uus05]
	$1/2^+$	6707(5)	2000(200)	87(10) [a]	[Smi99]
	$1/2^+$	6707	3700(2500)	47(32) [a]	[Coe86]

[a] Values of δ^2_α were calculated according to Rasmussen prescription [Ras59] using input values (E_α and $T_{1/2}$) from cited references.

(ER-γ)-α1 correlations Fig. 5.17(a) shows a part of the γ-ray spectrum detected in the germanium clover detector without any selection conditions applied. Panel (b) shows γ rays detected within a 5-μs coincidence time with ERs implanted into the PSSD. Panel (c) was obtained applying the condition of detecting an α decay from ^{201}Fr within 320 ms after ER-γ coincidences from panel (b). Insets in panels (a), (b), (c) show a broader energy range for the corresponding spectra. As the most intense peaks from panels (a) and (b) are not reproduced in panel (c), we assume that the peak at 85.7 keV (7 counts) in this panel is not random, but may originate from the decay of a short-lived isomer ^{201}Fr^{m2}. The energy of the peak corresponds to the energy of $K_{\alpha1}$ X-rays of francium, which is 86.105 keV [Fir04]. As the intensity ratio $I_{K_{\alpha2}}/I_{K_{\alpha1}}$ = 0.61(2) [Fir04], one should expect the detection of about four $K_{\alpha2}$ X-rays. Since none were observed, we note that possibly at least some of the events at

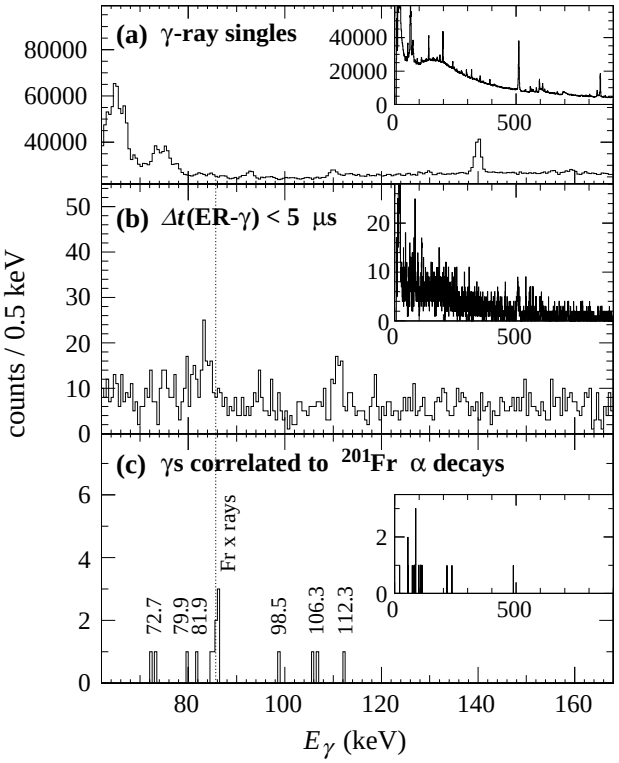

Fig. 5.17 (a) A part of the γ-ray spectrum detected in the germanium clover detector in the reaction $^{56}\mathrm{Fe} + {}^{149}\mathrm{Sm}$ at $E_{beam} = 256\,\mathrm{MeV}$. (b) Gamma rays from (a) within a 5-μs coincidence time with ERs implanted into the PSSD. (c) Gamma rays from (b) correlated with α decays of ^{201}Fr. Insets in each panel show unzoomed spectra from 0 to 900 keV.

85.7 keV may not be X-rays, but γ rays. Other weak γ-ray lines were registered at 72.7 and 106.3 keV (2 counts for each line). The half-life of the isomer is $0.7^{+0.5}_{-0.2}\,\mu$s.

Within a 320-ms time after ER implantations we registered 340(20) α decays attributed to $^{201}\mathrm{Fr}^{g}$ (not corrected for the geometric detection efficiency for α particles with full energy). About 10 of these ER-α correlated events had a γ ray attributed to the decay of $^{201}\mathrm{Fr}^{m2}$ registered within a 5-μs coincidence time after the ER implantations. Calculated time of flight for ^{201}Fr nuclei through the 11-m long separator is $1.4\,\mu$s, which is two times longer than the half-life of the $^{201}\mathrm{Fr}^{m2}$ isomer. Corrected for the γ-ray detection efficiency ($\sim 11\,\%$ for $E_\gamma \approx 80\,\mathrm{keV}$) and the time of flight through the separator ($\sim 75\,\%$ of $^{201}\mathrm{Fr}^{m2}$ isomers decay during the flight to $^{201}\mathrm{Fr}^{g}$) we get about 360(110) nuclei of $^{201}\mathrm{Fr}^{m2}$ produced in complete-fusion reactions (not corrected for the geometric detection efficiency for α particles with full energy). Comparing this number with the 340(20) nuclei of $^{201}\mathrm{Fr}^{g}$ obtained from the ER-α correlations we conclude that all (or at least the most) of the produced ^{201}Fr nuclei are in the 0.7-μs isomeric

state.

Discussion

Our measurement confirms the presence of the α-decaying isomeric $1/2^+$ level in ^{201}Fr reported at RITU [Uus05]. Besides this level, we observed a short-lived activity, which may be assigned to another isomeric level in ^{201}Fr. This assignment is based on the detection of francium $K_{\alpha 1}$ X-rays (7 counts) and two weak lines in the γ-ray spectrum at 72.7 and 106.3 keV (2 counts for each line) within a 5-μs coincidence time with ERs of ^{201}Fr. We note that the detection setup was not optimized for the detection of L X-rays, as the detection efficiency is below 4 % for energies below 20 keV (see Fig. 4.3 in Sect. 4.1.2). The source of $K_{\alpha 1}$ X-rays must be a transition with an energy higher than the K-shell binding energy of francium (101.13 keV [Fir04]). We can consider two possibilities: observed $K_{\alpha 1}$ X-rays come from the internal conversion of (a) the 106.3-keV internal transition, or (b) an unobserved internal transition with an energy larger than the K-shell binding energy (101.13 keV). The K-shell internal conversion coefficient (α_K) from experimental data is roughly 4 for variant (a) and more than 7 for variant (b).

For both variants we exclude an electric character of the internal transition producing $K_{\alpha 1}$ X-rays because the expected α_K values are too low. (See Tab. 5.6 showing expected α_K values for the 106.3-keV transition corresponding to variant (a). For transitions of higher energies the α_K values would be even lower excluding variant (b) as well.) In contrast, $M2$ and higher magnetic multipolarities have too high α_K values for case (a), but for case (b) all multipolarities for magnetic transitions would be compatible with experimental α_K.

Tab. 5.6 Comparison of total (α_{tot}), K- (α_K), L- (α_{L}), and M-shell (α_{M}) internal conversion coefficients from Ref. [Kib08] and single-particle half-lives ($T_{1/2,SP}$) according to Weisskopf [Wei51] for the 106.3-keV internal transition of different multipolarities in the nuclide ^{201}Fr. From experimental data we evaluated α_K to be more or equal to 4 and a half-life to be $0.7^{+0.5}_{-0.2}\,\mu$s.

multipolarity	α_{tot}	α_K	α_L	α_M	$T_{1/2,SP}$
$E1$	0.406(6)	0.315(5)	0.0691(10)	0.01659(24)	0.1 ps
$E2$	6.91(10)	0.311(5)	4.86(7)	1.316(19)	80 ns
$E3$	167.5(24)	0.1302(19)	120.0(17)	35.6(5)	20 ms
$M1$	12.00(17)	9.64(14)	1.79(3)	0.428(6)	1 ps
$M2$	89.2(13)	54.0(8)	26.0(4)	6.91(10)	0.8 μs
$M3$	645(9)	72.8(11)	405(6)	125.0(18)	0.6 s

Considering the Weisskopf estimates for single-particle half-lives ($T_{1/2,SP}$) [Wei51], we exclude $E1$, $E2$ and $M1$ characters as candidates for the transition producing observed $K_{\alpha 1}$ X-rays, because their $T_{1/2,SP}$ is much shorter than

the measured value of $0.7^{+0.5}_{-0.2}\,\mu$s (see Tab. 5.6). On the other hand, $T_{1/2,SP}$ for transitions of $E3$ and $M3$ characters (and higher multipolarities) is significantly longer than the measured value. We note that there are several known cases of isomers decaying by $E1$ transitions with relatively long half-lives (see, e.g., Ref. [Rig08]), but as we also excluded electric characters based on α_K values, it does not influence our conclusions. Therefore, considering the measured half-life, $M2$ is the most likely multipolarity for the transition producing the observed $K_{\alpha 1}$ X-rays.

To conclude, we assume the observed $K_{\alpha 1}$ X-rays arise from an internal transition of $M2$ character, for which γ-ray events were not observed due to a high α_K value. Assuming that the isomer decays directly by this transition to the $9/2^-$ ground state, we tentatively assign a spin and parity of $13/2^+$ to this isomeric state (see the decay scheme in Fig. 5.18). The excitation energy of the isomer must be higher than the K-shell atomic-electron binding energy of francium, which is 101.13 keV [Fir04]. As α_K decreases with increasing transition energy, we estimate the upper limit for the excitation energy of the isomer to be roughly 300 keV. Values of α_K for $M2$ transitions with higher energies are too low compared to experimental α_K.

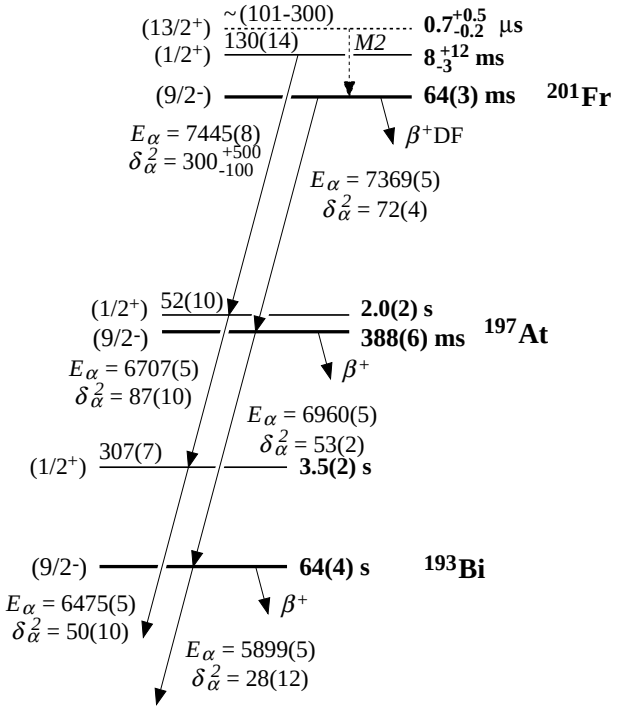

Fig. 5.18 Decay scheme for ^{201}Fr. Values for ^{201}Fr are from this work, for ^{197}At from Refs. [Smi99, Coe86] and for ^{193}Bi from Ref. [Coe85] and references therein. Alpha-decay energies, reduced widths and energies of excited levels are in keV.

Considering the tentative excitation energy range of $(101-300)$ keV, the transition strength for the $M2$ multipolarity is $(0.2-1.1)$ W.u.. This is comparable to $B(M2)$ values for neighboring odd-A francium isotopes: 0.10(2) W.u. for ^{203}Fr [Jak13], 0.17(4) W.u. for ^{205}Fr [Jak12] and astatine isotopes: 0.09(1) for ^{197}At [And08], 0.16(5) W.u. for ^{199}At [Jak10], 0.15(1) for ^{201}At [Dyb83].

We note that an isomeric state with spin and parity $13/2^+$ decaying through an $M2$ internal transition to the $9/2^-$ ground state was observed in ^{203}Fr at $E^* = 426$ keV with $T_{1/2} = 0.37(5)$ μs [Jak13] and in ^{205}Fr at $E^* = 544$ keV with $T_{1/2} = 80(20)$ ns [Jak12]. The estimated energy range for the excitation energy of the isomer in ^{201}Fr, $\sim(101-300)$ keV, confirms the trend of the decreasing excitation energy of the $13/2^+$ isomer with decreasing N in odd-A francium isotopes (see Fig. 5.19). This level is also present in odd-A astatine and bismuth isotopes and its energy decreases with decreasing neutron numbers as well.

The ground states of odd-A francium isotopes from $A = 219$ down to $A = 201$ are presumed to have the spherical configuration $\pi(h_{9/2})^5$ [Fir04]. Along with this level, the $1/2^+$, $13/2^+$, $7/2^-$ levels were identified at low excitation energies in the lightest odd-A francium ($Z = 8$), astatine ($Z = 85$), and bismuth ($Z = 83$) isotopes (see Fig. 5.19). The $13/2^+$ and $1/2^+$ states appear very close in energy in the most neutron-deficient francium isotopes, while in astatine and bismuth

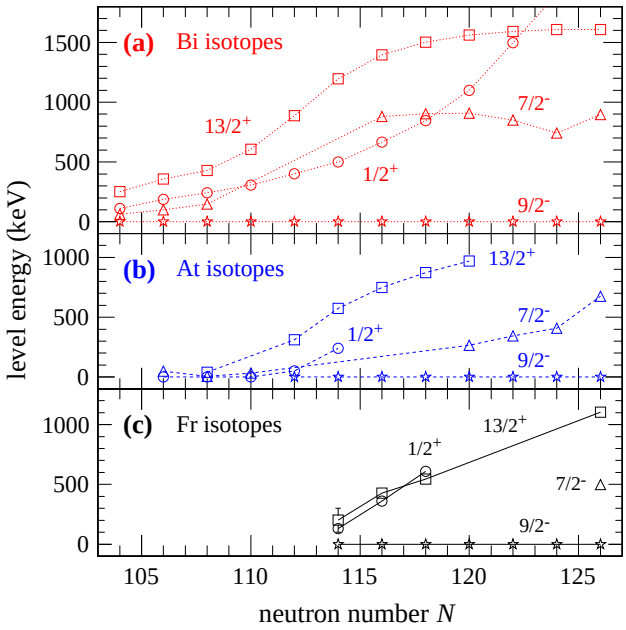

Fig. 5.19 Single-particle level systematics for odd-A (a) bismuth ($Z = 83$), (b) astatine ($Z = 85$) and (c) francium ($Z = 87$) isotopes. The error bar for the $13/2^+$ state in ^{201}Fr ($N = 114$) corresponds to the possible energy interval for this state; the exact value is not known. The values of excitation energies are taken from Refs. [Jak13, Jak12, nndc] except for the values for ^{201}Fr, which are from our data.

isotopes clear differences in excitation energy between these states exist (see Fig. 5.19). It might mean that in the lightest francium isotopes the $13/2^+$ state becomes the ground state, in contrast to the lightest astatine isotopes, where the intruder $1/2^+$ state becomes the ground state. Besides the $13/2^+$ and $1/2^+$ levels, the $7/2^-$ level has decreasing energy with decreasing N in astatine and bismuth isotopes as well. We observed decays of this level ($7/2^-$) in ^{199}Fr ($N = 112$) and ^{197}Fr ($N = 110$), but we could not establish its excitation energy (see Sect. 5.2.1 and 5.2.3 on ^{199}Fr and ^{197}Fr, respectively). We also reported a possible observation of the $1/2^+$ level 47(7) keV below the $7/2^-$ level in ^{199}Fr. Besides our study, another study of ^{199}Fr was performed [Uus13], where three levels were suggested: the ground $1/2^+$ state, the $7/2^-$ state at 56 keV and the $13/2^+$ state at ≤ 300 keV. As the results from both experiments are not unambiguous, we did not place these levels in ^{199}Fr in Fig. 5.19. To investigate the energy levels in the most neutron-deficient francium isotopes in more detail, measurements with higher statistics must be performed.

5.1.7 Isotope ^{202}Fr

Experimental data known prior to this work

The presence of two α-decaying states in ^{202}Fr was reported for the first time in measurement at Leuven Isotope Separator On-Line (LISOL) facility (Louvain-la-Neuve, Belgium) [Huy92]. The states with spins and parities 3^+ (ground state) and 10^- (isomeric state) were assumed to decay to corresponding levels in ^{198}At. Although two states were reported, only one α line was observed, which was interpreted as a line doublet. Also only a common half-life for both states was given. In later experiments at RITU (JYFL) these two α lines were confirmed and disentangled using the α-α correlation technique [Enq96b, Uus05] (see Tab. 5.7). Recently, both long-lived α-decaying states in ^{202}Fr were studied and confirmed in the Collinear Resonance Ionization Spectroscopy (CRIS) experiment [Lyn14].

Our experimental results

In our study we collected the data for ^{202}Fr at several beam energies in the range of $(244-275)$ MeV in front of the ^{149}Sm target. The majority of ^{202}Fr nuclei were produced at $E_{beam} = 256$ MeV corresponding to a 39-MeV excitation energy of compound nuclei. Alpha-decay energy spectrum from this reaction is shown in Fig. 5.20. The peak at 7237 keV is composed of two α lines: 7238(5) keV (^{202}Fr^g) and 7226(5) keV (^{202}Fr^m), which are not resolved in this spectrum. However, we can distinguish both decays in a two-dimensional plot of parent-daughter (α1-α2) correlations, which is shown in Fig. 5.21. Alpha decays of two states in

Tab. 5.7 The α-decay properties of $^{202}Fr^{g,m}$ and its daughter $^{198}At^{g,m}$.

isotope	I^π	E_α (keV)	$T_{1/2}$ (s)	δ^2_α (keV)	ref.
^{202}Fr	3^+	7238(5)	0.372(12)	33(2)	this work
	3^+	7241(8)	0.30(5)	40(7) [a]	[Uus05]
	3^+	7243(6)	$0.23^{+0.08}_{-0.04}$	52^{+18}_{-9} [a]	[Enq96b]
	3^+	7237(8)	0.34(4)	≤ 53	[Huy92]
	10^-	7226(5)	0.286(13)	48(3)	this work
	10^-	7235(8)	0.29(5)	44(8) [a]	[Uus05]
	10^-	7242(6)	$0.23^{+0.14}_{-0.5}$	52^{+32}_{-12} [a]	[Enq96b]
	10^-	7237(8)	0.34(4)	≤ 53	[Huy92]
^{198}At	3^+	6747(5)	3.0(1)	39(2)	this work
	3^+	6748(6)	3.8(4)	27(5) [a]	[Uus05]
	3^+	6753(4)	$4.6^{+1.8}_{-1.0}$	22^{+9}_{5} [a]	[Enq96b]
	3^+	6755(4)	4.2(3)	$26-37$	[Huy92]
	10^-	6849(5)	1.24(6)	39(3)	this work
	10^-	6850(6)	1.04(15)	39(10) [a]	[Uus05]
	10^-	6855(4)	$1.3^{+0.8}_{-0.3}$	30^{+19}_{-9} [a]	[Enq96b]
	10^-	6856(4)	1.0(2)	$37-73$	[Huy92]

[a] Values of δ^2_α were calculated according to Rasmussen prescription [Ras59] using input values (E_α and $T_{1/2}$) from cited references, but are not introduced directly in the original reference.

^{202}Fr correlated with the α decays of two corresponding states in the daughter nuclide ^{198}At are visible in this spectrum.

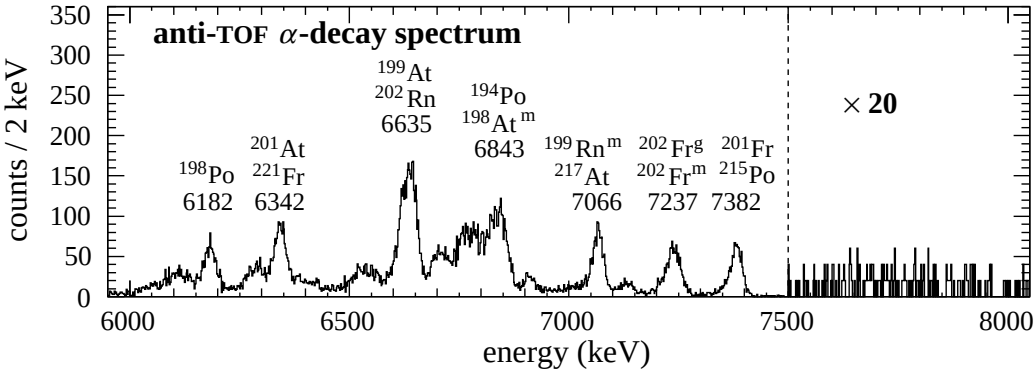

Fig. 5.20 Alpha-decay energy spectrum measured in the PSSD in anticoincidence with the TOF detectors in the reaction $^{56}Fe + ^{149}Sm$ at $E_{beam} = 244$ and 256 MeV.

In total around 500 α1-α2 pairs of ^{202}Fr-^{198}At were registered. The isomeric ratio is 0.6(1) from our data. For the sum of both states, the maximum cross section of 25(2) nb was measured at $E_{beam} = 260$ MeV ($E^*_{CN} = 42$ MeV) corresponding to the maximum of the ^{202}Fr excitation function.

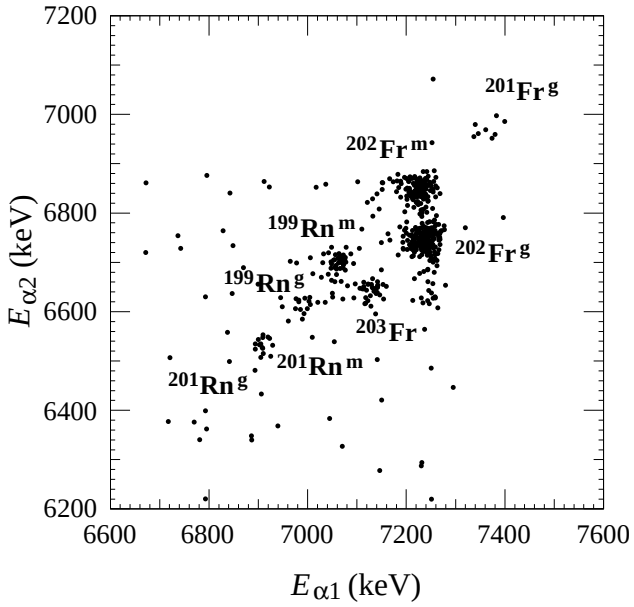

Fig. 5.21 Parent-daughter α1-α2 correlation energy spectrum measured in the PSSD in anticoincidence with the TOF detectors in the reaction ^{56}Fe + ^{149}Sm at $E_{beam} = 256$ MeV. The correlation search times were optimized for ^{202}Fr: Δt(ER-α1) < 1.5 s and Δt(α1-α2) < 10 s.

5.2 Reaction ^{60}Ni + ^{141}Pr

In the measurement described in this section we aimed at decay studies of the very neutron-deficient francium isotopes. The lightest francium isotope, for which decay data had been published prior to this work, is ^{199}Fr with only five registered decay chains. We aimed at the study of this isotope in more detail, and also at the study of even more neutron-deficient isotopes, ^{197,198}Fr. As we are approaching the proton drip-line, a search for the proton emission was also the motivation for our work.

Measurement was performed at SHIP (for more details see Sect. 4.1.1) using the fusion-evaporation reaction ^{60}Ni + ^{141}Pr $\rightarrow$ ^{201}Fr*. Irradiations were performed at several beam energies in the range of $(262 - 300)$ MeV in front of the target to cover the maximum cross sections for the $2n - 4n$ evaporation channels. An average beam intensity was ~ 400 pnA (particle nA), i.e. ~ 20 μA (electric μA) in the pulse (1 pnA $= 6.242 \times 10^9$ particles/s). A charge state of the projectiles was 13+ in the first part of the experiment and 14+ in the second one. An average thickness of the targets prepared from the $^{141}PrF_3$ material was ~ 520 μg/cm^2, which is equivalent to a contribution of ~ 370 μg/cm^2 of pure ^{141}Pr.

In this experiment only two TOF detectors were used. Energy resolution for single strips of the PSSD was $\sim(30 - 35)$ keV (FWHM) for α particles. For

energy calibration of the PSSD we used α lines at 6311(5), 6520(3), 6609(5), 6843(3), and 6958(5) keV from decays of ^{191}Bi, ^{196}Po, ^{195}Po^{g}, ^{194}Po, and ^{197}At^{g}, respectively [Fir04]. For the energy calibration of the germanium detector we used γ lines from ^{133}Ba and ^{152}Eu sources.

Results from this section were published in *Physical Review C* [Kal13a] and *GSI Scientific Report* [Kal13b].

5.2.1 Isotope ^{199}Fr

Experimental data known prior to this work

The ^{199}Fr isotope was observed for the first time in the $6n$ evaporation channel in the fusion-evaporation reaction $^{36}\mathrm{Ar} + {}^{169}\mathrm{Tm}$ at a beam energy of 215(5) MeV at GARIS at RIKEN in Japan [Tag99]. Five α-decay chains were attributed to the decay of ^{199}Fr on the basis of correlations with the known α decay of the daughter isotope ^{195}At. The measured α-decay energy and half-life of ^{199}Fr were 7655(40) keV and 12^{+10}_{-4} ms.

Another study of the decay of ^{199}Fr was performed at RITU at JYFL [Uus13]. Results from that study were published several months after our paper [Kal13a] and will be discussed later in this section.

Our experimental results

We collected data for the isotope ^{199}Fr at several beam energies from 262 to 272 MeV in front of the target. The corresponding excitation energy of the compound nucleus ^{201}Fr* was from 24 to 31 MeV. This energy interval was chosen to cover the maximum of the $2n$ evaporation channel according to calculations performed using the statistical model code HIVAP [Rei81]. We also produced ^{199}Fr at a beam energy of 276 MeV, but we had to exclude this part of data from analysis because of the production of ^{198}Fr in the $3n$ evaporation channel at this energy as well. Decay characteristics of ^{199}Fr and ^{198}Fr are very similar and these isotopes could not be distinguished when produced simultaneously.

ER-α1-α2 correlations A part of the α-decay spectrum from 6400 to 8000 keV measured in the PSSD in anticoincidence with the TOF system is presented in Fig. 5.22(a). The spectrum is dominated by the decays of polonium and radon isotopes produced in the αpxn and pxn evaporation channels, respectively. The measured α-decay energies of these isotopes (Fig. 5.22(a)) are in agreement with the reference values [Fir04] within 4 keV. No distinct α peaks with $E_\alpha >$ 7500 keV were observed due to the background (see the right side of Fig. 5.22(a)). Using a time window $\Delta t(\text{ER-}\alpha 1) < 60$ ms for position-correlated events, the background and longer-lived activities are strongly reduced, while a peak with $E_\alpha \approx 7675$ keV becomes visible (Fig. 5.22(b)). The spectrum of parent-daughter

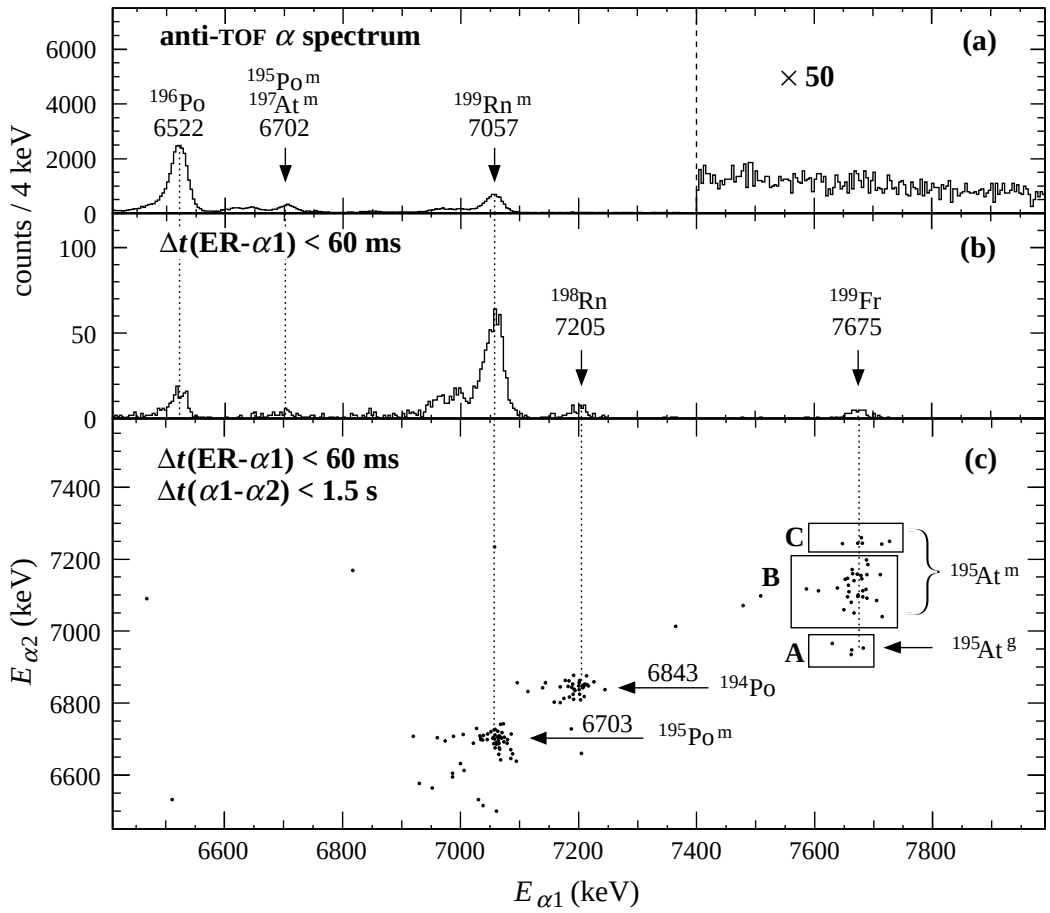

Fig. 5.22 (a) The sum of α-decay energy spectra measured in the PSSD in anticoincidence with the TOF detectors in the reaction $^{60}\mathrm{Ni} + ^{141}\mathrm{Pr}$ at several beam energies in the range of $(262 - 272)$ MeV. (b) α decays from (a) detected within 60 ms after ER implantation. (c) Parent-daughter $\alpha 1$-$\alpha 2$ correlation spectrum. $\alpha 2$ decays were detected within 1.5 s after $\alpha 1$ decays from (b).

$\alpha 1$-$\alpha 2$ correlations shown in Fig. 5.22(c) was obtained using a time window $\Delta t(\alpha 1\text{-}\alpha 2) < 1.5$ s for $\alpha 1$ decays from panel (b). The dominant groups in this spectrum are radon($\alpha 1$)-polonium($\alpha 2$) correlations. Three groups of $\alpha 2$ decays were observed in correlation with the $\alpha 1$ decay at 7675 keV. In Fig. 5.22(c) these groups are marked as 'A' (4 full-energy events in the PSSD for both $\alpha 1$ and $\alpha 2$), 'B' (26 events), and 'C' (6 events). By considering the escaped events measured by the PSSD + BOX system, the total number of observed events in regions A, B, and C increases to 58.

Decay properties from our data, $E_{\alpha 2} = 6955(8)$ keV and $T_{1/2} = 350^{+240}_{-100}$ ms, for the $\alpha 2$ decay in region A of Fig. 5.22(c) are in agreement with the reported values for the α decay of $^{195}\mathrm{At}^{g}$ ($E_\alpha = 6953(3)$ keV, $T_{1/2} = 328(20)$ ms [Ket03b]). Therefore, we assign the parent $\alpha 1$ decay for region A with an energy

of 7664(11) keV and a half-life of $4.5^{+3.1}_{-1.3}$ ms to ^{199}Fr.

The measured half-lives of 120^{+25}_{-20} ms and 130^{+70}_{-40} ms for the $\alpha 2$ decay of the groups B and C, respectively, correspond to the half-life of ^{195}At^m ($T_{1/2}$ = 147(5) ms [Ket03b]). The measured energy range of $(7040 - 7200)$ keV for $\alpha 2$ decays from region B and $E_{\alpha 2} = 7248(6)$ keV for region C are also in line with the values for α decay of ^{195}At^m (see Fig. 5.23). Therefore we assign the parent $\alpha 1$ decay for events in regions B and C with an energy of 7676(6) keV and a half-life of $6.2^{+1.1}_{-0.8}$ ms to ^{199}Fr.

Small differences in half-lives and α-decay energies for $\alpha 1$ transitions at 7664(11) keV (region A) and 7676(6) keV (regions B and C) may indicate a presence of two different isomeric states in ^{199}Fr decaying to two isomeric states in ^{195}At. However, those differences could also be due to low statistics and limited energy resolution of the PSSD, which would suggest the presence of only one α-decaying state in ^{199}Fr with an α-decay energy of 7675(6) keV and a half-life of $6.0^{+1.0}_{-0.7}$ ms. We present the discussion on both scenarios (see the 'Discussion' part further in this section). Decay properties of ^{199}Fr are summarized in Tab. 5.8. The maximum cross-section for ^{199}Fr production, 3(1) nb, was deduced at the beam energy of 272 MeV ($E^*_{CN} = 31$ MeV).

Tab. 5.8 The α-decay properties of ^{199}Fr. We show here α-decay properties for both proposed decay patterns of ^{199}Fr, [1] and [2] (for more details see the text). Based on present data we cannot make any preference for either of the scenarios.

isotope	I^π	E_α (keV)	$T_{1/2}$ (ms)	δ^2_α (keV)	ref.
^{199}Fr	$7/2^-$	7675(6)	$6.0^{+1.0}_{-0.7}$	85^{+15}_{-11}	this work[1]
	$7/2^-$	7676(6)	$6.2^{+1.1}_{-0.8}$	81^{+15}_{-11}	this work[2]
	$1/2^+$	7664(11)	$4.5^{+3.1}_{-1.3}$	120^{+80}_{-40}	this work[2]
	–	7655(40)	12^{+10}_{-4}	49^{+43}_{-22} [a]	[Tag99]
	$1/2^+$	7644(20)	5^{+7}_{-2}	130^{+120}_{-80}	[Uus13]
	$7/2^-$	7668(15)	7^{+3}_{-2}	80^{+60}_{-30}	[Uus13]
	$13/2^+$	7808(20)	$1.6^{+1.6}_{-0.6}$	120^{+110}_{-70}	[Uus13]

[a] Value of δ^2_α was calculated according to Rasmussen [Ras59] using input values (E_α and $T_{1/2}$) from cited reference.

Discussion

Two α-decaying states are presently known in ^{195}At with assumed spins and parities $7/2^-$ (isomeric state) and $1/2^+$ (ground state). Our data indicate that the α decay of ^{199}Fr with $E_\alpha \approx 7675$ keV is correlated with α decays from both states, ^{195}At^m and ^{195}At^g. We present two possible scenarios for this observation as our data do not allow to discriminate between them.

1st scenario One possible interpretation illustrated in the left panel of Fig. 5.23 is that two α-decaying states exist in ^{199}Fr with similar decay characteristics: 12(5) % of the decays having an α-decay energy of 7664(11) keV and a half-life of $4.5^{+3.1}_{-1.3}$ ms populating ^{195}At^{g} (region A in Fig. 5.22(c)), and 88(5) % decays with an α-decay energy of 7676(6) keV and a half-life of $6.2^{+1.1}_{-0.8}$ ms populating ^{195}At^{m} (regions B and C in Fig. 5.22(c)). Following this scenario, the reduced α-decay widths (δ^2_α) calculated using the Rasmussen prescription [Ras59] assuming $\Delta L = 0$ for transitions populating ^{195}At^{g} and ^{195}At^{m} are 120^{+80}_{-40} and 81^{+15}_{-11} keV, respectively. These values are comparable with the reduced α-decay width of the heavier isotope ^{201}Fr ($\delta^2_\alpha = 75(8)$ keV). The hindrance factors (HFs) for these transitions of $0.7^{+0.5}_{-0.2}$ and 1.1(2), respectively, were evaluated by comparing the δ^2_α of these transitions with those of neighboring even-even isotopes ($\delta^2_\alpha(^{198}\mathrm{Rn}) = 111(6)$ keV, $\delta^2_\alpha(^{200}\mathrm{Rn}) = 64^{+11}_{-3}$ keV). The values of HFs indicate unhindered decays for both transitions. Therefore, spins and parities of the α-decaying levels in ^{199}Fr should be the same as in the daughter ^{195}At. Ratio of the transitions (12(5) % for $E_\alpha = 7664$ keV and 88(5) % for $E_\alpha = 7676$ keV) agree with the expectation of the higher population of high-spin states in comparison with low-spin states in complete-fusion reactions. In this scenario, based on the 32(7)-keV excitation energy of ^{195}At^{m} [Ket03b], the level in ^{199}Fr decaying to ^{195}At^{m} lies 47(7) keV above the level decaying to ^{195}At^{g}. An estimated upper limit for the deexcitation of the $7/2^-$ state in ^{195}At by an $E3$ internal transition to the ground $1/2^+$ state is 5 %. The corresponding upper limit for the $B(E3)$ value of this possible (unobserved) $E3$ internal transition between the $7/2^-$ and $1/2^+$ levels in ^{195}At is $B(E3) < 0.03$ Weisskopf units.

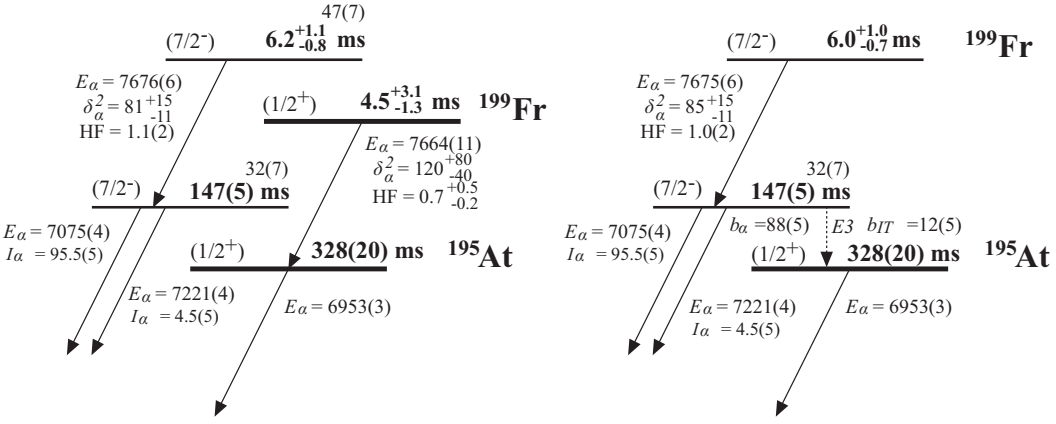

Fig. 5.23 Two possible α-decay schemes suggested for ^{199}Fr. The values for ^{199}Fr are from our measurement and for ^{195}At are from [Ket03b]. All spin and parity values are tentative. Alpha-decay energies, reduced width and energies of excited levels are in keV. Relative intensities and branching ratios are in %.

2nd scenario There is an alternative interpretation of our data, which is illustrated in the right panel of Fig. 5.23. As the energies of the $\alpha 1$ decays correlated with the $\alpha 2$ decays from $^{195}\mathrm{At}^m$ and $^{195}\mathrm{At}^g$ are comparable within their statistical uncertainty, they may represent the same α decay from only one α-decaying state in ^{199}Fr with an α-decay energy of 7675(6) keV and a half-life of $6.0^{+1.0}_{-0.7}$ ms. This transition populates an isomeric $7/2^-$ level in ^{195}At, which is required to have two decay modes in this scenario: α decay ($b_\alpha = 88(5)\,\%$) and deexcitation through an unobserved 32(7)-keV $E3$ internal transition to the ground state ($b_{IT} = 12(5)\,\%$). The $B(E3)$ value for the $E3$ internal transition is $0.09^{+0.14}_{-0.05}$ W.u. in this scenario. A similar value of 0.09 W.u. was deduced for the $E3$ internal transition connecting the same levels, $1/2^+$ and $7/2^-$, in ^{191}Bi, the α-decay daughter of ^{195}At [Ket03b]. The reduced α-decay width for the 7675(6)-keV transition is 85^{+15}_{-11} keV and the HF value is 1.0(2) indicating an unhindered decay. Therefore, in this scenario, we would assign a spin and parity of $7/2^-$ to the observed α-decaying state in ^{199}Fr.

***Experiment at* RITU** Shortly after our conclusions had been published [Kal13a], results of decay studies of ^{198,199}Fr produced at RITU at JYFL were reported [Uus13]. In that measurement, ^{199}Fr was produced in the $2n$ evaporation channel of the same fusion-evaporation reaction, $^{60}\mathrm{Ni} + ^{141}\mathrm{Pr}$, like in our experiment. Three α lines originating from ^{199}Fr were reported. The identification of the first one was based on three ER-$\alpha 1$-$\alpha 2$(-$\alpha 3$) correlations yielding $E_\alpha = 7644(20)$ keV and $T_{1/2} = 5^{+7}_{-2}$ ms. The decay was attributed to the ground state of ^{199}Fr with tentative spin and parity $1/2^+$. The identification of the second α line was based on 17 ER-$\alpha 1$-$\alpha 2$(-$\alpha 3$) correlation chains yielding $E_\alpha = 7668(15)$ keV and $T_{1/2} = 7^{+3}_{-2}$ ms. The identification of the third α line was based on four correlations yielding $E_\alpha = 7808(20)$ keV and $T_{1/2} = 1.6^{+1.6}_{-0.6}$ ms. In three correlation chains, implantation of ER was followed by parent and daughter α decay, while one correlation chain was composed of ER implantation followed by parent and granddaughter α decay. The second and third α lines were attributed to the decays of isomeric states with tentative spins and parities $7/2^-$ and $13/2^+$, respectively.

Alpha-decay properties for ^{199}Fr obtained from our data are in line with the values measured at GARIS [Tag99] and also agree with two α lines observed at RITU [Uus13] (see Tab. 5.8). Relative intensities of the decays of ^{199}Fr correlated to $1/2^+$ and $7/2^-$ states in ^{195}At from our data, 12(5) and 88(5) %, respectively, agree with relative intensities of 15(8) and 85(8) % for corresponding decays observed at RITU [Uus13], where the possibility of both decays being actually one α transition is also discussed. Despite (more than two times) higher statistics in our data, we did not confirm the α line reported at RITU at 7808(20) keV with $T_{1/2} = 1.6^{+1.6}_{-0.6}$ ms. We attributed the activity with similar characteristics

($T_{1/2} = 1.1(7)$ ms and α-decay energy in the range from 7580 to 7930 keV) seen in our data to the isotope ^{198}Fr (see next Sect. 5.2.2 on ^{198}Fr for more details). We remind that we did not make any conclusions from the measurement at a beam energy of 276 MeV, where both ^{199}Fr and ^{199}Fr were produced, because of their similar decay properties. However, the measurement at RITU was performed only at one beam energy, at which both isotopes were produced.

To summarize, significantly improved data for ^{199}Fr were obtained in our work, which can be interpreted in two possible ways (see the decay schemes in Fig. 5.23). No preference for either of the scenarios can be expressed due to the relatively low statistics. To confirm one of the scenarios we would need more statistics to decide whether there is one or two α lines in the α-decay energy spectrum of ^{199}Fr. For the discussion of the energy-level systematics for francium isotopes see Sect. 5.1.6. We note that in heavier neutron-deficient odd-A francium isotopes, the ground state is presumably spherical with spin and parity $9/2^-$. As we did not observe decays of this state in ^{199}Fr, our data imply a possible change in the ground-state deformation for francium isotopes from $A = 199$, as both $1/2^+$ and $7/2^-$ states are presumably oblate.

5.2.2 Isotope ^{198}Fr

Experimental data known prior to this work

No registered decay events of ^{198}Fr were reported prior to this study. However, shortly after our conclusions had been published [Kal13a], results from the study of experimental decay properties of ^{198}Fr performed at RITU at JYFL were reported [Uus13]. We will discuss results from RITU later in this section.

Our experimental results

We collected the data for the isotope ^{198}Fr at several beam energies in the range of $(282-300)$ MeV in front of the target resulting in the excitation energy of $(38-51)$ MeV of the compound nucleus ^{201}Fr*. The energy range was chosen to cover the maximum of the $3n$ evaporation channel and to minimize the contribution from ^{199}Fr produced in the $2n$ evaporation channel.

ER-α1-α2 correlations A part of the α-decay spectrum from 6400 to 8000 keV measured in the PSSD in anticoincidence with the TOF system is shown in Fig. 5.24(a). The dominant α lines belong to polonium isotopes produced in the αpxn evaporation channels and astatine isotopes produced in the $2pxn$ or αxn evaporation channels. Within 80 ms after ER implantations, α1 decays with a broad energy distribution in the range of $(7470 - 7930)$ keV were detected (see Fig. 5.24(b)). The spectrum of parent-daughter α1-α2 correlations shown in Fig. 5.24(c) was obtained by applying the condition $\Delta t(\alpha 1\text{-}\alpha 2) < 1.5$ s. The

dominant groups in this spectrum are decays of ^{198,197}Rn (α1) produced in the *pxn* evaporation channels correlated with their daughters ^{194,193}Po (α2).

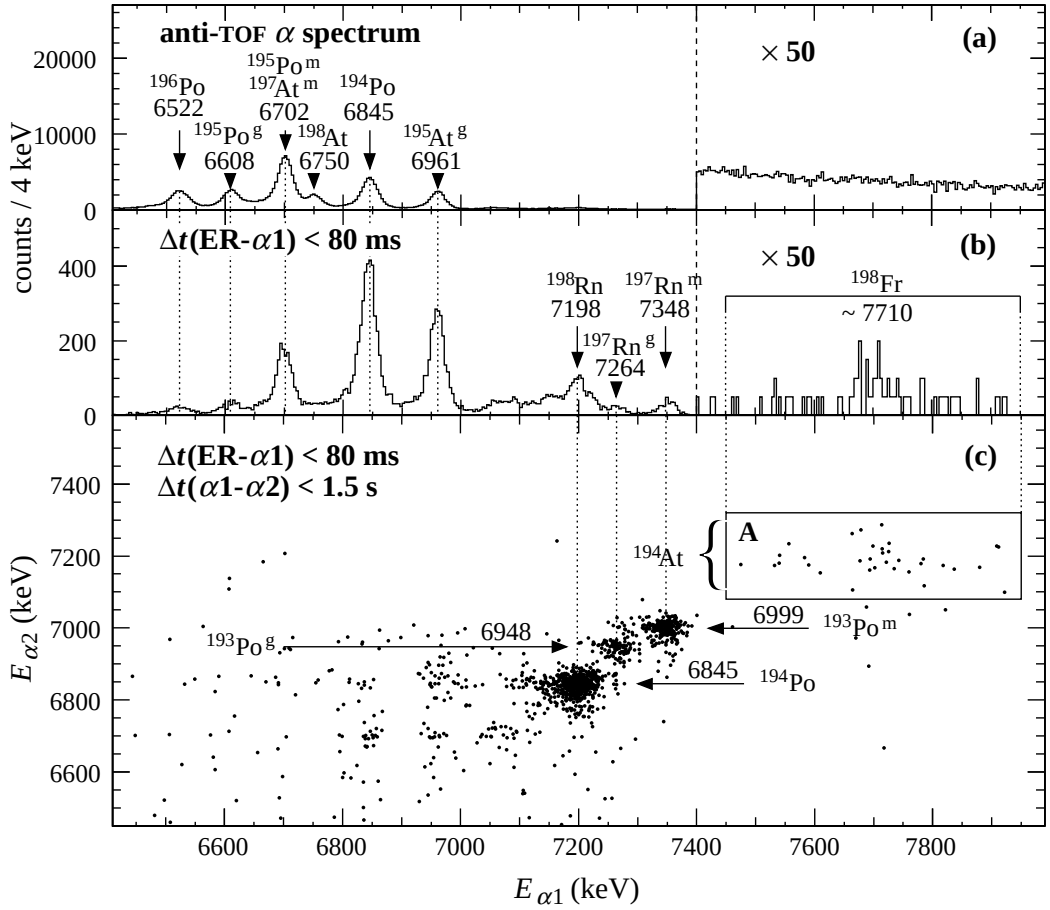

Fig. 5.24 (a) The sum of α-decay energy spectra measured in the PSSD in anticoincidence with the TOF detectors in the reaction ^{60}Ni + ^{141}Pr at several beam energies in the range of (282 − 300) MeV. (b) α decays from (a) detected within 80 ms after ER implantation. (c) Parent-daughter α1-α2 correlation spectrum. α2 decays were detected within 1.5 s after α1 decays from (b).

The α1 decays in region 'A' of Fig. 5.24(c) are correlated with an α2 activity with a half-life of 210^{+30}_{-20} ms. This value is in agreement with the half-life of 253(10) ms for ^{194}At^{m1} and compatible within 3σ intervals with the half-life of 310(8) ms for ^{194}At^{m2} [And09]. The measured energy distribution of α2 decays in the range of (7140 − 7290) keV agrees with reference values for both ^{194}At^{m1} and ^{194}At^{m2}, for which two main α lines were observed at 7178(15) and 7190(15) keV [And09]. Based on the ER-α1-α2 analysis, we attribute the parent decay in region A of Fig. 5.24(c) to the isotope ^{198}Fr.

In total 72 ER-α1-α2 (^{198}Fr-^{194}At) correlation chains were detected including events with coincidence signals between the PSSD and BOX system; 37 events were registered with full-energy release in the PSSD. Despite the overlapping α-decay energy regions of ^{198}Fr and ^{199}Fr, both isotopes can be clearly distinguished using different beam energies for their production. For ^{199}Fr a single peak at 7675 keV was observed (see Fig. 5.25(a)), while for ^{198}Fr a broad α-decay energy range of $(7470 - 7930)$ keV was measured (see Fig. 5.25(b)).

Time distribution Time distribution of ^{198}Fr decays can be explained by a presence of two components (see Fig. 5.26). The fit to the experimental decay curve was obtained with a combination of a shorter-lived component with a half-life of 1.1(7) ms and a longer-lived component with a half-life of 15(3) ms. We used the binned-likelihood fit method, as it reproduces experimental data

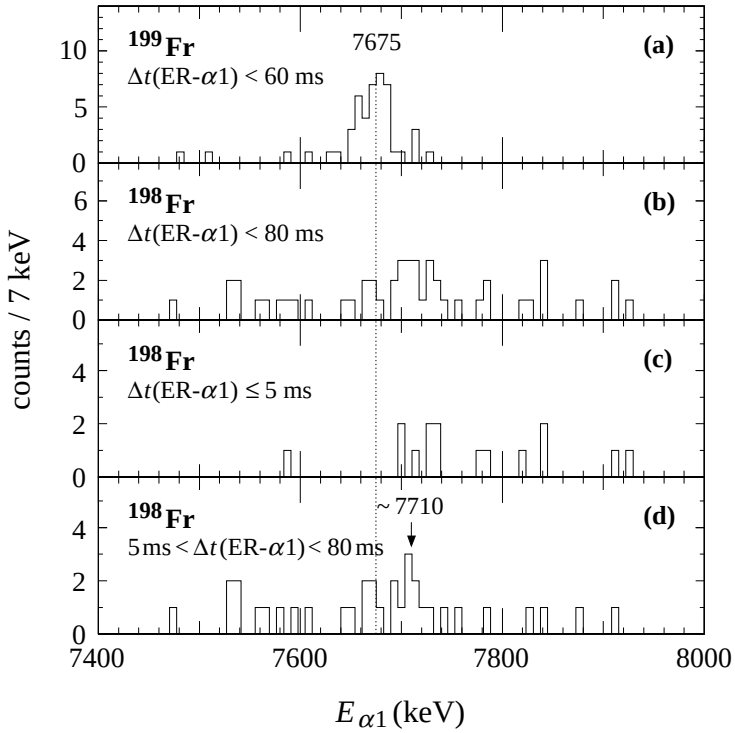

Fig. 5.25 Alpha-decay energy spectra measured in the PSSD in anticoincidence with the TOF system in the reaction ^{60}Ni + ^{141}Pr. (a) Events measured at several beam energies in the range of $(262 - 272)$ MeV attributed to α1 decays of ^{199}Fr. These events were correlated with α2 decays of ^{195}At (including escaped α particles recorded by the PSSD + BOX system). Used time windows for correlation search: Δt(ER-α1) < 60 ms and Δt(α1-α2) < 1.5 s. (b) Events measured at several beam energies in the range of $(282 - 300)$ MeV attributed to α1 decays of ^{198}Fr. These events were correlated with α2 decays of ^{194}At. Used time windows for correlation search: Δt(ER-α1) < 80 ms and Δt(α1-α2) < 1.5 s. (c) α decays from (b) occurring within 5 ms after ER implantations. (d) α decays from (b) occurring between 5 and 80 ms after ER implantations.

based on low statistics better than the chi-square fit method. Within the limited statistics, the α-decay energy distribution of the shorter-lived state seems to be concentrated at energies higher than 7700 keV (see Fig. 5.25(c)). In contrast to this, the α decay of the longer-lived state has a broader energy distribution in the range of $(7470 - 7920)$ keV with an indication of a distinct α line at ~ 7710 keV (see Fig. 5.25(d)).

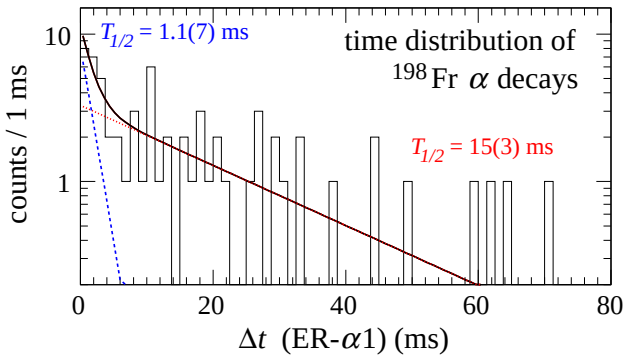

Fig. 5.26 The decay curve of ^{198}Fr (for the events from Fig. 5.25(b) including the escaped events detected by the PSSD + BOX system). The fit function was obtained as a combination of two exponential components with half-lives of 1.1(7) (blue dashed line) and 15(3) ms (red dotted line). The total decay curve as a sum of exponential components is drawn by a black solid line.

α3 decay The granddaughter α3 decay was searched for within a correlation time of 10 s after an α2 decay. The detected α3-decay energy was in the range of $\sim (6410 - 6475)$ keV corresponding to ^{190}Bi^{m1,m2} (see Fig. 5.27). (Reference values for ^{190}Bi are: $E_\alpha = 6431(5)$ keV, $T_{1/2} = 6.3(1)$ s for ^{190}Bi^{m1}, and $E_\alpha = 6456(5)$ keV, $T_{1/2} = 6.2(1)$ s for ^{191}Bi^{m2} [Van91, Huy88].) The lower number of α3 decays in Fig. 5.27 compared to the number of events in Fig. 5.24(c) (region A) is due to the α-decay branching ratio of ^{190}Bi ($b_\alpha = 90^{+10}_{-30}$ % for ^{190}Bi^{m1} and $b_\alpha = 70(9)$ % for ^{190}Bi^{m2} [Van91]) and the limited α2-α3 correlation time. The α3 decays also support the presence of two states in ^{198}Fr. The α1 decays with Δt(ER-α1) ≤ 5 ms correlate with the ~ 6415- and ~ 6460-keV decays from both ^{190}Bi^{m1} and ^{190}Bi^{m2} states (see Fig. 5.27(a)), while the α1 decays with Δt(ER-α1) > 5 ms only correlate with ~ 6425-keV decays of ^{190}Bi^{m1} (see Fig. 5.27(b)). For the summary of α-decay characteristics of both isomers in ^{198}Fr see Tab. 5.9.

The observation of two different half-lives (1.1(7) and 15(3) ms) and different energy distributions for the decay of ^{198}Fr (see Figs. 5.25(c) and 5.25(d)) implies two isomeric states in this isotope. Furthermore, α1 decays of ^{198}Fr with Δt(ER-α1) > 5 ms are correlated only with α3 decays of ^{190}Bi^{m1} (see Fig. 5.27(b)), while α1 decays with Δt(ER-α1) ≤ 5 ms seem to be followed by α3 decays from both

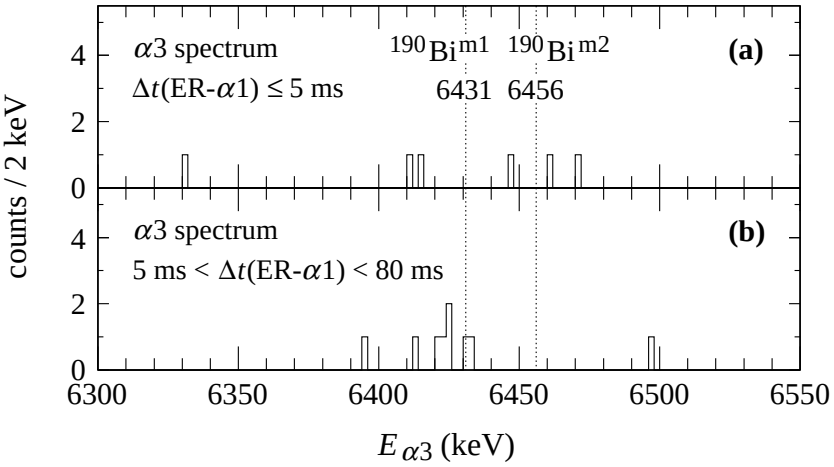

Fig. 5.27 The ^{198}Fr granddaughter α3-decay energy spectrum correlated with events from region A of Fig. 5.24(c) within 10 s. The dotted lines represent the reference energies [Van91] for ^{190}Bi^{m1,m2}. (a) α3 decays correlated with α1 decays of ^{198}Fr with Δt(ER-α1)$\leq$ 5 ms. (b) α3 decays correlated with α1 decays of ^{198}Fr with 5 ms$<\Delta t$(ER-α1)$<$ 80 ms.

Tab. 5.9 The α-decay properties of ^{198}Fr.

isotope	I^π	E_α (keV)	I_α (%)	$T_{1/2}$ (ms)	δ^2_α (keV)	ref.
^{198}Fr	–	7580 − 7930		1.1(7)	30 − 380	this work
	–	7470 − 7920	∼50	15(3)	1 − 30	this work
	–	∼7710	∼50	15(3)	14(6)	this work
	2^-	7613(15)		15^{+12}_{-5}	60^{+40}_{-30}	[Uus13]
	6^+,7^+	7684(15)		16^{+13}_{-5}	30(20)	[Uus13]

^{190}Bi^{m1} and ^{190}Bi^{m2} (see Fig. 5.27(a)). However, the appearance of correlations with decays from ^{190}Bi^{m1} for α1 decaying with Δt(ER-α1) $\leq$ 5 ms is most probably due to the contribution of α decays from the 15(3)-ms state within 5 ms after ER implantation. Therefore, we assume that the shorter-lived state decays predominantly to ^{190}Bi^{m2} and the longer-lived state decays to ^{190}Bi^{m1} (see the proposed decay scheme in Fig. 5.28). From the total number of ^{198}Fr decays and their time distribution after ER implantations (see Figs. 5.25(c),(d) and 5.26) we estimate a population of 15(5) % for the 1.1-ms state and 85(5) % for the 15-ms state. At the beam energy of 282 MeV (E^*_{CN} = 38 MeV), a maximum production cross-section of 1.3(3) nb was deduced for the sum of the two isomers in ^{198}Fr.

α-γ coincidences Searching for ER-(α1-γ)-α2-α3 correlations, two photons with an energy of 81.5(7) keV were detected in coincidence with 7836(14)-keV α1 decays. The energy of these photons agrees with the energy of $K_{\alpha1}$ X-rays of astatine (reference values: $E_{K_{\alpha1}}$ = 81.517 keV, I_{rel} = 46.1(9) % [Fir96]). The

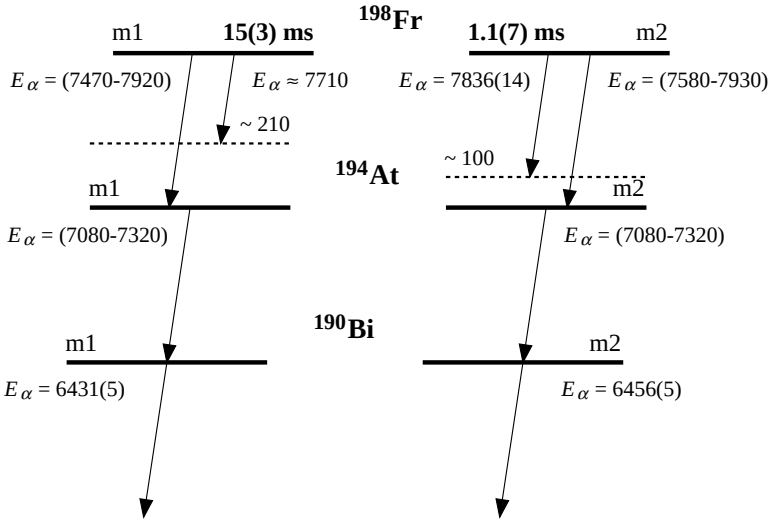

Fig. 5.28 Proposed simplified decay schemes for two α-decaying states in ^{198}Fr. The order and energy difference between the isomeric states are not known. As the α-decay energy distributions of both states are ranging over several hundreds of keV, we note that the depicted decays of $^{198}\mathrm{Fr}^{m1,m2}$ may also include transitions to low-lying excited states over $^{194}\mathrm{At}^{m1,m2}$. Energy of excited level and α-decay energies are in keV.

Q_α value for the 7836(14)-keV α transition is $Q_{\alpha(7836)} = 7998(14)$ keV. The time differences between the implantations of ERs and the detection of the α1-γ coincidences were 3.3 and 4.7 ms. Although the α2 particle from one decay chain was only registered with part of its energy in the PSSD, the α3 particle was fully stopped in the PSSD for both decay chains. The energies of the α3 decays, 6470(15) and 6461(15) keV, are consistent with the 6456(5)-keV α decay of $^{190}\mathrm{Bi}^{m2}$. Based on the energies of correlated α3 decays corresponding to the decay of $^{190}\mathrm{Bi}^{m2}$ and on the time differences between ERs and α1 decays (both within 5 ms), the α1-γ coincidences belong to the decay of $^{198}\mathrm{Fr}^{m2}$.

Discussion

In the even-A francium isotope ^{200}Fr only one α-decaying state has been observed so far (see Sect. 5.1.5), while in ^{202,204,206}Fr at least two α-decaying states have been identified [Huy92]. In ^{198}Fr we observed two α decaying states as well (see the proposed decay scheme in Fig. 5.28).

The broad α-decay energy distribution with a hint of a peak at $\sim$7710 keV for ^{198}Fr indicates its complex decay pattern (see Figs. 5.24(b), 5.24(c) (region A) and 5.25(b)). For the 15(3)-ms state, if one assumes a relative intensity of $\sim$50 % for the $\sim$7710-keV α line (see Fig. 5.25(d)), then $\delta^2_\alpha \approx 10$ keV can be deduced. This value suggests a hindrance (by about a factor of 10) of the $\sim$7710-keV transition relative to both ^{199}Fr ($\delta^2_\alpha = (81 - 120)$ keV) and neighboring even-

even nuclei ($\delta^2_\alpha(^{196}\mathrm{Rn}) = 250^{+80}_{-50}\,\mathrm{keV}$, $\delta^2_\alpha(^{198}\mathrm{Rn}) = 111(6)\,\mathrm{keV}$, $\delta^2_\alpha(^{200}\mathrm{Rn}) = 64^{+11}_{-3}\,\mathrm{keV}$). This decay should populate an excited state at $\sim$210 keV in ^{194}At (see Fig. 5.28), as α decays from 15(3)-ms state have energies up to $\sim$7920 keV. We assume that this level deexcites partly through internal conversion, as we did not detect any $\sim$210-keV γ rays in coincidence with the α decays of ^{198}Fr. The energy summing of an α particle and conversion electrons can also explain the broad α-decay energy distribution of this state (see Fig. 5.25(d)). However, the non-observation of γ rays at $\sim$210 keV can also be explained by the low statistics and a detection efficiency of only $\sim$8.5 % for γ rays with $E_\gamma \approx 200\,\mathrm{keV}$ (see the γ-ray detection efficiency curve in Fig. 4.3 in Sect. 4.1.2) or by the existence of other levels below the $\sim$210-keV state and then the deexcitation through a cascade of lower-energy transitions instead of a single transition. As there is a strong contribution of α decays below 7710 keV, also at least one level above $\sim$210 keV must be populated by the α decay of ^{198}Fr.

α-γ coincidences We may assume that the α decays of $^{198}\mathrm{Fr}^{m2}$ with the highest energy ($E_\alpha \approx 7930\,\mathrm{keV}$, see Fig. 5.25(b)) connect the 1.1(7)-ms level in ^{198}Fr directly with the $^{194}\mathrm{At}^{m2}$ level. The Q_α value of these decays is $Q_{\alpha(7930)} \approx 8090\,\mathrm{keV}$. In the decay of $^{198}\mathrm{Fr}^{m2}$ we detected α-γ coincidences with $E_\alpha = 7836(14)\,\mathrm{keV}$, $Q_{\alpha(7836)} = 7998(14)\,\mathrm{keV}$, and $E_\gamma = 81.5(7)\,\mathrm{keV}$ corresponding to K X-rays of astatine. Since the K X-rays were detected, the excitation energy of the level populated by the 7836(14)-keV α decay must be higher than the K-binding energy of astatine ($E_B = 96\,\mathrm{keV}$ [Fir96]).

The difference between the $Q_{\alpha(7836)}$ and $Q_{\alpha(7930)}$ values, which could give an excitation energy of the level populated by the 7836(14)-keV transition, is $\approx$ 90 keV. As this value is close to the K-binding energy of astatine ($E_B = 96\,\mathrm{keV}$), we may assume that the 7836(14)-keV α transition populates the level with E^* only slightly higher than E_B. As a result the emitted conversion electron would have a very low energy, which would be summed with the α-particle energy. In this case we can roughly estimate the excitation energy of the level populated by the 7836(14)-keV transition to be $\sim$100 keV.

However, the detected photons could also be γ-ray transitions that by chance have the same energy as $K_{\alpha 1}$ X-rays of astatine, which would lower the limit for the E^* of the level populated by the 7836(14)-keV α transition to 82 keV.

***Experiment at* RITU** Shortly after our conclusions on the decay properties of ^{198}Fr had been published [Kal13a], the results on ^{198}Fr decay measured at RITU were reported [Uus13]. In that measurement, ^{198}Fr was produced in the $3n$ evaporation channel of the same fusion-evaporation reaction, $^{60}\mathrm{Ni} + ^{141}\mathrm{Pr}$, like in our study. Two α lines were reported at 7613(15) and 7684(15) keV with half-lives of 15^{+12}_{-5} and 16^{+13}_{-5} ms, respectively. For each α line five ER-α1-α2(-α3) decay chains were observed.

In contrast to two α peaks at 7613(15) and 7684(15) keV observed at RITU [Uus13], we detected two broad α-decay energy distributions ranging from about 7500 keV and exceeding 7900 keV for both decays. Unlike our data, the 1.1-ms state state in ^{198}Fr was not observed at RITU [Uus13]. This is consistent with our data, as we estimated only a 15(5) % intensity for the 1.1-ms state compared to an 85(5) % intensity for the 15-ms state and at RITU only 10 decays were observed in total for ^{198}Fr. We recall that an α-decaying state with $T_{1/2} = 1.6$ ms was observed at RITU, but it was attributed to ^{199}Fr (see previous Sect. 5.2.1 on ^{199}Fr).

In summary, the isotope ^{198}Fr was identified and an indication for two isomeric states was observed. Due to the complexity of the data and the limited statistics only a simplified decay scheme is proposed (see Fig. 5.28).

5.2.3 New isotope ^{197}Fr

Prior to our study, no experimental information on the decay of ^{197}Fr was reported.

Our experimental results

ER-α1-α2-α3 correlation chain We observed one ER-α1-α2-α3 correlation chain with Δt(ER-α1) = 0.9 ms and $E_{\alpha 1}$ = 7728(15) keV (see Fig. 5.29) at a beam energy of 300 MeV. This energy was chosen intentionally for the $4n$ evaporation channel and resulted in a 51-MeV excitation energy of a compound nucleus ^{201}Fr*. The α1 decay was followed by a 7375(30)-keV α2 decay after 45 ms. The granddaughter 6665(30)-keV α3 decay was detected 294 ms after the α2 decay. The α1 particle was fully stopped in the PSSD, while the α2 and α3 particles escaped from the PSSD, but their residual energies were registered by the BOX system. The α1 and α2 decays were registered in the pause between beam pulses, while the α3 decay was detected in the pulse. The decays were registered in the middle part of the PSSD (strip No. 10 and about 1/3 of the strip length). The positions from the bottom and top of the strip are shown in Fig. 5.29.

The energy of the ER before the implantation into the PSSD calculated by LISE++ [Tar08] is 73 MeV. The registered energy of implanted ER was only 47.2 MeV. The detected energy is lower than the expected energy due to the pulse-height defect, which may be up to several tens of % [Ant01].

Fig. 5.30 shows the location of the ER in a two-dimensional plot showing the time of flight and energy of implanted particles. In this figure, the group of events from the bottom to the upper right corner comprises the scattered projectiles, events in the middle are complete-fusion reaction products, and below them are the scattered target or target-like nuclei from elastic scattering

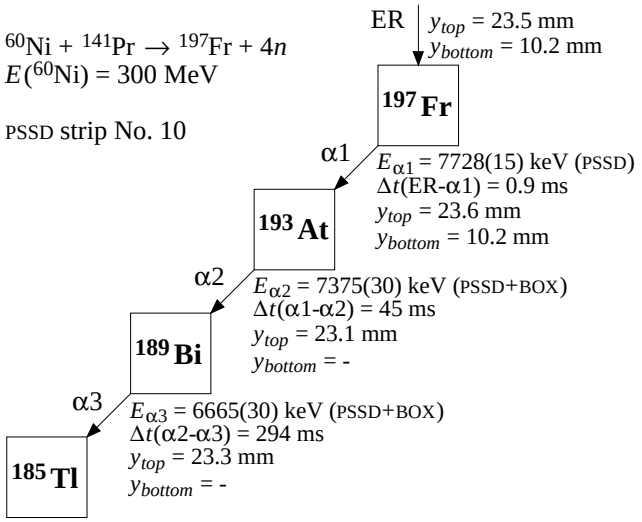

Fig. 5.29 Correlation α-decay chain attributed to ^{197}Fr observed in the reaction $^{60}\mathrm{Ni} + ^{141}\mathrm{Pr}$ at $E_{beam} = 300\,\mathrm{MeV}$. Measured energies, time differences between subsequent signals, and positions obtained from the top and bottom of the strip are shown. In the case of the escaped α particles $\alpha 2$ and $\alpha 3$, the signals from the bottom of the strip were too low for detection.

or transfer reactions, respectively.

We associate the daughter $\alpha 2$ decay with the known α decay of the $7/2^-$ state in ^{193}At (reference values: $E_\alpha = 7325(5)\,\mathrm{keV}$, $T_{1/2} = 21(5)\,\mathrm{ms}$ [Ket03a]) and the granddaughter $\alpha 3$ decay with the decay of the $9/2^-$ state in ^{189}Bi (reference values: $E_\alpha = 6667(4)\,\mathrm{keV}$, $T_{1/2} = 580(25)\,\mathrm{ms}$ [Ket03a]). Therefore we attribute the parent 7728(15)-keV $\alpha 1$ decay with a half-life of $0.6^{+3.0}_{-0.3}\,\mathrm{ms}$ to the new isotope ^{197}Fr (see Tab. 5.10).

Tab. 5.10 The α-decay properties of ^{197}Fr.

isotope	I^π	E_α (keV)	$T_{1/2}$ (ms)	δ^2_α (keV)	ref.
^{197}Fr	$7/2^-$	7728(15)	$0.6^{+3.0}_{-0.3}$	600^{+2900}_{-300}	this work

The probability of detecting such a triple-α correlation chain randomly, calculated using the method from Ref. [Sch84], is 10^{-9}. The probability includes the detection of a chain with $\Delta t(\mathrm{ER}\text{-}\alpha 1) < 60\,\mathrm{ms}$, $\Delta t(\alpha 1\text{-}\alpha 2) < 150\,\mathrm{ms}$ and $\Delta t(\alpha 2\text{-}\alpha 3) < 2\,\mathrm{s}$. The energy windows were set to include the range corresponding to decays of the $7/2^-$ state in ^{193}At and $9/2^-$ state in ^{189}Bi for the $\alpha 2$ and $\alpha 3$ decays, respectively. The energy window for the parent $\alpha 1$ decay was set to $(7500 - 8000)\,\mathrm{keV}$. Another argument for the correlation chain not being

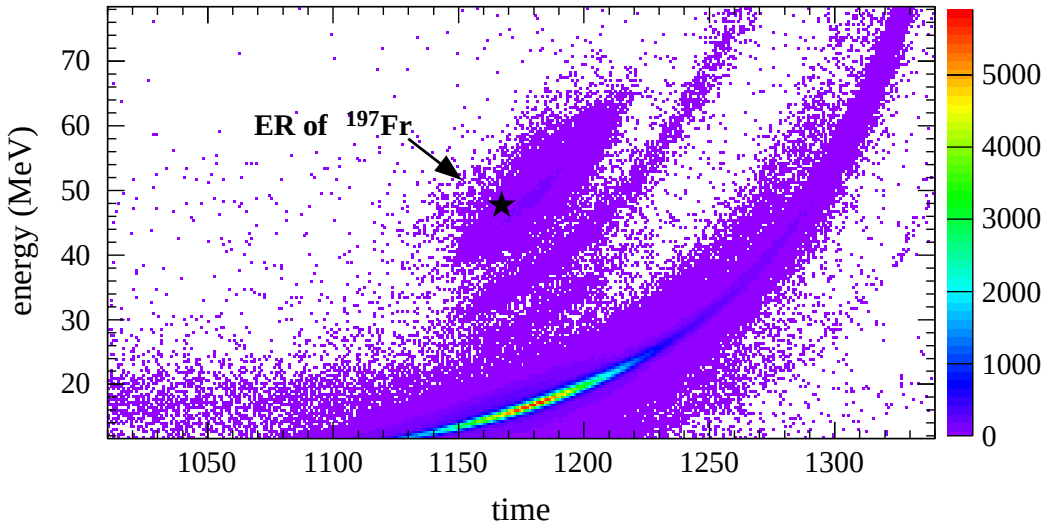

Fig. 5.30 A two-dimensional plot showing time of flight (horizontal axis) and energy (vertical axis) of implanted particles. A position of the evaporation residue (ER) attributed to ^{197}Fr is marked by the black full star. The color scale corresponds to the number of events in one pixel. Events in the middle are complete-fusion reaction products, below them are the scattered target or target-like nuclei from elastic scattering or transfer reactions, respectively, and the most numerous group of events from the bottom to the upper right corner are the scattered projectiles. Time on the horizontal axis is not calibrated and is in reverse order: higher values correspond to shorter times of flight and vice versa.

random is that the $\alpha 1$, $\alpha 2$ and $\alpha 3$ decays have energies different from energies of the most intensive peaks present in the α-decay energy spectrum detected at considered beam energy of 300 MeV (see Fig. 5.31).

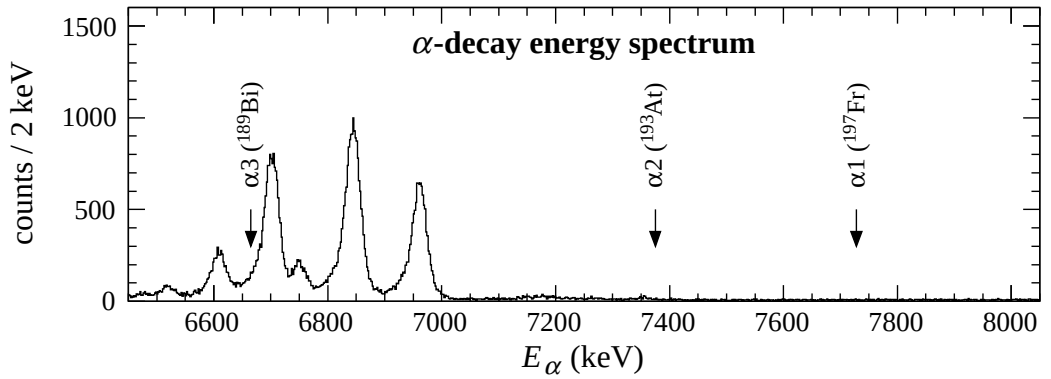

Fig. 5.31 A part of the α-decay energy spectrum measured in the PSSD in anticoincidence with the TOF system in the reaction ^{56}Fe + ^{141}Pr at E_{beam} = 300 MeV. The positions of α particles from the ER-α1-α2-α3 correlation chain attributed to the decay of ^{197}Fr are marked by arrows.

We were also searching for the decay of the next member of the ^{197}Fr correlation chain, ^{185}Tl^m. The isomeric 1.93(8)-s level at 454.8(15) keV in ^{185}Tl decays

predominantly by a cascade of two internal transitions with energies 168.8 and 284 keV to the ground state [nndc]. It also has a small α branch with a probability of around 2 %. We registered neither an α particle nor an electron-γ coincidence from the decay of ^{195}Tl^m within a 10-s correlation time after the α3 decay from ^{189}Bi. Looking for a single γ-ray decay (without coincidence with an electron) is impossible due to high rate of random (background) γ rays. The ground state of ^{185}Tl undergoes an electron capture with a half-life of 19.5(5) s. This half-life itself is too long for a correlation search, and moreover, the SHIP setup is not optimized for the detection of signals from the electron-capture process (high rate of background γ rays and an energy threshold for electrons of around 300 keV for this experiment).

A careful search for a possible proton emission of ^{197}Fr was made by searching for ER-proton-α(^{196}Rn) correlations, but no evidence for this was found. The expected half-life for the proton emission according to [Med07] is 2.1E+4 s. Assuming one recorded α particle and zero protons from the decay of ^{197}Fr, we estimated the lower limit for the partial proton-emission half-life to be more than 6 ms. Our estimate is consistent with the predicted half-life.

The Q_α value of the 7728(15)-keV decay is 7888(15) keV. The production cross-section of ^{197}Fr was determined as 18^{+41}_{-15} pb at $E_{beam} = 300$ MeV ($E^*_{CN} =$ 51 MeV).

Discussion

The reduced α-decay width for the α transition at 7728(15) keV attributed to the decay of ^{197}Fr is 600^{+2900}_{-300} keV. This suggests a HF of $0.3^{+1.5}_{-0.2}$ compared to neighboring even-even isotopes ($\delta^2_\alpha(^{194}\text{Rn}) = 270(60)$ keV, $\delta^2_\alpha(^{196}\text{Rn}) = 250^{+80}_{-50}$ keV, $\delta^2_\alpha(^{198}\text{Rn}) = 111(6)$ keV). Although the uncertainty is large, the very low HF value indicates an allowed transition. Therefore, we assume no spin or parity change between the levels connected by this transition.

In ^{193}At, the $1/2^+$ and $7/2^-$ levels were observed to be very close in energy and it is presently not known unambiguously which one of them represents the ground state [Ket03a]. The α-decay energy and half-life for the α2 decay correlated with the parent ^{197}Fr decay agree with the α-decay properties of the $7/2^-$ state in ^{193}At (see Fig. 5.32). Based on the unhindered nature of the 7728(15)-keV α1 decay, we assume that it originates from the $7/2^-$ state in ^{197}Fr. This would also be in agreement with the expected higher population of higher-spin states compared with lower-spin states in complete-fusion reactions.

Assuming that the detected 7728(15)-keV decay originates from the ground state of ^{197}Fr, we calculated a mass of 183.47099(8) GeV for ^{197}Fr. The corresponding atomic mass excess is 11.7(1) MeV. This value follows the trend of masses of francium isotopes (see Fig. 5.33(a)). We compared experimental values of atomic mass excess with predictions made by several theoretical models

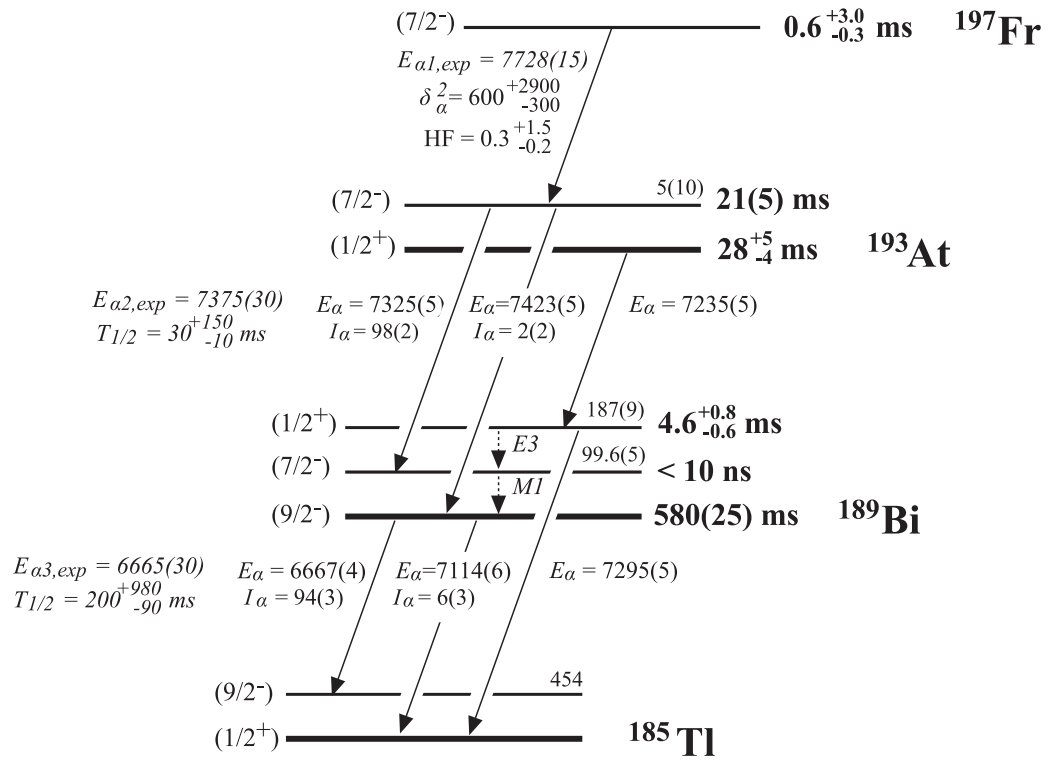

Fig. 5.32 The proposed decay scheme for ^{197}Fr. The reference values for decays of ^{193}At and ^{189}Bi are from Ref. [Ket03a]. The experimental values for $\alpha 1$, $\alpha 2$, and $\alpha 3$ decays from our measurement are written in bold italic font. Alpha-decay energies, reduced width and energies of excited levels are in keV and relative intensities are in %.

[lbnl] (see Fig. 5.33(b)). Commonly used finite-range droplet model (FRDM) [Möl95] reproduces experimental data well down to $A = 200$, but for the lightest francium isotopes, ^{199}Fr and ^{197}Fr, its predictions differ from experimental data by up to 2 MeV. On the other hand, finite-range liquid-drop model (FRLDM) [Möl95], which gives values differing from experimental data by about 1 MeV for masses between 200 and 205, reproduces the experimental mass of ^{197}Fr very precisely (within a 1σ interval).

Systematics of reduced α-decay widths The δ^2_α systematics for odd-A francium, astatine and even-A radon isotopes in the vicinity of the shell closure $N = 126$ are shown in Fig. 5.34. The francium isotopes exhibit a trend of increasing δ^2 at decreasing neutron number from $N = 126$ down to $N = 114$. The value of the reduced α-decay width for ^{199}Fr ($N = 112$) in the range of $(81 - 120)$ keV (depending on the considered scenario, see the Discussion in Sect. 5.2.1) obtained from our data indicates no significant change compared to ^{201}Fr. However, the deduced reduced α-decay width for ^{197}Fr of 600^{+2900}_{-300} keV is considerably larger than in the heavier isotopes ^{199,201}Fr (see Fig. 5.34). Neighboring even-even

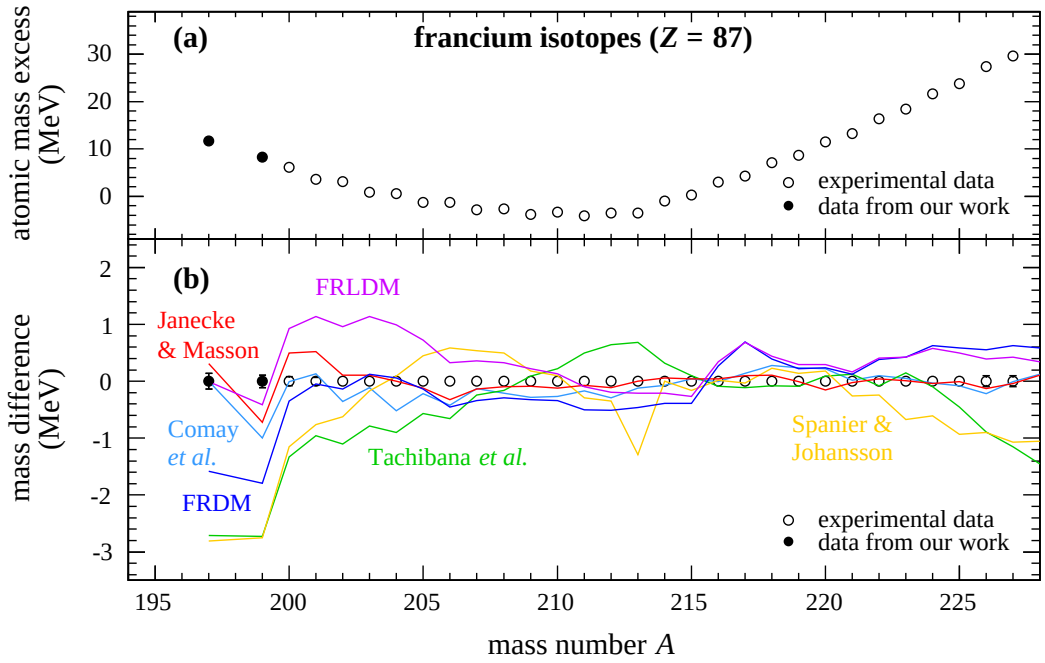

Fig. 5.33 (a) Experimental atomic mass excesses for francium isotopes. (b) The relative differences between experimental (black circles) and theoretical values (colored lines) for atomic mass excesses of francium isotopes. Experimental values were set to zero and values predicted by several models are compared with them. Experimental values were taken from Ref. [Wan12] (open circles) except for ^{197,199}Fr (full circles), which are from our data. Theoretical values were taken from Ref. [lbnl].

radon isotopes ($Z = 86$) have reduced α-decay widths of 270(60) keV (^{194}Rn) [And06], 250^{+80}_{-50} keV (^{196}Rn) [Ket01] and 111(6) keV (^{198}Rn) [Bij95].

We note that the values of reduced α-decay widths of the isotopes in this region (including ^{197}Fr) are higher than for transitions in regions above the doubly magic nuclei ^{100}Sn (e.g., with reduced α-decay widths of 140(20) and 220^{+100}_{-80} keV for ^{105}Te [Lid06] and ^{106}Te [Jan05a, Sch81], respectively) and ^{208}Pb (e.g., with reduced α-decay widths of 70(1) and 90(20) keV for ^{212}Po [Fir04] and ^{213}Po [Fir04], respectively). One explanation for high values of reduced α-decay widths of α decays leading to doubly-magic or nearby nuclei is the possibility, that an α-particle is pre-formed from valence nucleons outside the doubly-magic core [Mac65, Var92]. The enhanced stability of the doubly-magic core makes such α transitions very allowed. However, nuclei in the vicinity of ^{197}Fr do not decay to regions of doubly-magic nuclei, and still their reduced α-decay widths are so high. To investigate this issue, experimental data with much higher statistics would be necessary.

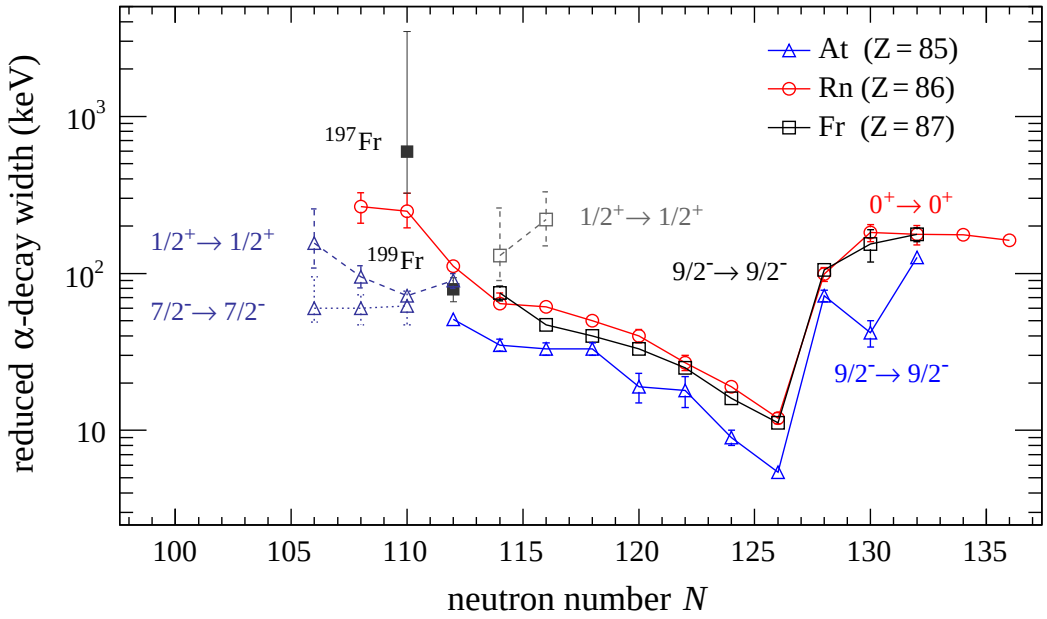

Fig. 5.34 Systematics of reduced α-decay widths in the vicinity of the shell closure $N = 126$ for odd-A francium ($Z = 87$) isotopes and neighboring odd-A astatine ($Z = 85$) and even-A radon ($Z = 86$) isotopes. The $9/2^- \rightarrow 9/2^-$ and $0^+ \rightarrow 0^+$ transitions are connected by solid lines. The transitions $7/2^- \rightarrow 7/2^-$ and $1/2^+ \rightarrow 1/2^+$ are represented by dashed lines. The values of reduced α-decay widths except for ^{197,199}Fr are taken from Refs. [Kal14, DeW05, Chu99, Ket03a, Ket03b, Smi99, And06, Ket01, Bij95, Wau93, Cal84]. The values for ^{197,199}Fr, which are from our measurement, are shown by solid symbols. They are not connected by a line with the symbols of other francium isotopes representing $9/2^- \rightarrow 9/2^-$ transitions, because they probably represent $7/2^- \rightarrow 7/2^-$ transitions (and possibly also $1/2^+ \rightarrow 1/2^+$ for ^{199}Fr, see Sect. 5.1.6 on ^{199}Fr for more details).

5.3 Hindrance factors

As we already mentioned in Sect. 3.1.1, a measure of a suppression of an α decay can be expressed by a hindrance factor (HF) of the α transition. An unhindered decay (HF ≈ 1) connects two states with the same configuration. The more different are the states connected by the α transition, the higher is the HF of the α transition. As an example of this dependence, we can look at the decay scheme of ^{253}No in Fig. 7.1 in Appendix B: The α transition connecting the states with the same configuration, $9/2^-[734]$, in the parent ^{253}No and daughter ^{249}Fm nuclei, has a hindrance factor of 3.1. On the other hand, for the transition, which requires a sizable change between the states in the parent and daughter nuclei, e.g., the transition connecting ground states of ^{253}No and ^{249}Fm, the hindrance factor is more than 8000.

We calculated hindrance factors for decays studied in this work by comparing reduced α-decay widths (δ_α^2) for a given α decay with δ_α^2 of unhindered α

decays in neighboring isotopes. Reduced α-decay widths were evaluated using the approach introduced by J.O. Rasmussen [Ras59]. In this section, we compare hindrance factors obtained by comparing reduced α-decay widths with the ones determined by comparing experimental ($T_{1/2,exp}$) and expected ($T_{1/2,theor}$) half-lives calculated using several approaches (see Sect. 3.1.1). We chose three methods for the calculation of expected half-lives:

- Semi-empirical relationship based on the fission theory of α decay. The method was originally proposed by D.N. Poenaru, *et al.* in 1980 [Poe80]. Later, the fit parameters were updated according to enhanced set of experimental α-decay data [Poe06].
- Method for the calculation of half-lives for cluster decays introduced by D.N. Poenaru, *et al.* [Poe06]. In this approach, the parameters were extracted both from a set of α-decay data and from a set of (cluster+α)-decay data.
- Universal decay law for cluster decays introduced by C. Qi, *et al.* [Qi09]. In this approach, the parameters were extracted both from a set of α-decay data and from a set of (cluster+α)-decay data.

We applied these methods to obtain expected half-lives of isotopes studied in this work; both for known decays already measured with high accuracy ($^{200-202}$Fr) and for new data (^{197}Fr, ^{201,202}Ra) (see Figs. 5.35 and 5.36). For all the considered transitions, all methods give hindrance factors around 1, which corresponds to an unhindered nature of studied α decays. This result is independent on the used method. Two of the approaches (1. Poenaru (2006), semiFIS and 2. Poenaru (2006), univ (α), see Figs. 5.35 and 5.36) predict half-lives by about one order of magnitude longer than the experimentally measured ones (resulting in hindrance factors of about 0.1). This difference indicates that these transitions are even more allowed than one would expect from the systematics. The fact that these transitions are very allowed, can be also seen in systematics of reduced α-decay widths, which was discussed in Sect. 5.1.1 on ^{202}Ra (Fig. 5.4(a)) and Sect. 5.2.3 on ^{197}Fr (Fig. 5.34).

5.4 Cross sections

In this section we present evaluated experimental production cross sections for radium and francium isotopes studied in this work. Isotopes were produced in fusion-evaporation reactions (^{56}Fe + ^{149}Sm, ^{56}Fe + ^{147}Sm, ^{60}Ni + ^{141}Pr), for which we estimated the transmission of SHIP to be 40 % based on the Monte-Carlo code for fusion-evaporation residues traversing through an ion-optical system [Maz08].

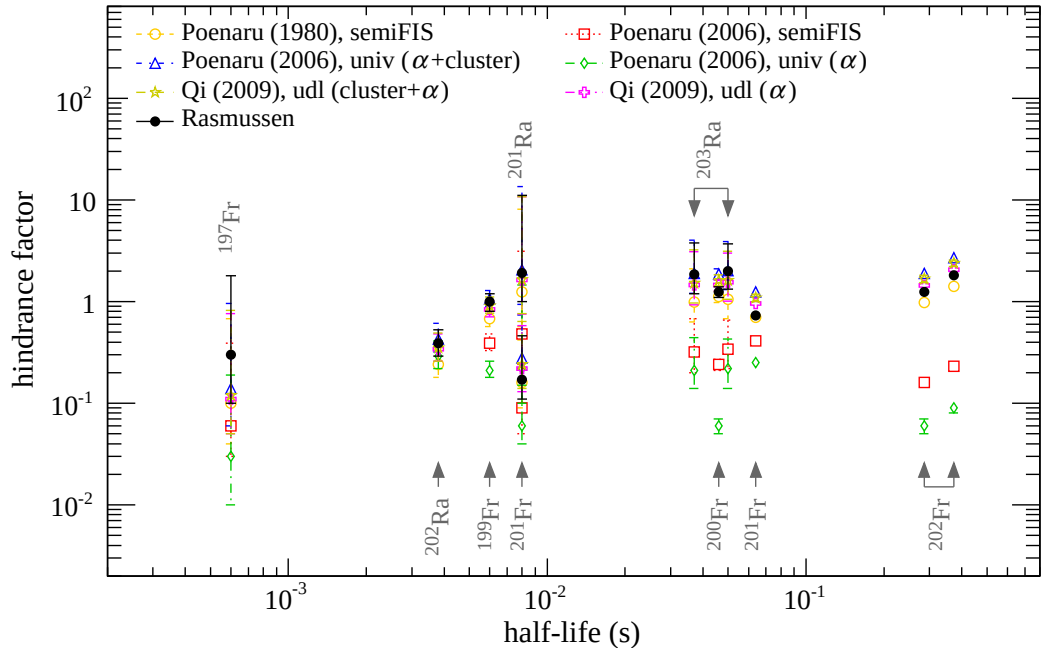

Fig. 5.35 Hindrance factors evaluated using different approaches for some of the α decays studied in this work. See the text for more details.

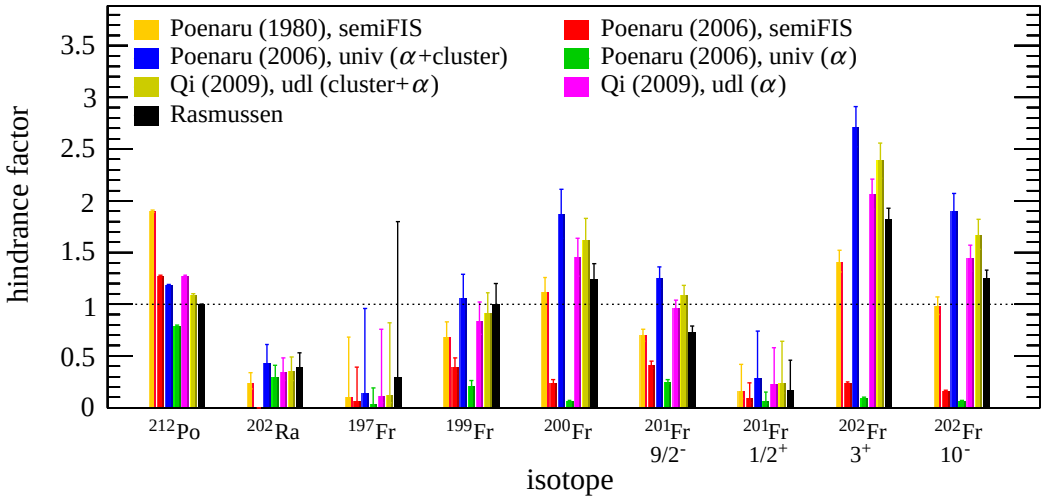

Fig. 5.36 Hindrance factors evaluated using different approaches for some of the α decays studied in this work. HF for an α decay of ^{212}Po is shown here for comparison, as it is an example of an unhindered α decay leading to a doubly-magic ^{208}Pb. See the text for more details.

Reactions $^{56}Fe + ^{149}Sm$ and $^{56}Fe + ^{147}Sm$ In the first experiment, radium and francium isotopes were produced in xn and pxn evaporation channels, respectively, in the fusion-evaporation reactions $^{56}\mathrm{Fe} + ^{149}\mathrm{Sm} \rightarrow ^{205}\mathrm{Ra}^*$ and $^{56}\mathrm{Fe} + ^{147}\mathrm{Sm} \rightarrow ^{203}\mathrm{Ra}^*$. Irradiations of the ^{149}Sm and ^{147}Sm targets were performed

at several beam energies resulting in different excitation energies of compound nuclei ^{205}Ra and ^{203}Ra, respectively, which are summarized in Tabs. 5.11 and 5.12. Production cross sections from these reactions are shown in Figs. 5.37 and 5.38. The cross sections for the *pxn* evaporation channels are about two orders of magnitude higher than for the *xn* channels due to a large neutron deficit of produced isotopes.

Tab. 5.11 Experimental cross sections for the production of radium and francium isotopes in the reaction $^{56}\mathrm{Fe} + {}^{149}\mathrm{Sm}$.

E_{beam} (MeV)	E^*_{CN} (MeV)	cross section (nb)			
		^{200}Ra ($5n$)	**^{201}Ra** ($4n$)	**^{202}Ra** ($3n$)	**^{203}Ra** ($2n$)
244	30	–	–	0.2(1)	0.2(1)
256	39	–	–	0.17(6)	$0.06^{+0.04}_{-0.03}$
275	42	–	–	$0.02^{+0.03}_{-0.01}$	$0.02^{+0.03}_{-0.01}$
		^{200}Fr ($p4n$)	**^{201}Fr** ($p3n$)	**^{202}Fr** ($p2n$)	**^{203}Fr** (pn)
244	30	–	–	5(1)	3.9(8)
256	39	–	0.6(2)	24(2)	4.1(5)
260	42	–	0.5(2)	25(2)	0.9(4)
275	53	$0.023^{+0.053}_{-0.019}$	4.0(4)	5.9(6)	1.0(2)

Tab. 5.12 Experimental cross sections for the production of radium and francium isotopes in the reaction $^{56}\mathrm{Fe} + {}^{147}\mathrm{Sm}$.

E_{beam} (MeV)	E^*_{CN} (MeV)	cross section (nb)	
		^{200}Ra ($3n$)	**^{201}Ra** ($2n$)
249	27	–	$0.04^{+0.08}_{-0.03}$
263	37	< 0.03	–
		^{200}Fr ($p2n$)	**^{201}Fr** (pn)
249	27	–	0.3(2)
260	35	0.5(1)	0.3(1)
263	37	1.8(2)	$0.36^{+0.09}_{-0.08}$

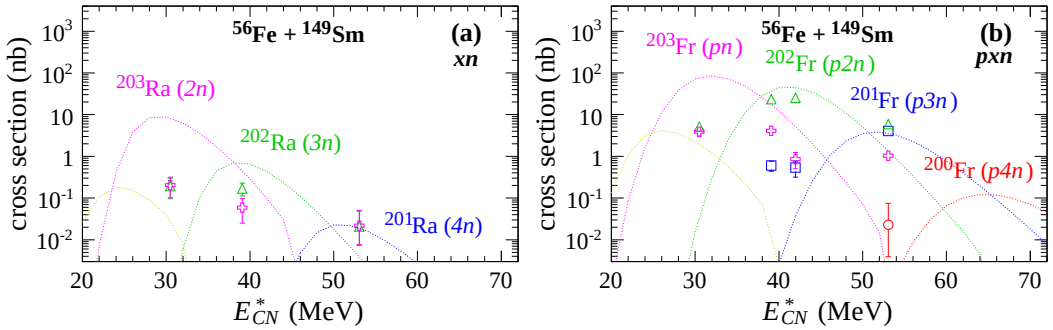

Fig. 5.37 Experimental production cross sections (symbols) for radium (panel (a)) and francium (panel (b)) isotopes produced in the xn and pxn evaporation channels, respectively, in the fusion evaporation reaction $^{56}\mathrm{Fe} + {}^{149}\mathrm{Sm}$. Solid lines represent the cross sections calculated using the HIVAP code [Rei81, Ant12].

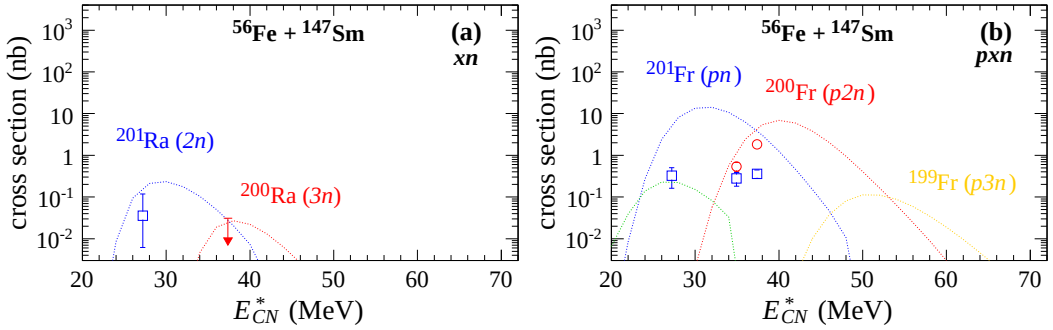

Fig. 5.38 Experimental production cross sections (symbols) for radium (panel (a)) and francium (panel (b)) isotopes produced in the xn and pxn evaporation channels, respectively, in the fusion evaporation reaction $^{56}\mathrm{Fe} + {}^{147}\mathrm{Sm}$. Solid lines represent the cross sections calculated using the HIVAP code [Rei81, Ant12]. For the ^{200}Ra isotope we present only an upper limit for the experimental cross section (red arrow), as no event was observed.

Reaction $^{60}\boldsymbol{Ni} + {}^{141}\boldsymbol{Pr}$ In the second experiment, we produced $^{199-197}$Fr isotopes in the $(2n-4n)$ evaporation channels in the fusion-evaporation reaction $^{60}\mathrm{Ni} + {}^{141}\mathrm{Pr}$. Irradiations of the ^{141}Pr target were performed at several beam energies from 266 to 300 MeV resulting in excitation energies of a compound nucleus ^{201}Fr in the range of $(51-27)$ MeV (see Tab. 5.13 and Fig. 5.39). We recall that at a beam energy of 276 MeV, $E^*_{CN} = 34$ MeV, both ^{198}Fr and ^{199}Fr isotopes were produced. As their decay properties are very similar, it was not possible to distinguish them when both were produced simultaneously (see Sections 5.2.1 and 5.2.2 on ^{199}Fr and ^{198}Fr for more details). The cross section for the sum of both isotopes is plotted as a black diamond symbol between the maxima of excitation functions for ^{199}Fr and ^{198}Fr in Fig. 5.39.

We compared experimental production cross sections for studied isotopes with the cross sections calculated using a statistical model code HIVAP [Rei81, Ant12].

Tab. 5.13 Experimental cross sections for the production of $^{197-199}$Fr isotopes in the reaction ^{60}Ni + ^{141}Pr.

E_{beam} (MeV)	E^*_{CN} (MeV)	cross section (nb)		
		^{197}Fr ($4n$)	**^{198}Fr** ($3n$)	**^{199}Fr** ($2n$)
266	27	–	–	2(1)
272	31	–	–	3(1)
282	38	–	1.3(3)	–
286	41	–	0.8(4)	–
291	44	–	$0.8^{+0.6}_{-0.5}$	–
297	49	–	$0.14^{+0.10}_{-0.08}$	–
300	51	$0.018^{+0.041}_{-0.015}$	$0.06^{+0.13}_{-0.05}$	–

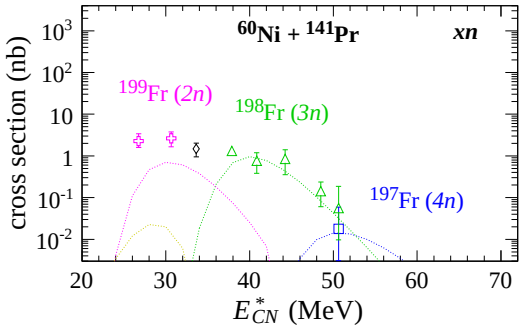

Fig. 5.39 Experimental production cross sections (symbols) for francium isotopes produced in the xn evaporation channels in the fusion evaporation reaction ^{60}Ni + ^{141}Pr. Solid lines represent the cross sections calculated using the HIVAP code [Rei81, Ant12]. The black diamond shows the common cross section for ^{199}Fr and ^{198}Fr, as at a beam energy of 276 MeV (E^*_{CN} = 34 MeV) both isotopes were produced.

Experimental and calculated values are mostly consistent within one order of magnitude. The HIVAP calculations were performed before the analysis of experimental data. This may explain the difference between experimental and calculated values, which is apparent mainly at low excitation energies. It is well known that HIVAP may not be optimal for the reactions close to the fusion barrier. The input parameters for the HIVAP calculations related to the fusion barrier and its fluctuations may not be known for the particular reactions, which results in sizable uncertainties of the final values.

Chapter 6

Summary

In this Thesis, we present results of decay studies for neutron-deficient radium and francium isotopes. For some of these isotopes, only very limited experimental information has been available prior to our work. Studied isotopes are in the region of the nuclide chart where several interesting nuclear-structure phenomena occur, for example, β-delayed fission and coexisting states with different shapes within a single nucleus. This motivated us to study the most neutron-deficient isotopes from this region.

Two experiments aimed at the production of neutron-deficient radium and francium isotopes were performed at the velocity filter SHIP (GSI, Darmstadt). We analyzed data from these measurements using the methods of α- and γ-decay spectroscopy. Identification of isotopes was based on correlations of their decays with known decays of their daughter (and granddaughter) isotopes. The method of the isotope identification based on time- and position-correlated events is very selective and enabled us to identify specific decay chains, even if the number of background signals was several orders of magnitude higher than the number of studied events. This technique was successfully used, for example, in the identification of several new superheavy elements (see, e.g., Ref. [Hof00]).

We investigated in detail decay properties of nine isotopes:

- $^{201-203}$Ra and $^{200-202}$Fr produced in the fusion-evaporation reactions $^{56}\mathrm{Fe} + {}^{149}\mathrm{Sm}$ and $^{56}\mathrm{Fe} + {}^{147}\mathrm{Sm}$,
- $^{197-199}$Fr produced in the fusion-evaporation reaction $^{60}\mathrm{Ni} + {}^{141}\mathrm{Pr}$.

In the following paragraphs we list the results for individual isotopes obtained from our experiments. (We recall that all spins and parities assigned to nuclear energy levels in our work are tentative.)

Reactions ^{56}Fe + ^{147,149}Sm

^{201}Ra We observed a new isomeric α-decaying state in ^{201}Ra yielding an α-decay energy of 7842(12) keV and a half-life of 8^{+40}_{-4} ms. Based on the value of reduced α-decay width, we consider this decay to be unhindered, and we assume that it connects states with spins and parities $3/2^-$ in the parent ^{201}Ra and daughter ^{197}Rn isotope.

^{202}Ra For the heavier radium isotope, ^{202}Ra, we significantly improved the α-decay data by detecting 16 decay chains, while in both previous measurements only one decay chain was recorded [Lei96, Uus05]. We measured an α-decay energy of 7722(7) keV and a half-life of $3.8^{+1.3}_{-0.8}$ ms for ^{202}Ra resulting in the reduced α-decay width of 210^{+70}_{-50} keV. This value showed that reduced α-decay widths for even-A radium isotopes continue to increase with decreasing neutron number. Such trends of reduced α-decay widths were also reported for even-A isotopes of neighboring elements — radon [And06, Ket01] and thorium [Her10].

^{200}Fr Besides the known α-decaying state, we also observed a new short lived γ-decaying state with a half-life of $0.6^{+0.5}_{-0.2}$ μs in ^{200}Fr. Based on one fission event, we identified a process of β-delayed fission in this isotope. The estimated lower limit for the probability of this decay mode in ^{200}Fr is 1.4 %, which is one of the highest observed values for the probability of β-delayed fission. For ^{196}At, the α-decay daughter of ^{200}Fr, we detected a new weak α line at 6732(8) keV.

^{201}Fr Our data confirmed decay properties of the ground (spherical) $9/2^-$ state and the intruder (oblate) $1/2^+$ state in ^{201}Fr. Besides these two states, we also identified a short-lived γ-decaying state with a half-life of $0.7^{+0.5}_{-0.2}$ μs in this nuclide and tentatively assigned a spin and parity of $13/2^+$ to this state. Recently, the $13/2^-$ isomeric states were also identified in heavier francium isotopes, ^{203}Fr [Jak13] and ^{205}Fr [Jak12].

^{203}Ra, ^{202}Fr We observed α decay of the $13/2^+$ and $3/2^-$ states in ^{203}Ra and α decays of the 3^+ and 10^- states in ^{202}Fr. Half-lives and α-decay energies for these states evaluated from our data confirmed known values.

^{200}Ra In the reaction ^{56}Fe + ^{147}Sm, we estimated an upper limit of 30 pb for the production cross section of ^{200}Ra at the expected maximum of ^{200}Ra excitation function.

Reaction $^{60}\mathbf{Ni} + {}^{141}\mathbf{Pr}$

^{199}Fr Compared to a previous measurement [Tag99], we collected statistics higher by one order of magnitude for ^{199}Fr, which enabled us to significantly improve its α-decay properties. Based on our data, we proposed two possible scenarios for the decay of ^{199}Fr: One of them considers the existence of two α-decaying states with similar decay properties: the $1/2^+$ state with an α-decay energy of 7664(11) keV and a half-life of $4.5^{+3.1}_{-1.3}$ ms decaying to a ground state in ^{195}At and the $7/2^-$ state with an α-decay energy of 7676(6) keV and a half-life of $6.2^{+1.1}_{-0.8}$ ms decaying to an isomeric state in ^{195}At. The second scenario considers only one α-decaying state in ^{199}Fr with tentative spin and parity $7/2^-$, α-decay energy of 7675(6) keV and a half-life of $6.0^{+1.0}_{-0.7}$ ms. To confirm one of the scenarios, more statistics is needed. As for the heavier odd-A francium isotopes the ground state is presumably spherical with spin and parity $9/2^-$, our data indicate a change in the ground-state deformation from $A = 199$, since both $7/2^-$ and $1/2^+$ states are presumably oblate.

^{198}Fr To our knowledge, no experimental data for ^{198}Fr were published prior to our work. We recorded several tens of ^{198}Fr nuclei with a broad α-decay energy distribution in the range of $(7470 - 7930)$ keV. The energy and time distribution of α decays as well as correlated granddaughter decays indicate the presence of two α-decaying states in ^{198}Fr with half-lives of 1.1(7) and 15(3) ms.

^{197}Fr We identified a new isotope ^{197}Fr based on one correlation chain consisting of the implantation of an evaporation residue followed by three α decays. We assume, that this chain originates from the $7/2^-$ state in ^{197}Fr. A measured α-decay energy for this state was 7728(15) keV and a half-life was $0.6^{+3.0}_{-0.3}$ ms. A remarkably high reduced α-decay width, $0.6^{+2.9}_{-0.3}$ MeV, was deduced for this transition. Although the uncertainty is large, this value, along with the values of reduced α-decay widths for some other nearby isotopes, is higher than reduced α-decay widths of nuclei decaying to regions of doubly magic ^{208}Pb and ^{100}Sn. To investigate this issue in more detail, experimental data with higher statistics would be necessary.

Chapter 7

Conclusion

In this Thesis, the results of two experiments aimed at the investigation of neutron-deficient radium and francium isotopes are discussed. Isotopes were produced in fusion-evaporation reactions, $^{56}\mathrm{Fe} + ^{147,149}\mathrm{Sm}$ and $^{60}\mathrm{Ni} + ^{141}\mathrm{Pr}$, at the velocity filter SHIP at GSI in Darmstadt. Data were analyzed by α- and γ-decay spectroscopy.

A new isotope, ^{197}Fr, was identified. New isomeric α-decaying states were observed in ^{201}Ra and ^{198}Fr. For ^{202}Ra and ^{199}Fr, significantly improved values for α-decay energies and half-lives were evaluated compared to previously known data. Short-lived γ-decaying states were identified in ^{200}Fr and ^{201}Fr. A process of β-delayed fission was observed in ^{200}Fr for the first time. In addition, known α-decay properties were confirmed for ^{203}Ra and ^{202}Fr.

In the ^{199}Fr isotope, decays of the $7/2^-$ and possibly also $1/2^+$ states were observed. Both states are associated with a presumably oblate deformation. On the other hand, the ground $9/2^-$ state of heavier odd-A francium isotopes is associated with a presumably spherical shape. Therefore, starting from $A = 199$, the ground-state deformation in francium isotopes may change from spherical to oblate.

A high reduced α-decay width evaluated for ^{202}Ra shows that a trend of increasing reduced α-decay widths for even-A radium isotopes continues with decreasing neutron number. Similarly, a very high reduced α-decay width was evaluated for ^{197}Fr, which exhibits increasing reduced α-decay widths with decreasing neutron number for odd-A francium isotopes as well. These values along with the values of reduced α-decay widths for several other nearby nuclides are comparable with or even higher than reduced α-decay widths of transitions leading to regions of doubly-magic nuclei ^{208}Pb and ^{100}Sn. However, to investigate this topic in more detail, experimental data with higher statistics are necessary.

Zhrnutie

V dizertačnej práci prezentujeme výsledky štúdia rozpadových vlastností neutrónovo-deficitných izotopov rádia a francia. Pre niektoré z týchto izotopov bolo doteraz známych len veľmi málo experimentálnych informácií. Študované jadrá sa nachádzajú v oblasti tabuľky izotopov, kde sa vyskytuje niekoľko zaujímavých javov z hľadiska výskumu jadrovej štruktúry, napríklad oneskorené štiepenie po β premene alebo koexistencia stavov s rôznou deformáciou v rámci jedného jadra. To nás motivovalo ku štúdiu veľmi neutrónovo-deficitných izotopov z tejto oblasti.

Na rýchlostnom filtri SHIP (GSI, Darmstatd) boli uskutočnené dva experimenty zamerané na produkciu neutrónovo-deficitných izotopov rádia a francia. Dáta z týchto meraní sme analyzovali metódami rozpadovej α a γ spektroskopie. Izotopy sme identifikovali na základe korelácií ich rozpadov so známymi rozpadmi ich dcérskych izotopov. Metóda identifikácie jadier založená na časových a pozičných koreláciách eventov je veľmi selektívna a umožňuje nám identifikovať jednotlivé konkrétne rozpadové reťazce aj pri početnostiach pozaďových signálov prevyšujúcich študované eventy o niekoľko rádov. Táto metóda bola úspešne aplikovaná pri identifikácii niekoľkých nových superťažkých prvkov (viď napr. Ref. [Hof00]).

Podrobne sme študovali rozpadové vlastnosti deviatich izotopov:

- $^{201-203}$Ra a $^{200-202}$Fr produkovaných vo fúzno-výparných reakciách $^{56}\mathrm{Fe} + {}^{149}\mathrm{Sm}$ a $^{56}\mathrm{Fe} + {}^{147}\mathrm{Sm}$,
- $^{197-199}$Fr produkovaných vo fúzno-výparnej reakcii $^{60}\mathrm{Ni} + {}^{141}\mathrm{Pr}$.

V nasledujúcich odstavcoch stručne uvádzame výsledky pre jednotlivé izotopy získané z našich experimentov. (Poznamenávame, že spiny a parity priradené energetickým hladinám v tejto práci sú predbežné.)

Reakcie ^{56}Fe + ^{147,149}Sm

^{201}Ra Registrovali sme nový izomérny stav v ^{201}Ra rozpadajúci sa α rozpadom s energiou 7842(12) keV a dobou polpremeny 8^{+40}_{-4} ms. Na základe hod-

noty redukovanej šírky sme tento rozpad vyhodnotili ako nepotlačený, a predpokladáme, že spája hladiny so spinom a paritou $3/2^-$ v materskom jadre ^{201}Ra a dcérskom jadre ^{197}Rn.

^{202}Ra Pre ťažší izotop, ^{202}Ra, sme výrazne upresnili doteraz známe rozpadové dáta registrovaním 16 rozpadových reťazcov, pričom v oboch predošlých experimentoch bol registrovaný iba jeden reťazec [Lei96, Uus05]. Energia α rozpadu ^{202}Ra z našich dát má hodnotu 7722(7) keV a doba polpremeny je $3.8^{+1.3}_{-0.8}$ ms. Z vyhodnotenej redukovanej šírky tohto α rozpadu, 210^{+70}_{-50} keV, je zrejmé, že s klesajúcim počtom neutrónov redukované šírky párno-párnych izotopov rádia ďalej stúpajú. Stúpajúci trend redukovaných šírok bol pozorovaný aj pre párno-párne izotopoy susedných prvkov — radónu [And06, Ket01] a tória [Her10].

^{200}Fr Okrem známeho α rozpadu ^{200}Fr sme registrovali aj nový krátkožijúci stav v tomto jadre s dobou polpremeny $0.6^{+0.5}_{-0.2}$ μs rozpadajúci sa vnútornými prechodmi. Na základe jedného štiepneho eventu sme pozorovali po prvýkrát proces oneskoreného štiepenia po β premene v izotope ^{200}Fr. Dolný limit pre pravdepodobnosť tohto spôsobu rozpadu pre ^{200}Fr je 1.4 %, čo je jedna z najvyšších pozorovaných hodnôt pravdepodobnosti oneskoreného štiepenia po β premene. Pre ^{196}At, dcérsky izotop po α rozpade ^{200}Fr, sme registrovali novú α čiaru s energiou 6732(8) keV.

^{201}Fr Naše dáta potvrdili rozpadové vlastnosti základného stavu $9/2^-$ (predpokladaný sférický tvar) a izomérneho stavu $1/2^+$ (predpokladaný sploštený[1] tvar) v jadre ^{201}Fr. Okrem týchto stavov sme v izotope ^{201}Fr identifikovali tiež krátkožijúci izomérny stav s dobou polpremeny $0.7^{+0.5}_{-0.2}$ μs rozpadajúci sa vnútornými prechodmi. Predbežne sme mu priradili spin a paritu $13/2^+$. Izoméry so spinom a paritou $13/2^+$ boli nedávno identifikované aj v ťažších izotopoch francia, ^{203}Fr [Jak13] a ^{205}Fr [Jak12].

^{203}Ra, ^{202}Fr Registrovali sme α rozpady stavov $3/2^-$ a $13/2^+$ v jadre ^{203}Ra a α rozpady stavov 3^+ a 10^- v jadre ^{202}Fr. Doby polpremeny a energie α rozpadov týchto stavov vyhodnotené z našich dát potvrdili známe hodnoty.

^{200}Ra V reakcii ^{56}Fe + ^{147}Sm sme vyhodnotili horný limit pre účinný prierez produkcie ^{200}Ra v očakávanom maxime excitačnej funkcie. Jeho hodnota je 30 pb.

[1] z angl. 'oblate'

Reakcia ^{60}Ni + ^{141}Pr

^{199}Fr Oproti predošlému meraniu [Tag99] sme pre izotop ^{199}Fr získali rádovo vyššiu štatistiku, čo nám umožnilo výrazne upresniť jeho rozpadové vlastnosti. Na základe našich dát sme navrhli dva možné rozpadové scenáre pre ^{199}Fr. V prvom uvažujeme existenciu dvoch stavov s veľmi podobnými vlastnosťami α rozpadu: stav $1/2^+$ s energiou 7664(11) keV a dobou polpremeny $4.5^{+3.1}_{-1.3}$ ms rozpadajúci sa na základný stav ^{195}At a stav $7/2^-$ s energiou 7676(6) keV a dobou polpremeny $6.2^{+1.1}_{-0.8}$ ms rozpadajúci sa na izomérny stav ^{195}At. Druhý scenár predpokladá iba jeden stav rozpadajúci sa α rozpadom v ^{199}Fr s predbežným spinom a paritou $7/2^-$, energiou 7676(6) keV a dobou polpremeny $6.0^{+1.0}_{-0.7}$ ms. Aby sme mohli potvrdiť jeden zo scenárov, potrebujeme dáta s vyššou štatistikou. Nakoľko v ťažších nepárno-párnych izotopoch francia má základný stav $9/2^-$ predpokladaný sférický tvar, naše dáta naznačujú zmenu deformácie základného stavu od $A = 199$, keďže predpokladáme, že oba stavy $7/2^+$ aj $1/2^+$ sú sploštené.

^{198}Fr Pokiaľ vieme, pred našou štúdiou neboli publikované žiadne experimentálne dáta o izotope ^{198}Fr. My sme registrovali niekoľko desiatok jadier ^{198}Fr so širokou energetickou distribúciou α rozpadu v rozsahu $(7470 - 7930)$ keV. Energetická a časová distribúcia α rozpadov, ako aj korelácie s dcérskymi jadrami ^{190}Bi, naznačujú prítomnosť dvoch stavov v ^{198}Fr s dobami polpremeny 1.1(7) a 15(3) ms.

^{197}Fr Identifikovali sme nový izotop, ^{197}Fr, na základe jedného korelačného reťazca pozostávajúceho z implantácie jadra a následných troch α rozpadov. Predpokladáme, že reťazec pochádza z rozpadu stavu $7/2^-$ v ^{197}Fr. Nameraná energia α rozpadu tohto stavu je 7728(15) keV a doba polpremeny $0.6^{+3.0}_{-0.3}$ ms. Redukovaná šírka tohto α rozpadu, $0.6^{+2.9}_{-0.3}$ MeV, je pozoruhodne vysoká. Hoci má veľkú neistotou, táto hodnota spolu s hodnotami redukovaných šírok α rozpadov niekoľkých ďalších okolitých izotopov, je vyššia než redukované šírky izotopov rozpadajúcich sa na dvojito-magické jadrá ^{208}Pb a ^{100}Sn.

Záver V dizertačnej práci sú diskutované výsledky experimentov zameraných na štúdium neutrónovo-deficitných izotopov rádia a francia. Izotopy boli produkované vo fúzno-výparných reakciách ^{56}Fe + ^{147,149}Sm a ^{60}Ni + ^{141}Pr na rýchlostnom filtri SHIP v GSI, Darmstadt. Dáta boli analyzované metódami rozpadovej α a γ spektroskopie.

Bol identifikovaný nový izotop ^{197}Fr. Nové izomérne stavy rozpadajúce sa α rozpadom boli pozorované v jadrách ^{201}Ra a ^{198}Fr. Pre ^{202}Ra a ^{199}Fr boli získané výrazne presnejšie hodnoty dôb polpremien a energií α rozpadov oproti

predošlým dátam. Registrovanie rozpadov zo stavov s predpokladaným splošteným tvarom v ^{199}Fr naznačuje zmenu deformácie základného stavu oproti ťažším nepárno-párnym izotopom francia, kde má základný stav predpokladaný sférický tvar. V jadrách ^{200}Fr a ^{201}Fr boli identifikované nové krátkožijúce izomérne hladiny rozpadajúce sa vnútornými prechodmi. Po prvýkrát bolo pre izotop ^{200}Fr registrované oneskorené štiepenie po β premene. Známe rozpadové dáta boli potvrdené pre izotopy ^{203}Ra a ^{202}Fr.

Dáta pre ^{202}Ra preukázali pokračovanie trendu zvyšujúcich sa redukovaných šírok s klesajúcim počtom neutrónov pre párno-párne izotopy rádia. Podobný trend bol preukázaný aj pre nepárno-párne izotopy francia vyhodnotením redukovaných šírok pre ^{199}Fr a ^{197}Fr. Pre vysvetlenie nezvyčajne vysokých redukovaných šírok rozpadov ^{197}Fr, ^{202}Ra, a aj niektorých ďalších okolitých jadier, je potrebné získať experimentálne dáta s vyššou štatistikou.

Appendix A

Summary of spectroscopic results

Tabs. 7.1, 7.2, and 7.3 contain the summary of all spectroscopic results obtained in this work compared with values from the literature.

Tab. 7.1 The α-decay properties of $^{201-203}$Ra produced in the fusion-evaporation reaction $^{56}\mathrm{Fe} + {}^{147,149}\mathrm{Sm}$. Spin and parity assignments (I^π) are tentative.

isotope	I^π	E_α (keV)	$T_{1/2}$ (ms)	δ^2_α (keV)	ref.
^{201}Ra	$3/2^-$	7842(12)	8^{+40}_{-4}	43^{+204}_{-20}	this work
	$13/2^+$	7905(20)	$1.6^{+7.7}_{-0.7}$	140^{+680}_{-70} [a]	[Uus05]
^{202}Ra	0^+	7722(7)	$3.8^{+1.3}_{-0.8}$	210^{+70}_{-50}	this work
	0^+	7740(20)	16^{+30}_{-7}	44^{+83}_{-20} [a]	[Uus05]
	0^+	7860(60)	$0.7^{+3.3}_{-0.3}$	430^{+2020}_{-260} [a]	[Lei96]
^{203}Ra	$3/2^-$	7575(10)	50^{+40}_{-15}	45^{+37}_{-14}	this work
	$3/2^-$	7589(8)	31^{+17}_{-9}	66^{+36}_{-20} [a]	[Uus05]
	$3/2^-$	7577(20)	$1.0^{+5.0}_{-0.5}$	2200^{+11200}_{-1200} [a]	[Lei96]
	$13/2^+$	7607(8)	37^{+37}_{-12}	48^{+48}_{-16}	this work
	$13/2^+$	7612(8)	24^{+6}_{-4}	72^{+18}_{-13} [a]	[Uus05]
	$13/2^+$	7615(20)	33^{+22}_{-10}	51^{+35}_{-17} [a]	[Lei96]

[a] Values of δ^2_α were calculated according to Rasmussen prescription [Ras59] using input values (E_α and $T_{1/2}$) from cited references.

Tab. 7.2 The α-decay properties of $^{197-199}$Fr produced in the fusion-evaporation reaction ^{60}Ni + ^{141}Pr. We show here α-decay properties for both proposed decay patterns of ^{199}Fr, [1] and [2] (for more details see Sect. 5.2.1). Based on present data we cannot make any preference for either of the scenarios. Unless stated otherwise, we assume a relative intensity of the α lines (I_α) to be 100 %. Spin and parity assignments (I^π) are tentative.

isotope	I^π	E_α (keV)	I_α (%)	$T_{1/2}$ (ms)	δ^2_α (keV)	ref.
^{197}Fr	$7/2^-$	7728(15)		$0.6^{+3.0}_{-0.3}$	600^{+2900}_{-300}	this work
^{198}Fr	–	7580 − 7930		1.1(7)	30 − 380	this work
	–	7470 − 7920	∼ 50	15(3)	1 − 30	this work
	–	∼ 7710	∼ 50	15(3)	14(6)	this work
	2^-	7613(15)		15^{+12}_{-5}	60^{+40}_{-30}	[Uus13]
	6^+,7^+	7684(15)		16^{+13}_{-5}	30(20)	[Uus13]
^{199}Fr	$7/2^-$	7675(6)		$6.0^{+1.0}_{-0.7}$	85^{+15}_{-11}	this work[1]
	$7/2^-$	7676(6)		$6.2^{+1.1}_{-0.8}$	81^{+15}_{-11}	this work[2]
	$1/2^+$	7664(11)		$4.5^{+3.1}_{-1.3}$	120^{+80}_{-40}	this work[2]
	–	7655(40)		12^{+10}_{-4}	49^{+43}_{-22} [a]	[Tag99]
	$1/2^+$	7644(20)		5^{+7}_{-2}	130^{+120}_{-80}	[Uus13]
	$7/2^-$	7668(15)		7^{+3}_{-2}	80^{+60}_{-30}	[Uus13]
	$13/2^+$	7808(20)		$1.6^{+1.6}_{-0.6}$	120^{+110}_{-70}	[Uus13]

[a] Values of δ^2_α were calculated according to Rasmussen prescription [Ras59] using input values (E_α and $T_{1/2}$) from cited references.

Tab. 7.3 The α-decay properties of $^{200-202}$Fr and their α-decay daughters $^{196-198}$At produced in the fusion-evaporation reactions ^{56}Fe + ^{147,149}Sm. Unless stated otherwise, we assume a relative intensity of the α lines (I_α) to be 100 %. Spin and parity assignments (I^π) are tentative.

isotope	I^π	E_α (keV)	I_α (%)	$T_{1/2}$ (ms)	δ^2_α (keV)	ref.
^{200}Fr	–	7470(5)		46(4)	48(5)	this work
	–	7473(12)		49(4)	44(5) [a]	[DeW05]
	–	7468(9)		19^{+13}_{-6}	120^{+80}_{-40} [a]	[Enq96b]
	–	7500(30)		570^{+270}_{-140}	$3.1^{+1.6}_{-1.0}$ [a]	[Mor95]
^{196}At	–	7045(5)	96(2)	340(90)	29(7)	this work
	–	6732(8)	4(2)	340(90)	16(9)	this work
	3^+	7048(12)		350^{+290}_{-110}	27(2)	[Uus13]
	–	7055(12)		389(54)	25(4) [a]	[DeW05]
	3^+	7048(5)		388(7)	27(1) [a]	[Smi00]

Tab. 7.3 (continued): The α-decay properties of $^{200-202}$Fr and their α-decay daughters $^{196-198}$At produced in the fusion-evaporation reactions ^{56}Fe + ^{147,149}Sm. Unless stated otherwise, we assume a relative intensity of the α lines (I_α) to be 100 %. Spin and parity assignments (I^π) are tentative.

isotope	I^π	E_α (keV)	I_α (%)	$T_{1/2}$ (ms)	δ^2_α (keV)	ref.
	–	7065(30)		253(9)	36(9) [a]	[Pu97]
	–	7044(7)		390^{+270}_{-120}	28^{+19}_{-9} [a]	[Enq96b]
	–	7053(30)		320^{+220}_{-90}	31^{+23}_{-12} [a]	[Mor95]
^{201}Fr	$9/2^-$	7369(5)		64(3)	72(4)	this work
	$9/2^-$	7379(7)		67(3)	64(4)	[DeW05]
	$9/2^-$	7369(8)		53(4)	87(8) [a]	[Uus05]
	$9/2^-$	7361(7)		69^{+16}_{-11}	71^{+17}_{-12} [a]	[Enq96b]
	$9/2^-$	7388(15)		48(15)	83(28) [a]	[Ewa80]
	$1/2^+$	7445(8)		8^{+12}_{-3}	300^{+500}_{-100}	this work
	$1/2^+$	7454(8)		19^{+19}_{-6}	130^{+130}_{-40} [a]	[Uus05]
^{197}At	$9/2^-$	6963(5)		354^{+17}_{-15}	57^{+4}_{-3}	this work
	$9/2^-$	6963(4)		390(16)	51(3)	[DeW05]
	$9/2^-$	6959(6)		340(20)	61(5) [a]	[Uus05]
	$9/2^-$	6960(5)		388(6)	53(2) [a]	[Smi99]
	$9/2^-$	6956(5)		370^{+90}_{-60}	57^{+14}_{-10} [a]	[Enq96b]
	$1/2^+$	6698(16)		$2.8^{+3.8}_{-1.0}$ s	70^{+90}_{-30}	this work
	$1/2^+$	6706(9)		$1.1^{+1.1}_{-0.4}$ s	106^{+160}_{-60} [a]	[Uus05]
	$1/2^+$	6707(5)		2.0(2) s	87(10) [a]	[Smi99]
	$1/2^+$	6707		3.7(25) s	47(32) [a]	[Coe86]
^{202}Fr	3^+	7238(5)		372(12)	33(2)	this work
	3^+	7241(8)		300(50)	40(7) [a]	[Uus05]
	3^+	7243(6)		230^{+80}_{-40}	52^{+18}_{-9} [a]	[Enq96b]
	3^+	7237(8)		340(40)*	≤ 53	[Huy92]
	10^-	7226(5)		286(13)	48(3)	this work
	10^-	7235(8)		290(50)	44(8) [a]	[Uus05]
	10^-	7242(6)		230^{+140}_{-50}	52^{+32}_{-12} [a]	[Enq96b]
	10^-	7237(8)		340(40)*	≤ 53	[Huy92]
^{198}At	3^+	6747(5)		3.0(1) s	39(2)	this work
	3^+	6748(6)		3.8(4) s	27(5) [a]	[Uus05]
	3^+	6753(4)		$4.6^{+1.8}_{-1.0}$ s	22^{+9}_{-5} [a]	[Enq96b]
	3^+	6755(4)	80 – 100	4.2(3) s	26 – 37	[Huy92]
	10^-	6849(5)		1.24(6) s	39(3)	this work
	10^-	6850(6)		1.04(15) s	39(10) [a]	[Uus05]
	10^-	6855(4)		$1.3^{+0.8}_{-0.3}$ s	30^{+19}_{-9} [a]	[Enq96b]
	10^-	6856(4)	67 – 100	1.0(2) s	37 – 73	[Huy92]

[a] Values of δ^2_α were calculated according to Rasmussen prescription [Ras59] using input values (E_α and $T_{1/2}$) from cited references.
* Value is from Ref. M. R. Schmorak, *Nucl. Data Sheets* **50**, 669 (1987).

Appendix B

GEANT 4 simulations of the α decay of ^{253}No

Isotopes with odd proton and/or neutron number are known for their complex decay patters. Therefore, the construction of their decay scheme from experimental data may be difficult. Computer Monte-Carlo simulations of a potential decay process are a valuable tool, that can help to support or exclude our hypotheses. At SHIP we performed an experiment aimed at the study of ^{253}No ($Z = 102$), which is a nice example of the isotope with a complex decay pattern. We performed Monte-Carlo simulations of the decay of ^{253}No using GEANT 4 [Ago03] and compared the results of the simulations with the experimental α-decay spectra. Results were published in *The European Physical Journal A* and *GSI Scientific Report* [Heß12, Kal12] and are presented in this Appendix.

The ^{253}No isotope decays predominantly (96 %) by the 8004-keV α line to the 279.5-keV excited level in ^{249}Fm (see the proposed decay scheme in Fig. 7.1). Less probable are the decays with $E_\alpha = 8075\,\mathrm{keV}$ (4 %) and $E_\alpha = 7620\,\mathrm{keV}$ (0.25 %) populating 209.3- and 669.5-keV excited levels, respectively. In all cases, the daughter nucleus ^{249}Fm promptly deexcites to the ground state by one or more internal transitions. The process of internal transition is realized by the emission of either a γ ray or a conversion electron. The latter induces the emission of a cascade of X-rays and/or Auger electrons.

In the case when nuclei are implanted into the detector and then undergo radioactive disintegration, one must be aware of the 'energy-summing' effect while analyzing experimental spectra [Heß89]. This is the case of the experimental setup used at SHIP, where nuclei are implanted into a 16-strip position-sensitive silicon detector (see Sect. 4.1). Energy summing occurs when two signals arise in the detector within such a short time that the electronic system cannot resolve them and signals are piled-up.

In the case of ^{253}No, α decay populates excited levels in ^{249}Fm promptly deexciting by internal transition(s). As the internal transition occurs rapidly after the α decay, the electronics does not resolve individual steps. The energy of the α particle is summed with the energy of electrons and/or X-rays from

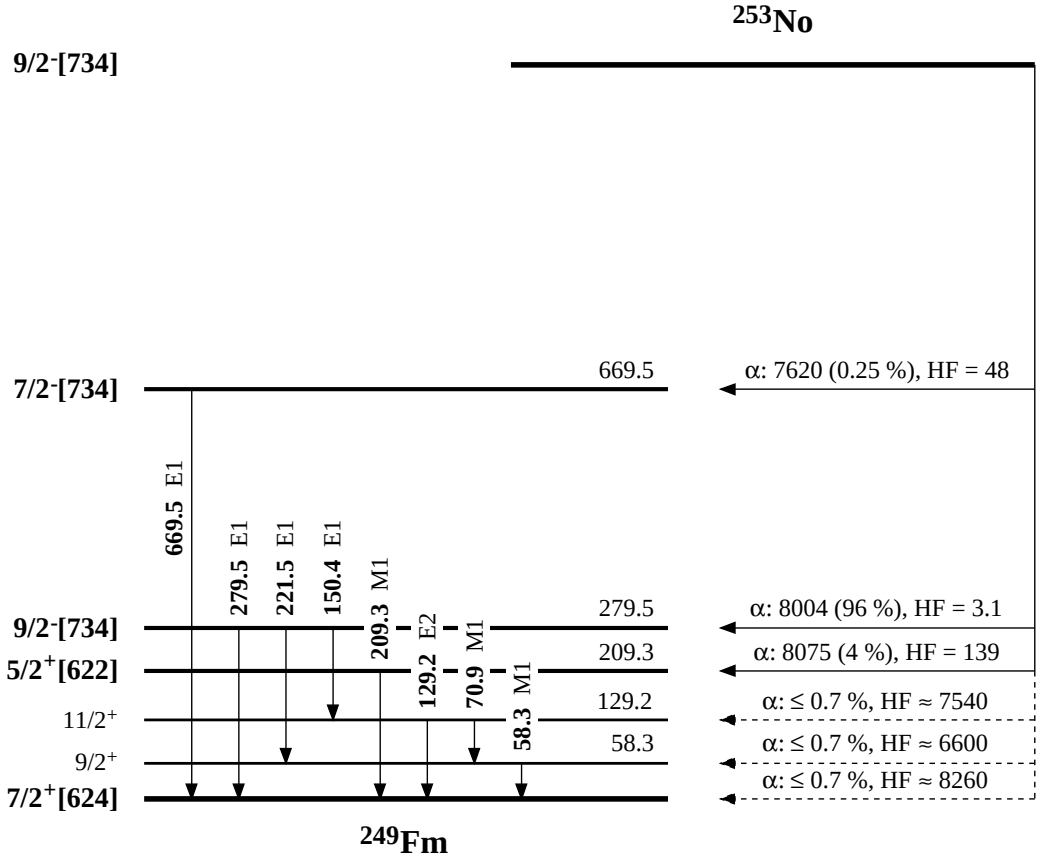

Fig. 7.1 Proposed decay scheme for ^{253}No [Heß12, Kal12]. Energies of α lines, excited levels and internal transitions are in keV.

the deexcitation process. The effect of energy summing causes:

- appearance of additional α lines in the α-decay spectrum,
- a change in shape and/or relative intensities of α lines in the α-decay spectrum.

In Monte-Carlo simulations of the decay of ^{253}No, we considered Gaussian distributions of spatial positions of nuclei within the detector and their implantation depths. Considered energy resolution of the detector was 30 keV (FWHM). Three decay paths with corresponding relative intensities were simulated following the decay scheme in Fig. 7.1:

- 0.25 % of α decays with $E_\alpha = 7620$ keV followed by the 669.5-keV $E1$ internal transition.
- 4 % of α decays with $E_\alpha = 8075$ keV followed by the 209.3-keV $M1$ internal transition.

- 96 % of α decays with $E_\alpha = 8004\,\mathrm{keV}$ followed by the $E1$ internal transition with one of the energies: 279.5, 221.5 or 150.4 keV.

We simulated the emission of an α particle and a subsequent deexcitation process. The deexcitation involved the emission of a γ ray or a conversion electron with the probability taken from Ref. [Kib08]. Internal conversion on K-, L- and M-shell was simulated assuming the corresponding binding energy of the electron. Internal conversion on N- or higher shell was simulated by the emission of conversion electron with energy equal to the energy of the internal transition and its binding energy ($\sim 2\,\mathrm{keV}$ or less) was neglected.

Vacancies in electron shells created by the emitted conversion electrons are promptly filled by electrons from higher shells. Difference between binding energies of atomic electrons on initial and final shell may be released either as photons (i.e. X-rays) or electrons (called Auger electrons). The radiative and non-radiative yield, i.e. relative intensities of X-rays and Auger electrons, respectively, were taken from Ref. [Fir04]. In the process of Auger-electron emission we also included the Coster-Kronig transition, in which the initial vacancy is filled by the electron from a higher subshell within the same shell. Propagating and filling of the vacancies was simulated up to the electron M-shell for each shell individually. The probability for the process to occur on a given shell was equal to the sum of intensities of all its subshells. Binding energy of a given shell was considered as a weighted mean of all its subshells. All processes appearing in higher shells were simulated in one step with the relative intensity corresponding to the sum of all included shells and zero binding energy.

In Fig. 7.2 we show a comparison of experimental and simulated α-decay spectrum of ^{253}No. In the experimental data, besides ^{253}No, a small contribution of ^{254}No was expected as well. That is the reason why we also simulated the α decay of ^{254}No with one α line at 8093 keV. The 'artificial' peaks at about 8060, 8133, and 8274 keV in the spectrum are due to the energy-summing effect. Alpha lines with these energies are not present in the α-decay scheme of ^{253}No (Fig. 7.1).

In the region from 8200 to 8300 keV experimental data exceed counts obtained from simulation. This excess could indicate a weak transition connecting ground state of ^{253}No with ground state in ^{249}Fm or its two lowest-lying rotational levels. These potential transitions are depicted by the dashed lines in the decay scheme in Fig. 7.1. The total intensity of ~ 0.7 % for these three transitions was obtained from the discrepancy between experimental and simulated α-decay spectra in corresponding energy region (see the right side of Fig. 7.2). The best agreement between simulation and experimental data was obtained using the relative intensities of 45, 37 and 18 % for the transitions to the $7/2^+$, $9/2^+$ and $11/2^+$ states in ^{249}Fm, respectively. Corresponding hindrance factors of the transitions are about 8260, 6600 and 7540, respectively.

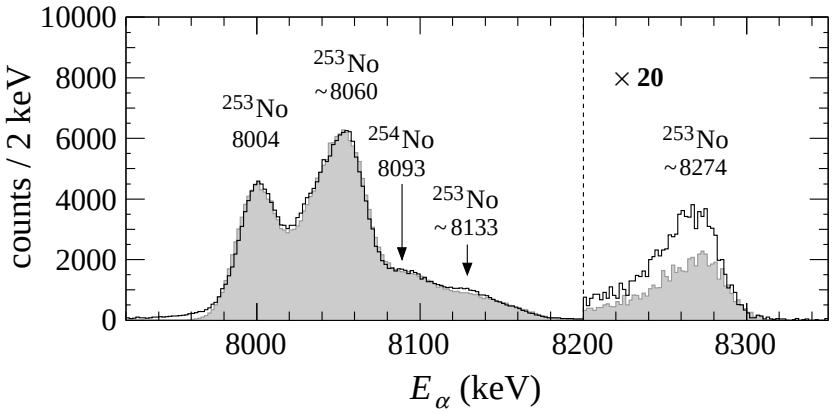

Fig. 7.2 A comparison of experimental (black solid line) and simulated (shaded area) α-decay energy spectra of ^{253}No. A small contribution from ^{254}No is visible at 8093 keV. Energies of α lines are in keV. A discrepancy between simulated and experimental spectra at about 8274 keV led us to a conclusion, that there may be a weak α transition between a ground state of ^{253}No and a ground state or its rotational band in ^{249}Fm. See text for more details.

The α transitions between mentioned levels were also observed in lighter $N = 151$ isotones: ^{247}Cm ($Z = 96$), ^{249}Cf ($Z = 98$) and ^{251}Fm ($Z = 100$). Total relative intensity of α decays to the $7/2^+$, $9/2^+$ and $11/2^+$ states in daughter isotopes is 20.7 % for ^{247}Cm, 4.1 % for ^{249}Cf, and 2.7 % for ^{251}Fm [Fir04]. The value of 0.7 % for ^{253}No from our data follows the decreasing trend of relative intensity with increasing proton number. The relative intensities of α decays to the $7/2^+$, $9/2^+$ and $11/2^+$ states separately are 67, 27 and 6 % for ^{247}Cm; 60, 32 and 8 % for ^{249}Cf; and 55, 34 and 11 % for ^{251}Fm [Fir04]. These values are similar to estimated relative intensities (45, 37, and 18 %) for corresponding transitions in the decay of ^{253}No. Although the transitions cannot be identified directly in the α-decay spectrum due to the energy-summing effect, the simulation indicates their presence in the decay of ^{253}No.

In the study of the dependence of energy summing on implantation depth, several measurements with plastic foils of different thickness placed in front of the detector were performed. As a result different implantation depths were achieved for ^{253}No nuclides. For five cases, where plastic foils with a thickness of 0, 2, 4, 6, and 8 μm were used, we performed GEANT 4 simulations. The resulting implantation depths of 7.0, 5.2, 3.6, 2.2, and 1.0 μm, respectively, were calculated using the computer code SRIM [Zie13]. The comparison of experimental and simulated α-decay energy spectra for these five cases is shown in Fig. 7.3. Different probability of the energy-summing effect is demonstrated as the different relative intensities of 8004- and 8060-keV peaks as a function of the implantation depth. Along with the decreasing implantation depth of ^{253}No nuclei (from Panel (a) to Panel (e)), the relative amount of counts at higher

energies decreases. This is caused by increasing probability for the conversion electron to escape from the detector and not to be registered with full energy at lowering implantation depths.

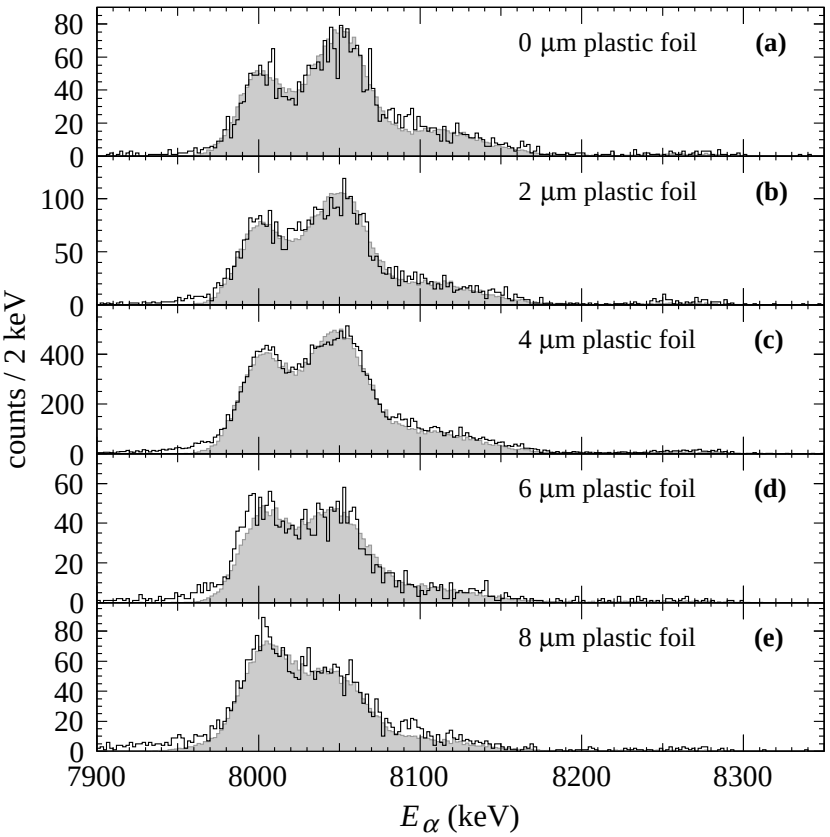

Fig. 7.3 Comparison of experimental (black solid line) and simulated (shaded area) α-decay energy spectra of ^{253}No. Five measurements were performed with plastic foils with a thickness of 0, 2, 4, 6, and 8 μm placed in front of the detector resulting in implantation depths of 7.0, 5.2, 3.6, 2.2, and 1.0 μm for ^{253}No nuclides, respectively. Different implantation depths resulted in different probability for the conversion electrons to be fully stopped in the detector, and thus for their full energy to be summed with the α-particle energy. This is manifested as different shapes of the spectra depending on implantation depth. See text for more details.

The GEANT 4 simulations were performed to verify the proposed decay scheme of ^{253}No and to study the influence of different implantation depths of ^{253}No nuclides on energy summing of α particles with conversion electrons. A fair agreement was achieved between the experimental and simulated α-decay energy spectra.

List of publications

Publications in current contents:

- **Decay of $^{201-203}$Ra and $^{200-202}$Fr**
  Z. Kalaninová, S. Antalic, A.N. Andreyev, F.P. Heßberger, D. Ackermann, B. Andel, L. Bianco, S. Hofmann, M. Huyse, B. Kindler, B. Lommel, R. Mann, R.D. Page, P.J. Sapple, J. Thomson, P. Van Duppen, M. Venhart
  Phys. Rev. C **89**, 054312 (2014)

- **New developments of the in-source spectroscopy method at RILIS/ISOLDE**
  B.A. Marsh, B. Andel, A.N. Andreyev, S. Antalic, D. Atanasov, A.E. Barzakh, B. Bastin, Ch. Borgmann, L. Capponi, T.E. Cocolios, T. Day Goodacre, M. Dehairs, X. Derkx, H. De Witte, D.V. Fedorov, V.N. Fedosseev, G.J. Focker, D.A. Fink, K.T. Flanagan, S. Franchoo, L. Ghys, M. Huyse, N. Imai, Z. Kalaninova, U. Köster, S. Kreim, N. Kesteloot, Yu. Kudryavtsev, J. Lane, N. Lecesne, V. Liberati, D. Lunney, K.M. Lynch, V. Manea, P.L. Molkanov, T. Nicol, D. Pauwels, L. Popescu, D. Radulov, E. Rapisarda, M. Rosenbusch, R.E. Rossel, S. Rothe, L. Schweikhard, M.D. Seliverstov, S. Sels, A.M. Sjödin, V. Truesdale, C. Van Beveren, P. Van Duppen, K. Wendt, F. Wienholtz, R.N. Wolf, S.G. Zemlyanoy
  Nucl. Instr. and Meth. B **317**, 550 (2013)

- **β-delayed fission and α decay of ^{178}Tl**
  V. Liberati, A.N. Andreyev, S. Antalic, A. Barzakh, T.E. Cocolios, J. Elseviers, D. Fedorov, V.N. Fedoseev, M. Huyse, D.T. Joss, Z. Kalaninová, U. Köster, J.F.W. Lane, B. Marsh, D. Mengoni, P. Molkanov, K. Nishio, R.D. Page, N. Patronis, D. Pauwels, D. Radulov, M. Seliverstov, M. Sjödin, I. Tsekhanovich, P. Van den Bergh, P. Van Duppen, M. Venhart, M. Veselský
  Phys. Rev. C **88**, 044322 (2013)

- **α decay of the very neutron-deficient isotopes $^{197-199}$Fr**
  Z. Kalaninová, A.N. Andreyev, S. Antalic, F.P. Heßberger, D. Ackermann, B. Andel, M.C. Drummond, S. Hofmann, M. Huyse, B. Kindler, J.F.W. Lane, V. Liberati, B. Lommel, R.D. Page, E. Rapisarda, K. Sandhu, Š. Šáro, A. Thornthwaite, P. Van

Duppen
Phys. Rev. C **87**, 044335 (2013)

- **β-delayed fission of ^{192,194}At**
  A.N. Andreyev, S. Antalic, D. Ackermann, L. Bianco, S. Franchoo, S. Heinz, F.P. Heßberger, S. Hofmann, M. Huyse, Z. Kalaninová, I. Kojouharov, B. Kindler, B. Lommel, R. Mann, K. Nishio, R.D. Page, J.J. Ressler, B. Streicher, Š. Šáro, B. Sulignano, P. Van Duppen
  Phys. Rev. C **87**, 014317 (2013)

- **Nuclear structure of heavy $N = 153$ isotones**
  S. Antalic, F.P. Heßberger, D. Ackermann, M. Block, S. Heinz, S. Hofmann, Z. Kalaninová, B. Kindler, M. Leino, B. Lommel, R. Mann, K. Nishio, Š. Šáro, B. Sulignano
  Acta Physica Polonica B **44**, 387 (2013)

- **Alpha-gamma decay studies of ^{253}No and its daughter products ^{253}Md, ^{249}Fm**
  F.P. Heßberger, S. Antalic, D. Ackermann, Z. Kalaninová, S. Heinz, S. Hofmann, B. Streicher, B. Kindler, I. Kojouharov, P. Kuusinniemi, M. Leino, B. Lommel, R. Mann, K. Nishio, Š. Šáro, B. Sulignano, M. Venhart
  Eur. Phys. J. A **48**, 75 (2012)

- **Isomeric states in ^{253}No and ^{253}Fm**
  S. Antalic, F.P. Heßberger, D. Ackermann, S. Heinz, S. Hofmann, Z. Kalaninová, B. Kindler, J. Khuyagbaatar, I. Kojouharov, P. Kuusiniemi, M. Leino, B. Lommel, R. Mann, K. Nishio, Š. Šáro, B. Streicher, B. Sulignano, M. Venhart
  Eur. Phys. J. A **47**, 62 (2011)

Other publications:

- **Decay of ^{200,201}Fr**
  Z. Kalaninová, S. Antalic,, A.N. Andreyev, F.P. Heßberger, D. Ackermann, B. Andel, L. Bianco, S. Hofmann, M. Huyse, B. Kindler, B. Lommel, R. Mann, R.D. Page, P.J. Sapple, J. Thomson, P. Van Duppen, M. Venhart
  submitted to GSI SCIENTIFIC REPORT 2013

- **Decay of $^{201-203}$Ra**
  Z. Kalaninová, S. Antalic,, A.N. Andreyev, F.P. Heßberger, D. Ackermann, B. Andel, L. Bianco, S. Hofmann, M. Huyse, B. Kindler, B. Lommel, R. Mann, R.D. Page, P.J. Sapple, J. Thomson, P. Van Duppen, M. Venhart
  submitted to GSI SCIENTIFIC REPORT 2013

- **Alpha Decay of $^{197-199}$Fr**
  Z. Kalaninová, A.N. Andreyev, S. Antalic, F.P. Heßberger, D. Ackermann, B. Andel, M.C. Drummond, S. Hofmann, M. Huyse, B. Kindler, J.F.W. Lane, V. Liberati, B. Lommel, R.D. Page, E. Rapisarda, K. Sandhu, Š. Šáro, A. Thornthwaite, P. Van Duppen
  GSI SCIENTIFIC REPORT 2012, PHN-ENNA-EXP-04 (2013)

- **Spontaneous Fission Properties of ^{259}Sg and ^{255}Rf**
  F.P. Heßberger, S. Antalic, D. Ackermann, M. Block, S. Heinz, S. Hofmann, Z. Kalaninová, I. Kojouharov, J. Khuyagbaatar, B. Kindler, B. Lommel, R. Mann
  GSI SCIENTIFIC REPORT 2012, PHN-ENNA-06 (2013)

- **Geant 4 simulations of ^{253}No α decay**
  Z. Kalaninová, S. Antalic, F.P. Heßberger, D. Ackermann, L.-L. Andersson, Š. Šáro
  GSI SCIENTIFIC REPORT 2011, PHN-NUSTAR-SHE-06 (2012)

- **Decay Study of ^{254}Sg**
  F.P. Heßberger, S. Antalic, D. Ackermann, S. Heinz, S. Hofmann, Z. Kalaninová, I. Kojouharov, J. Khuyagbaatar, B. Kindler, B. Lommel, R. Mann
  GSI SCIENTIFIC REPORT 2011, PHN-NUSTAR-SHE-05 (2012)

Conferences and workshops:

- **Alpha decay of $^{197-199}$Fr (Abstract)**
  Z. Kalaninová, A.N. Andreyev, S. Antalic, F.P. Heßberger, D. Ackermann and B. Andel and M.C. Drummond, S. Hofmann, M. Huyse, J.F.W. Lane, V. Liberati, B. Lommel, R.D. Page, E. Rapisarda, K. Sandhu, Š. Šáro, A. Thornthwaite, P. Van Duppen
  Workshop "Shape Coexistence Across the Chart of the Nuclides", 15.−16. 04. 2013, York (United Kingdom)
  Abstract book, p. 17 (2013)

- **Production and decay studies of $^{197-202}$Fr at SHIP (Abstract)**
  Z. Kalaninová, S. Antalic, A.N. Andreyev, F.P. Heßberger, D. Ackermann, B. Andel, M.C. Drummond, S. Hofmann, M. Huyse, J.F.W. Lane, V. Liberati, R.D. Page, E. Rapisarda, K. Sandhu, A. Thornthwaite, P. Van Duppen
  Conference "Nuclear Structure and Related Topics", 03. − 07. 07. 2012, Dubna (Russia)
  Abstract book, p. 50 (2012)

- **Studies of very neutron-deficient radium and francium isotopes**
  Z. Kalaninová
  17th Conference of Czech and Slovak Physicists, 05. − 08. 09. 2011, Žilina (Slovakia)
  Proceedings, p. 57 (2012)

- **Decay studies of neutron deficient Ra and Fr isotopes (Extended Abstract)**
  Z. Kalaninová
  Študentská vedecká konferencia FMFI UK, 19. 04. 2011, Bratislava (Slovakia)
  Proceedings, p. 213 (2011)

Bibliography

[Ago03] S. Agostinelli, *et al.*, *Nucl. Instr. and Meth. A* **506**, 250 (2003), http://geant4.cern.ch/.

[And00] A.N. Andreyev, M. Huyse, P. Van Duppen, L. Weissman, D. Ackermann, J. Gerl, F.P. Heßberger, S. Hofmann, A. Kleinböhl, G. Münzenberg, S. Reshitko, C. Schlegel, H. Schaffner, P. Cagarda, M. Matoš, Š. Šáro, A. Keenan, C. Moore, C.D. O'Leary, R.D. Page, M. Taylor, H. Kettunen, M. Leino, A. Lavrentiev, R. Wyss, and K. Heyde, *Nature* **405**, 430 (2000).

[And04a] A.N. Andreyev, D. Ackermann, F.P. Heßberger, K. Heyde, S. Hofmann, M. Huyse, D. Karlgren, I. Kojouharov, B. Kindler, B. Lommel, G. Münzenberg, R.D. Page, K. Van de Vel, P. Van Duppen, W.B. Walters, and R. Wyss, *Phys. Rev. C* **69**, 054308 (2004).

[And04b] A.N. Andreyev, D. Ackermann, F.P. Heßberger, S. Hofmann, M. Huyse, G. Münzenberg, R.D. Page, K. Van de Vel, and P. Van Duppen, *Nucl. Instr. and Meth. A* **533**, 409 (2004).

[And05] A.N. Andreyev, D. Ackermann, S. Antalic, I.G. Darby, S. Franchoo, F.P. Heßberger, S. Hofmann, M. Huyse, P. Kuusiniemi, B. Lommel, B. Kindler, R. Mann, G. Münzenberg, R.D. Page, Š. Šáro, B. Sulignano, B. Streicher, K. Van de Vel, P. Van Duppen, and D.R. Wiseman, *Phys. Rev. C* **72**, 014612 (2005).

[And06] A.N. Andreyev, S. Antalic, M. Huyse, P. Van Duppen, D. Ackermann, L. Bianco, D.M. Cullen, I.G. Darby, S. Franchoo, S. Heinz, F.P. Heßberger, S. Hofmann, I. Kojouharov, B. Kindler, A.-P. Leppänen, B. Lommel, R. Mann, G. Münzenberg, J. Pakarinen, R.D. Page, J.J. Ressler, Š. Šáro, B. Streicher, B. Sulignano, J. Thomson, and R. Wyss, *Phys. Rev. C* **74**, 064303 (2006).

[And08] K. Andgren, U. Jakobsson, B. Cederwall, J. Uusitalo, T. Bäck, S.J. Freeman, P.T. Greenlees, B. Hadinia, A. Hugues, A. Johnson, P.M. Jones, D.T. Joss, S. Juutinen, R. Julin, S. Ketelhut, A. Khaplanov, M. Leino, M. Nyman, R.D. Page, P. Rahkila, M. Sandzelius, P. Sapple, J. Sarén,

C. Scholey, J. Simpson, J. Sorri, J. Thomson, and R. Wyss, *Phys. Rev. C* **78**, 044328 (2008).

[And09] A.N. Andreyev, S. Antalic, D. Ackermann, L. Bianco, S. Franchoo, S. Heinz, F.P. Heßberger, S. Hofmann, M. Huyse, I. Kojouharov, B. Kindler, B. Lommel, R. Mann, K. Nishio, R.D. Page, J.J. Ressler, P. Sapple, B. Streicher, Š. Šáro, B. Sulignano, J. Thomson, P. Van Duppen, and M. Venhart, *Phys. Rev. C* **79**, 064320 (2009).

[And13a] A.N. Andreyev, S. Antalic, D. Ackermann, L. Bianco, S. Franchoo, S. Heinz, F.P. Heßberger, S. Hofmann, M. Huyse, Z. Kalaninová, I. Kojouharov, B. Kindler, B. Lommel, R. Mann, K. Nishio, R.D. Page, J.J. Ressler, B. Streicher, Š. Šáro, B. Sulignano, and P. Van Duppen, *Phys. Rev. C* **87**, 014317 (2013).

[And13b] A.N. Andreyev, M. Huyse, and P. Van Duppen, *Rev. Mod. Phys.* **85**, 1541 (2013).

[And13c] A.N. Andreyev, M. Huyse, P. Van Duppen, C. Qi, R.J. Liotta, S. Antalic, D. Ackermann, S. Franchoo, F.P. Heßberger, S. Hofmann, I. Kojouharov, B. Kindler, P. Kuusiniemi, S.R. Lesher, B. Lommel, R. Mann, K. Nishio, R.D. Page, B. Streicher, Š. Šáro, B. Sulignano, D. Wiseman, and R.A. Wyss, *Phys. Rev. Lett.* **110**, 242502 (2013).

[Ant01] S. Antalic and Š. Šáro, *Proceedings of the 5th International Conference on Dynamical Aspects of Nuclear Fission* , 524 (2001).

[Ant05] S. Antalic, *Synthesis and properties of neutron deficient isotopes of elements around Z = 100*, PhD thesis, Comenius University in Bratislava (2005).

[Ant11] S. Antalic, F.P. Heßberger, D. Ackermann, S. Heinz, S. Hofmann, Z. Kalaninová, B. Kindler, J. Khuyagbaatar, I. Kojouharov, P. Kuusiniemi, M. Leino, B. Lommel, R. Mann, K. Nishio, Š. Šáro, B. Streicher, B. Sulignano, and M. Venhart, *Eur. Phys. J. A* **47**, 62 (2011).

[Ant12] S. Antalic, *private communication.*

[Bij95] N. Bijnens, P. Decrock, S. Franchoo, M. Gaelens, M. Huyse, H.-Y. Hwang, I. Reusen, J. Szerypo, J. von Schwarzenberg, J. Wauters, J. G. Correia, A. Jokinen, P. Van Duppen, and The ISOLDE Collaboration, *Phys. Rev. Lett.* **75**, 4571 (1995).

[Boh51] A. Bohr, *Phys. Rev.* **81**, 134 (1951).

[Bru97] R. Brun and F. Rademakers, *Nucl. Instr. and Meth. A* **389**, 81 (1997), http://root.cern.ch/drupal/.

[Cal84] F. Calaprice, G.T. Ewan, R.-D. von Dincklage, B. Jonson, O.C. Jonsson, and H.L. Ravn, *Phys. Rev. C* **30**, 1671 (1984).

[Cas90] R.F. Casten, *Nuclear Structure From A Simple Perspective* (Oxford University Press, 200 Madison Avenue, New York, New York 10016, 1990).

[Cha32] J. Chadwick, *Proc. R. Soc. Lond. A* **136**, 692 (1932).

[Chu99] S.Y.F. Chu, L.P. Ekström, and R.B. Firestone, *The Lund/LBNL Nuclear Data Search* (1999), http://nucleardata.nuclear.lu.se/nucleardata/toi/perchart.htm.

[Coe85] E. Coenen, K. Deneffe, M. Huyse, P. Van Duppen, and J.L. Wood, *Phys. Rev. Lett.* **54**, 1783 (1985).

[Coe86] E. Coenen, K. Deneffe, M. Huyse, and P. Van Duppen, *Z. Phys. A* , 485 (1986).

[DeW05] H. De Witte, A.N. Andreyev, S. Dean, S. Franchoo, M. Huyse, O. Ivanov, U. Köster, W. Kurcewicz, J. Kurpeta, A. Plochocki, K. Van de Vel, J. Van de Walle, and P. Van Duppen, *Eur. Phys. J. A* **23**, 243 (2005).

[Dob02] D.J. Dobson, S.J. Freeman, P.T. Greenlees, A.N. Qadir, S. Juutinen, J.L. Durell, T. Enqvist, P. Jones, R. Julin, A. Keenan, H. Kettunen, P. Kuusiniemi, M. Leino, P. Nieminen, P. Rahkila, S. D. Robinson, J. Uusitalo, and B.J. Varley, *Phys. Rev. C* **66**, 064321 (2002).

[Dra98] G. D. Dracoulis, A. P. Byrne, and A. M. Baxter, **432**, 37 (1998).

[Dyb83] K. Dybdal, T. Chapuran, D.B. Fossan, W.F. Piel, Jr., D. Horn, and E.K. Warburton, *Phys. Rev. C* **28**, 1171 (1983).

[Enq96a] T. Enqvist, P. Armbruster, K. Eskola, M. Leino, V. Ninov, W.H. Trzaska, and J. Uusitalo, *Z. Phys. A* **354**, 9 (1996).

[Enq96b] T. Enqvist, K. Eskola, A. Jokinen, M. Leino, W.H. Trzaska, J. Uusitalo, V. Ninov, and P. Armbruster, *Z. Phys. A* **354**, 1 (1996).

[Ewa80] G.T. Ewan, E. Hagberg, B. Jonson, S. Mattsson, and P. Tidemand-Petersson, *Z. Phys. A* **296**, 223 (1980).

[Fir96] R.B. Firestone, V.S. Shirley, S.Y.F. Chu, C.M. Baglin, and J. Zipkin, *Table of Isotopes* (CD-ROM Edition, 1996).

[Fir04] R.B. Firestone and L.P. Ekström, *database version 2.1, URL: http://ie.lbl.gov/toi/perchart.htm* (2004).

[Gam28] G. Gamow, *Z. Phys.* **51**, 204 (1928).

[Gei09] H. Geiger and E. Marsden, *Proc. R. Soc. Lond. A* **82**, 495 (1909).

[Gei10] H. Geiger, *Proc. R. Soc. Lond. A* **83**, 492 (1910).

[Gei11] H. Geiger and J.M. Nuttall, *Phil. Mag.* **22**, 613 (1911).

[Gho50] S.N. Ghoshal, *Phys. Rev.* **80**, 939 (1950).

[Ghy14] L. Ghys, *et al., in preparation* (2014).

[Gur28] R.W. Gurney and E.U. Condon, *Nature* **122**, 439 (1928).

[Hal92] H.L. Hall and D.C. Hoffman, *Annu. Rev. Nucl. Part. Sci.* **42**, 147 (1992).

[Ham85] J.H. Hamilton, P.G. Hansen, and E.F. Zganjar, *Rep. Prog. Phys.* **48**, 631 (1985).

[Hel99] K. Helariutta, J.F.C. Cocks, T. Enqvist, P.T. Greenlees, P. Jones, R. Julin, S. Juutinen, P. Jämsen, H. Kankaanpää, H. Kettunen, P. Kuusiniemi, M. Leino, M. Muikku, M. Piiparinen, P. Rahkila, A. Savelius, W.H. Trzaska, S. Törmänen, J. Uuistalo, R.G. Allatt, P.A. Butler, R.D. Page, and M. Kapusta, *Eur. Phys. J. A* **6**, 289 (1999).

[Her10] J.A. Heredia, A.N. Andreyev, S. Antalic, S. Hofmann, D. Ackermann, V. F. Comas, S. Heinz, F.P. Heßberger, B. Kindler, J. Khuyagbaatar, B. Lommel, and R. Mann, *Eur. Phys. J. A* **46**, 337 (2010).

[Heß89] F.P. Heßberger, S. Hofmann, K.-H. Schmidt G. Münzenberg, and P. Armbruster, *Nucl. Instr. and Meth. A* **274**, 522 (1989).

[Heß06] F.P. Heßberger, S. Hofmann, D. Ackermann, S. Antalic, B. Kindler, I. Kojouharov, P. Kuusiniemi, M. Leino, B. Lommel, R. Mann, K. Nishio, A.G. Popeko, B. Sulignano, Š. Šáro, B. Streicher, M. Venhart, and A.V. Yeremin, *Eur. Phys. J. A* **29**, 165 (2006).

[Heß12] F.P. Heßberger, S. Antalic, D. Ackermann, Z. Kalaninová, S. Heinz, S. Hofmann, B. Streicher, B. Kindler, I. Kojouharov, P. Kuusiniemi, M. Leino, B. Lommel, R. Mann, K. Nishio, Š. Šáro, B. Sulignano, and M. Venhart, *Eur. Phys. J. A* **48**, 75 (2012).

[Hey83] K. Heyde, P. Van Isacker, M. Waroquier, J.L. Wood, and R.A. Meyer, **102**, 291 (1983).

[Hey99] K. Heyde, *Basic Ideas and Concepts in Nuclear Physics. An Introductory Approach* (Institute of Physics Publishing, Bristol and Philadelphia, 1999).

[Hey11] K. Heyde and J.L. Wood, *Rev. Mod. Phys.* **83**, 1467 (2011).

[Hir93] M. Hirsch, A. Staudt, K. Muto, and H.V. Klapdor-Kleingrothaus, *At. Data and Nucl. Data Tables* **53**, 165 (1993).

[Hof79] S. Hofmann, W. Faust, G. Münzenberg, W. Reisdorf, P. Armbruster, K. Güttner, and H. Ewald, *Z. Phys. A* **291**, 53 (1979).

[Hof00] S. Hofmann and G. Münzenberg, *Rev. Mod. Phys.* **72**, 733 (2000).

[Hof07] S. Hofmann, D. Ackermann, S. Antalic, H. G. Burkhard, V. F. Comas, R. Dressler, Z. Gan, S. Heinz, J.A. Heredia, F.P. Heßberger, J. Khuyagbaatar, B. Kindler, I. Kojouharov, P. Kuusiniemi, M. Leino, B. Lommel, R. Mann, G. Münzenberg, K. Nishio, A.G. Popeko, Š. Šáro, H.J. Schött, B. Streicher, B. Sulignano, J. Uusitalo, M. Venhart, and A.V. Yeremin, *Eur. Phys. J. A* **32**, 251 (2007).

[Huy88] M. Huyse, E. Coenen, K. Deneffe, P. Van Duppen, K. Heyde, and J. Van Maldeghem, *Phys. Lett. B* **201**, 293 (1988).

[Huy92] M. Huyse, P. Decrock, P. Dendooven, G. Reusen, P. Van Duppen, and J. Wauters, *Phys. Rev. C* **46**, 1209 (1992).

[Jak10] U. Jakobsson, J. Uusitalo, S. Juutinen, M. Leino, P. Nieminen, K. Andgren, B. Cederwall, P.T. Greenlees, B. Hadinia, P. Jones, R. Julin, S. Ketelhut, A. Khaplanov, M. Nyman, P. Peura, P. Rahkila, P. Ruotsalainen, M. Sandzelius, J. Sarén, C. Scholey, and J. Sorri, *Phys. Rev. C* **82**, 044302 (2010).

[Jak12] U. Jakobsson, J. Uusitalo, S. Juutinen, M. Leino, T. Enqvist, P.T. Greenlees, K. Hauschild, P. Jones, R. Julin, S. Ketelhut, P. Kuusiniemi, M. Nyman, P. Peura, P. Rahkila, P. Ruotsalainen, J. Sarén, C. Scholey, and J. Sorri, *Phys. Rev. C* **85**, 014309 (2012).

[Jak13] U. Jakobsson, S. Juutinen, J. Uusitalo, M. Leino, K. Auranen, T. Enqvist, P.T. Greenlees, K. Hauschild, P. Jones, R. Julin, S. Ketelhut, P. Kuusiniemi, M. Nyman, P. Peura, P. Rahkila, P. Ruotsalainen, J. Sarén, C. Scholey, and J. Sorri, *Phys. Rev. C* **87**, 054320 (2013).

[Jan05a] Z. Janas, C. Mazzocchi, L. Batist, A. Blazhev, M. Górska, M. Kavatsyuk, O. Kavatsyuk, R. Kirchner, A. Korgul, M. La Commara, K. Miernik, I. Mukha, A. Plochocki, E. Roeckl, and K. Schmidt, *Eur. Phys. J. A* **23**, 197 (2005).

[Jan05b] R.V.F. Janssens, *Nature* **435**, 897 (2005).

[Jul01] R. Julin, K. Helariutta, and M. Muikku, *J. Phys. G: Nucl. Part. Phys.* **27**, R109 (2001).

[Kal10] Z. Kalaninová, *Gama spektroskopia na separátore* SHIP*: Identifikácia a rozpad* ^{253}*No*, Master thesis, Comenius University in Bratislava (2010).

[Kal12] Z. Kalaninová, S. Antalic, F.P. Heßberger, D. Ackermann, L.-L. Andersson, and Š. Šáro, *GSI Scientific Report 2011* , 210 (2012).

[Kal13a] Z. Kalaninová, A.N. Andreyev, S. Antalic, F.P. Heßberger, D. Ackermann, B. Andel, M. C. Drummond, S. Hofmann, M. Huyse, B. Kindler, J.F.W. Lane, V. Liberati, B. Lommel, R.D. Page, E. Rapisarda, K. Sandhu, Š. Šáro, A. Thornthwaite, and P. Van Duppen, *Phys. Rev. C* **87**, 044335 (2013).

[Kal13b] Z. Kalaninová, A.N. Andreyev, S. Antalic, F.P. Heßberger, D. Ackermann, B. Andel, M. C. Drummond, S. Hofmann, M. Huyse, B. Kindler, J.F.W. Lane, V. Liberati, B. Lommel, R.D. Page, E. Rapisarda, K. Sandhu, Š. Šáro, A. Thornthwaite, and P. Van Duppen, *GSI Scientific Report 2012* , 134 (2013).

[Kal14] Z. Kalaninová, S. Antalic, A.N. Andreyev, F.P. Heßberger, D. Ackermann, B. Andel, L. Bianco, S. Hofmann, M. Huyse, B. Kindler, B. Lommel, R. Mann, R.D. Page, P.J. Sapple, J. Thomson, P. Van Duppen, and M. Venhart, *Phys. Rev. C* **89**, 054312 (2014).

[Ket01] H. Kettunen, J. Uusitalo, M. Leino, P. Jones, K. Eskola, P.T. Greenlees, K. Helariutta, R. Julin, S. Juutinen, H. Kankaanpää, P. Kuusiniemi, M. Muikku, P. Nieminen, and P. Rahkila, *Phys. Rev. C* **63**, 044315 (2001).

[Ket03a] H. Kettunen, T. Enqvist, T. Grahn, P.T. Greenlees, P. Jones, R. Julin, S. Juutinen, A. Keenan, P. Kuusiniemi, M. Leino, A.-P. Leppänen, P. Nieminen, J. Pakarinen, P. Rahkila, and J. Uusitalo, *Eur. Phys. J. A* **17**, 537 (2003).

[Ket03b] H. Kettunen, T. Enqvist, M. Leino, K. Eskola, P.T. Greenlees, K. Helariutta, P. Jones, R. Julin, S. Juutinen, H. Kankaanpää, H. Koivisto, P. Kuusiniemi, M. Muikku, P. Nieminen, P. Rahkila, and J. Uusitalo, *Eur. Phys. J. A* **16**, 457 (2003).

[Kib08] T. Kibédi, T. W. Burrows, M. B. Trzhaskovskaya, P. M. Davidson, and C. W. Nestor Jr., *Nucl. Instr. and Meth. A* **589**, 202 (2008), http://bricc.anu.edu.au/.

[Kra88] Kenneth S. Krane, *Introductory Nuclear Physics* (John Wiley & Sons Inc., Oregon State University, 1988).

[Lan13] J. F. W. Lane, A.N. Andreyev, S. Antalic, D. Ackermann, J. Gerl, F.P. Heßberger, S. Hofmann, M. Huyse, H. Kettunen, A. Kleinböhl, B. Kindler, I. Kojouharov, M. Leino, B. Lommel, G. Münzenberg, K. Nishio, R.D. Page, Š. Šáro, H. Schaffner, M. J. Taylor, and P. Van Duppen, *Phys. Rev. C* **87**, 014318 (2013).

[lbnl] LBNL Isotopes Project Nuclear Data Dissemination Home Page, *URL: http://ie.lbl.gov/toi.html* (2002).

[Lei96] M. Leino, J. Uusitalo, R.G. Allatt, P. Armbruster, T. Enqvist, K. Eskola, S. Hofmann, S. Hurskanen, A. Jokinen, V. Ninov, R.D. Page, and W.H. Trzaska, *Z. Phys. A* **355**, 157 (1996).

[Lid06] S.N. Liddick, R. Grzywacz, C. Mazzocchi, R.D. Page, K.P. Rykaczewski, J.C. Batchelder, C.R. Bingham, I.G. Darby, G. Drafta, C. Goodin, C.J. Gross, J.H. Hamilton, A.A. Hecht, J.K. Hwang, S. Ilyushkin, D.T. Joss, A. Korgul, W. Królas, K. Lagergren, K. Li, M.N. Tantawy, J. Thomson, and J.A. Winger, *Phys. Rev. Lett.* **97**, 082501 (2006).

[Lom02] B. Lommel, D. Gembalies-Datz, W. Hartmann, S. Hofmann, B. Kindler, J. Klemm, J. Kojouharova, and J. Steiner, *Nucl. Instr. and Meth. A* **480**, 16 (2002).

[Lyn14] K.M. Lynch, J. Billowes, M.L. Bissell, I. Budinčević, T.E. Cocolios, R.P. De Groote, S. De Schepper, V.N. Fedosseev, K.T. Flanagan, S. Franchoo, R.F. Garcia Ruiz, H. Heylen, B.A. Marsh, G. Neyens, T.J. Procter, R.E. Rossel, S. Rothe, I. Strashnov, H.H. Stroke, and K.D.A. Wendt, *Phys. Rev. X* **4**, 011055 (2014).

[Mac65] R. D. Macfarlane and A. Siivola, *Phys. Rev. Lett.* **14**, 114 (1965).

[May49] M.G. Mayer, *Phys. Rev.* **75**, 1969 (1949).

[Maz08] M. Mazzocco, D. Ackermann, M. Block, H Geissel, F. Herfurth, F.P. Heßberger, S. Hofmann, N. Iwasa, K. Nishio, W.R. Plaß, C. Scheidenberger, H. Weick, M. Winkler, and The SHIPTRAP Collaboration, *Nucl. Instr. and Meth. B* **266**, 3467 (2008).

[Med07] E.L. Medeiros, M.M.N. Rodrigues, S.B. Duarte, and O.A.P. Tavares, *Eur. Phys. J. A* **34**, 417 (2007).

[Möl95] P. Möller, J.R. Nix, W. D. Myers, and J. Swiatecki, *At. Data and Nucl. Data Tables* **59**, 185 (1995).

[Möl97] P. Möller, J.R. Nix, and K.-L. Kratz, *At. Data and Nucl. Data Tables* **66**, 131 (1997).

[Mor95] K. Morita, Y.H. Pu, J. Feng, M.G. Hies, K.O. Lee, A. Yoshida, S.C. Jeong, S. Kubono, T. Nomura, Y. Tagaya, M. Wada, M. Kurokawa, T. Motobayashi, H. Ogawa, T. Uchibori, K. Sueki, T. Ishizuka, K. Uchiyama, Y. Fujita, H. Miyatake, T. Shimoda, T. Shinozuka, H. Kudo, Y. Nagai, and S. A. Shin, *Z. Phys. A* **352**, 7 (1995).

[Mün79] G. Münzenberg, W. Faust, S. Hofmann, P. Armbruster, K. Güttner, and H. Ewald, *Nucl. Instr. and Meth.* **161**, 65 (1979).

[Nil55] S.G. Nilsson, **29**, 1 (1955).

[nndc] Data extracted using the NNDC On-Line Data Service from the ENSDF database, file revised as of 2014-01-08. M. R. Bhat, *Evaluated Nuclear Structure Data File (ENSDF),* **Nuclear Data for Science and Technology**, *URL: www.nndc.bnl.gov.*

[Poe80] D.N. Poenaru, M. Ivascu, and D. Mazilu, *J. Phys. Lett.* **41**, L589 (1980).

[Poe06] D.N. Poenaru, I.-H. Plonski, and W. Greiner, *Phys. Rev. C* **74**, 014312 (2006).

[Pu97] Y.H. Pu, K. Morita, M.G. Hies, K.O. Lee, A. Yoshida, T. Nomura, Y. Tagaya, T. Motobayashi, M. Kurokawa, H. Minemura, T. Uchibori, T. Ariga, K. Sueki, and S. A. Shin, *Z. Phys. A* **357**, 1 (1997).

[Qi09] C. Qi, F.R. Xu, R.J. Liotta, and R. Wyss, *Phys. Rev. Lett.* **103**, 072501 (2009).

[Rai50] J. Rainwater, *Phys. Rev.* **79**, 432 (1950).

[Ras59] J.O. Rasmussen, *Phys. Rev.* **113**, 1593 (1959).

[Rei81] W. Reisdorf, *Z. Phys. A* **300**, 227 (1981).

[Rig08] S.V. Rigby, D.M. Cullen, P.J.R. Mason, D.T. Scholes, C. Scholey, P. Rahkila, S. Eeckhaudt, T. Grahn, P. Greenlees, P.M. Jones, R. Julin, S. Juutinen, H. Kettunen, M. Leino, A.-P. Leppänen, P. Nieminen, M. Nyman, J. Pakarinen, and J. Uusitalo, *Phys. Rev. C* **78**, 034304 (2008).

[Rut07] E. Rutherford, *Phil. Mag.* **13**, 110 (1907).

[Rut11] E. Rutherford, *Phil. Mag.* **21**, 669 (1911).

[Rut19] E. Rutherford, *Phil. Mag.* **37**, 581 (1919).

[Šár96] Š. Šáro, R. Janik, S. Hofmann, H. Folger, F.P. Heßberger, V. Ninov, H.J. Schött, A.P. Kabachenko, A.G. Popeko, and A.V. Yeremin, *Nucl. Instr. and Meth. A* **381**, 520 (1996).

[Sau09] J. Sauvage, J. Genevey, B. Roussière, S. Franchoo, A.N. Andreyev, N. Barré, J.-F. Clavelin, H. De Witte, D.V. Fedorov, V.N. Fedoseyev, L.M. Fraile, X. Grave, G. Huber, M. Huyse, H.B. Jeppesen, U. Köster, P. Kunz, S.R. Lesher, B.A. Marsh, I. Mukha, J. Oms, M. Seliverstov, I. Stefanescu, K. Van de Vel, J. Van de Walle, P. Van Duppen, and Yu.M. Volkov, *Eur. Phys. J. A* **39**, 33 (2009).

[Sau13] J. Sauvage, B. Roussière, J. Genevey, S. Franchoo, A.N. Andreyev, N. Barré, A. Ben Braham, C. Bourgeois, J.-F. Clavelin, H. De Witte, D.V. Fedorov, V.N. Fedoseyev, L.M. Fraile, X. Grave, G. Huber, M. Huyse, P. Kilcher, U. Köster, P. Kunz, S.R. Lesher, B.A. Marsh, I. Mukha, J. Oms,

M.G. Porquet, M. Seliverstov, I. Stefanescu, K. Van de Vel, P. Van Duppen, Yu.M. Volkov, and A. Wojtasiewicz, *Eur. Phys. J. A* **49**, 109 (2013).

[Sch81] D. Schardt, T. Batsch, R. Kirchner, O. Klepper, W. Kurcewicz, E. Roeckl, and P. Tidemand-Petersson, *Nucl. Phys. A* **368**, 153 (1981).

[Sch84] K.-H. Schmidt, *Z. Phys. A* **316**, 19 (1984).

[Smi99] M.B. Smith, R. Chapman, J.F.C. Cocks, O. Dorvaux, K. Helariutta, P.M. Jones, R. Julin, S. Juutinen, H. Kankaanpää, H. Kettunen, P. Kuusiniemi, Y. Le Coz, M. Leino, D.J. Middleton, M. Muikku, P. Nieminen, P. Rahkila, A. Savelius, and K.-M. Spohr, *Eur. Phys. J. A* **5**, 43 (1999).

[Smi00] M.B. Smith, R. Chapman, J.F.C. Cocks, K.-M. Spohr, O. Dorvaux, K. Helariutta, P.M. Jones, R. Julin, S. Juutinen, H. Kankaanpää, H. Kettunen, P. Kuusiniemi, Y. Le Coz, M. Leino, D.J. Middleton, M. Muikku, P. Nieminen, P. Rahkila, and A. Savelius, *J. Phys. G: Nucl. Part. Phys.* **26**, 787 (2000).

[Tag99] Y. Tagaya, S. Hashimoto, K. Morita, Y.H. Pu, T. Ariga, K. Ohta, T. Minemura, I. Hisanaga, T. Motobayashi, and T. Nomura, *Eur. Phys. J. A* **5**, 123 (1999).

[Tak73] K. Takahashi, M. Yamada, and T. Kondoh, *At. Data and Nucl. Data Tables* **12**, 101 (1973).

[Tar08] O.B. Tarasov and D. Bazin, *Nucl. Instr. and Meth. B* **266**, 4657 (2008).

[Tho04] J.J. Thomson, *Phil. Mag.* **7**, 237 (1904).

[Tru14] V. Truesdale, *et al., in preparation* (2014).

[Uus05] J. Uusitalo, M. Leino, T. Enqvist, K. Eskola, T. Grahn, P.T. Greenlees, P. Jones, R. Julin, S. Juutinen, A. Keenan, H. Kettunen, H. Koivisto, P. Kuusiniemi, A.-P. Leppänen, P. Nieminen, J. Pakarinen, P. Rahkila, and C. Scholey, *Phys. Rev. C* **71**, 024306 (2005).

[Uus13] J. Uusitalo, J. Sarén, S. Juutinen, M. Leino, S. Eeckhaudt, T. Grahn, P.T. Greenlees, U. Jakobsson, P. Jones, R. Julin, S. Ketelhut, A.-P. Leppänen, M. Nyman, J. Pakarinen, P. Rahkila, C. Scholey, A. Semchenkov, J. Sorri, A. Steer, and M. Venhart, *Phys. Rev. C* **87**, 064304 (2013).

[Van91] P. Van Duppen, P. Decrock, P. Dendooven, M. Huyse, G. Reusen, and J. Wauters, *Nucl. Phys. A* **529**, 268 (1991).

[Var92] K. Varga, R.G. Lovas, and R.J. Liotta, *Phys. Rev. Lett.* **69**, 37 (1992).

[Wan12] M. Wang, G. Audi, A.H. Wapstra, F.G. Kondev, M. MacCormick, X. Xu, and B. Pfeiffer, *Chinese Phys. C* **36**, 1603 (2012).

[Wau93] J. Wauters, P. Dendooven, M. Huyse, G. Reusen, P. Van Duppen, P. Lievens, and the ISOLDE Collaboration, *Phys. Rev. C* **47**, 1447 (1993).

[Wei51] V.F. Weisskopf, *Phys. Rev.* **83**, 1073 (1951).

[Woo92] J.L. Wood, K. Heyde, W. Nazarewicz, M. Huyse, and P. Van Duppen, **215**, 101 (1992).

[Zie13] J.F. Ziegler, J.P. Biersack, and M.D. Ziegler, *SRIM-2013, The Stopping and Range of Ions in Matter* (2013).